CIZ1 as a therapeutic target for glioblastoma

Matheson Paxton

Department of Biomedical and Live Sciences

Faculty of Health and Medicine

Lancaster University

Thesis for degree of MSc by Research 2024

Declaration

I declare that everything written in this thesis is my own work and not the work of anybody else. This work has not been previously submitted in the same form for the award of a higher degree of qualification elsewhere.

Matheson Paxton

Abstract

Glioblastoma is a devastating disease with a median survival of 12 – 15 months. It is the most common brain tumour in adults and current standard treatments remain poor. Surgery and radiotherapy only improve patient prognosis short term (12.1 months median survival) and the only available chemotherapy (TMZ) extends median survival to just 14.6 months. Resistance mechanisms may explain the poor response of grade IV, IDH wildtype glioblastomas to TMZ. CIZ1 is a nuclear protein with DNA replication, epigenetic maintenance, and genome stability functions. CIZ1 is overexpressed in many cancers, including glioblastoma, and is evidenced to drive tumourigenesis. CDK inhibition therapy has showed recent promise in the treatment of cancer and some FDA approved CDK4/6 inhibitors are now used in routine breast cancer treatment. CDK inhibitors have been trialled in glioblastoma patients, showing some efficacy, however it is hypothesised that CDK inhibition may reduce CIZ1 levels to reduce glioblastoma growth. Our aim was to demonstrate the efficacy of CDK inhibitors on reducing proliferation and their toxicity in glioblastoma cultures, as well as showing reduced CIZ1 protein expression and comparing data to that of normal glia. Here, we assess the effect of a panel of six CDK inhibitors on glioblastoma (U-87 MG and BTNW914) and normal glia (SVG p12) cell lines. CDK inhibition causes significantly reduced glioblastoma cell proliferation compared with vehicle controls and normal glia. Cell cycle arrest and cell death is also observed in both in 2D and 3D glioblastoma cell culture. The effect on CIZ1 levels has proved inconclusive and requires further investigation. Overall, these data identify that CDK inhibitors have promising efficacy in reducing proliferation and increasing cell death in glioblastoma models *in vitro and* should be further investigated in pre-clinical models.

Table of Contents

Table of Figures

Table of Tables

Acknowledgements

Firstly, I would like to thank my supervisor Dr Nikki Copeland for his support and guidance during both the practical and writing parts of this work. I would also like to thank everyone in the cancer group at Lancaster University for their advice during meetings and sense of community. I also owe a big thank you to Dr James Tollitt for his teaching of lab techniques, patience, and humour.

1. Introduction

1.1. Glioblastoma

1.1.1. Overview

Glioblastoma is the most common brain tumour type with an incidence of 3.21 per 100,000 population and accounting for 47.7% of all brain and other central nervous system (CNS) tumours (Thakkar, Peruzzi and Prabhu, 2024). There are few direct causative links in glioblastoma, including inherited genetic syndromes (Narod, Stiller and Lenoir, 1991) and therapeutic ionising radiation (Hodges *et al.*, 1992; Preston-Martin and Mack, 1996; Socié *et al.*, 2000), but these only account for a small number of cases. The uneven prevalence of glioblastoma across sexes and ethnicities is poorly understood, with men more likely to develop the disease than women (Ostrom *et al.*, 2013; Chakrabarti *et al.*, 2005; McKinley *et al.*, 2000; Fleury *et al.*, 1997; Walker, Robins and Weinfeld, 1985) and a higher prevalence found in Caucasians than other ethnic groups (Ostrom *et al.*, 2013; Chakrabarti *et al.*, 2005).

Glioblastomas have been characterised into four subtypes: Proneural, Neural, Classical, and Mesenchymal (Verhaak *et al.*, 2010), based on molecular analysis of gene expression profiles. Different subtypes may have differing responses to treatments, which may help guide therapeutic interventions. Expression profiles of subtypes correlate somewhat to different neural lineages; however, subtypes may represent different differentiation pathways of the same precursor cell type. The newest (fifth) edition of the WHO Classification of Tumours of the Central Nervous System classifies primary glioblastoma by epidermal growth factor receptor (EFGR) amplification, an absence of isocitrate dehydrogenase (IDH) mutations, telomerase reverse transcriptase (TERT) promoter alterations, and common defects in chromosomes 7/10 (reviewed by Louis *et al.*, 2021). However, secondary glioblastomas are those that present evidence of being a malignant progression from another pre-existing tumour and are characterised by tumour protein 53 (TP53) mutations, IDH mutations, and lack of EGFR amplification (Parsons *et al.*, 2008). Despite these characteristic mutations, glioblastoma tumours are genetically heterogeneous. Variation in cell types within the tumour, mutations, protein expression,

epigenetics, and the tumour microenvironment all contribute to intra- and inter-patient heterogeneity.

1.1.2. Current Standard Treatments and Complications

The current standard treatments for glioblastoma are surgery, radiotherapy and temozolomide (TMZ) chemotherapy (reviewed by Alifieris and Trafalis, 2015). Concomitant and adjuvant TMZ resulted in a clinically significant survival benefit over just radiotherapy, so was included in the standard of care treatment for glioblastoma (Stupp *et al.*, 2005). TMZ (Figure 1.1) is a monofunctional DNA methylating agent, allowing modification of only one site per molecule, and an imidazotetrazinone (an organic heterobicyclic compound containing ortho-fused imidazole and tetrazine rings). TMZ is spontaneously converted to its active compound: the methyldiazonium cation (MTIC) at physiological pH. MITC adds methyl groups to the N^7 or O^6 positions of guanine, or the N^3 position of adenine (Figure 1.2). 7-methylguanine and N^3-methyladenine are excised by the base-excision repair (BER) pathway to repair DNA. BER is only rarely mutated in glioblastoma, providing a mechanism to develop resistance to TMZ. Typically, tumour cell death occurs through downregulation of the enzymes that repair TMZ-mediated DNA alkylation, including methylguanine-DNA methyltransferase (MGMT) and BER enzymes, whereas downregulation of mismatch repair (MMR) enzymes allows cell survival.

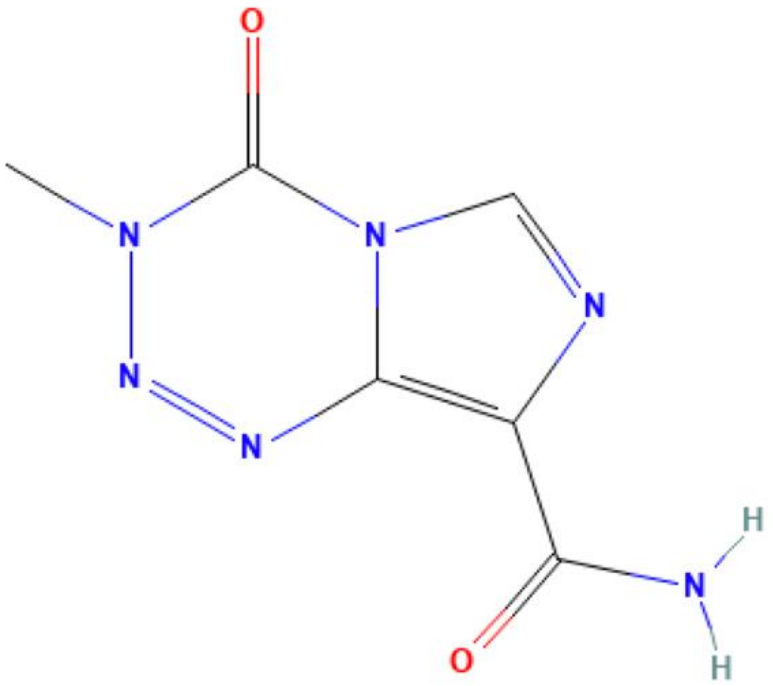

Figure 1. 1. Structure of temozolomide (NCBI, 2024). An imidazotetrazine that is 3,4-dihydroimidazo[5,1-d][1,2,3,5]tetrazine, with ortho-fused imidazole and tetrazine rings.

O^6-methylguanine adducts are repaired by MGMT. However, epigenetic regulation via methylation of the MGMT promoter is present in 30-60% of glioblastomas resulting in low or no protein expression. In glioblastoma cells with downregulated MGMT, unrepaired O^6-methylguanine mismatches to thymine on the opposite strand. Functional MMR machinery attempts to replace this, but another thymine enters its place. This leads to futile attempted repair cycles and ultimately autophagy. MMR cannot repair O^6-methylguanine and this causes replication fork stalling, double-strand DNA breaks and apoptosis. Non-functional MMR causes mutation tolerance and cell survival. Therefore, MGMT promoter methylation in combination with functional MMR in glioblastoma is clinically beneficial as these increase sensitivity to TMZ and increase cell death (reviewed by Strobel *et al.*, 2019).

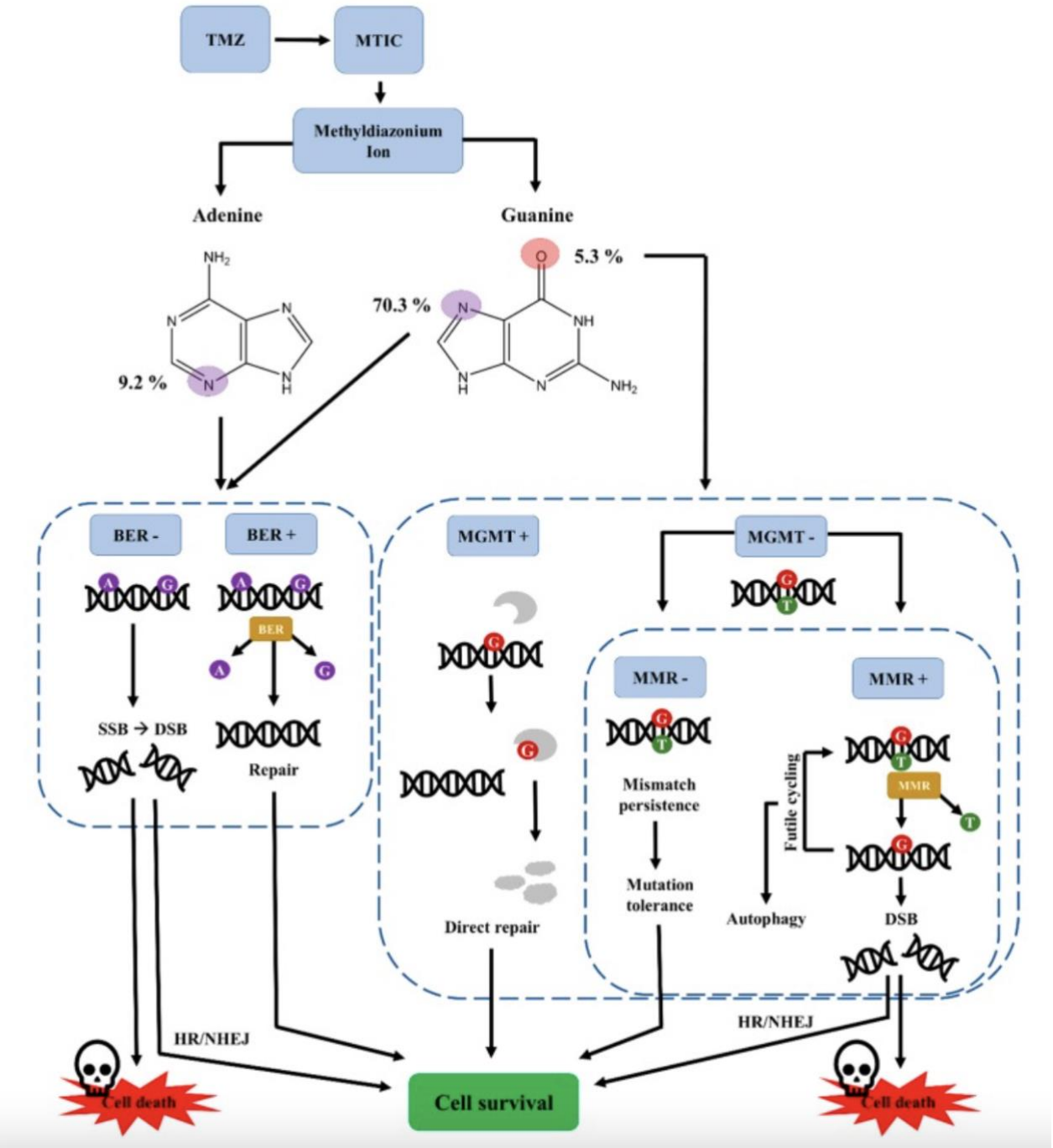

Figure 1. 2. TMZ-induced alterations and DNA repair mechanisms involved in cellular response (Strobel et al., 2019). 6-methylguanine and N7-methyladenine modifications by MTIC are repaired by BER. The methylated base is removed and replaced by a non-modified base of the same type. Dysfunctional BER is rare in glioblastoma but leads to cell death. If present, MGMT simply removes the methyl group from the base and the cell survives. MMR attempts to replace the mismatched thymine across from O6-methylguanine, but another thymine enters its place leading to futile repair cycles and autophagy or cell death. A combination of MGMT inactivation and functional MMR causes cell death. Abbreviations: SSB, single strand break; DSB, double strand break; HR, homologous recombination; NHEJ, non-homologous end joining.

There are many mechanisms that can confer resistance to TMZ in glioblastoma. Firstly, DNA repair mechanisms can repair the damage caused by TMZ and allow cells to survive. MGMT methylation is a prognostic marker for TMZ efficacy and patient survival in glioblastoma (Hegi *et al.*, 2005). MGMT removes the most toxic DNA alteration by TMZ the O^6-methylguanine and epigenetic methylation of cytosine-phosphate-guanine (CpG) islands in the MGMT promoter silences the gene and prevents TMZ-induced DNA damage repair. Despite the MGMT promoter being methylated in approximately 50% of grade IV gliomas (La Starza, Pierini and Metro, 2019), many of those that are MGMT deficient still have TMZ resistance (Hegi *et al.*, 2005) however the mechanism is not fully understood.
Other DNA repair mechanisms can impact the response of glioblastoma to TMZ. MMR machinery can cause double strand breaks (DSBs) when attempting to repair O^6-methylguanine adducts leading to cell death (Zhang, Stevens and Bradshaw, 2012; Mojas, Lopes and Jiricny, 2007). However, MMR gene deficiencies have been implicated in TMZ resistance where their loss has affected the clinical course of glioblastomas (Kawaguchi *et al.*, 2021) or showed to accelerate tumour growth during TMZ treatment (Cahill *et al.*, 2007). BER mechanisms also confer resistance to the TMZ-induced DNA adducts: N^7-methylguanine and N^3-methyladenine (Figure 1.2). BER is rarely mutated in glioblastoma and key enzymes are even overexpressed in some cases, conferring a stronger resistance to TMZ (Agnihotri *et al.*, 2012; Tang *et al.*, 2011; Thanasupawat *et al.*, 2017) even where there is an increase in MGMT mRNA (Serrano-Heras *et al.*, 2020). Figure 1.2 shows DNA that cannot be repaired by MGMT, MMR, or BER forms DSBs, which can still be repaired by homologous recombination (HR) or non-homologous end joining (NHEJ). These degenerate mechanisms provide several mechanisms to overcome TMZ-mediated DNA alkylation and promote resistance in glioblastoma.

In addition to DNA repair mechanisms, tumours can also develop TMZ resistance through survival autophagy (Zou *et al.*, 2014), conversion to glioma stem cells (GSCs) upon TMZ treatment (Auffinger *et al.*, 2014), altering microRNA expression (Wong *et al.*, 2012), and overexpression of efflux transporters that remove cytotoxic drugs (Liu *et al.*, 2015a; Zhang *et al.*, 2018). Due to the many ways glioblastomas can become resistant to TMZ, half of the patients who receive TMZ display a resistant phenotype (reviewed by Lee, 2016).

Surgery is the first line of treatment for glioblastoma and involves maximal resection using microsurgical techniques without compromising neurological function (Weller *et al.*, 2021). Naturally, technological developments have improved the amount of tumour volume that can be removed by surgery and over 98% removal of the visible tumour from a magnetic resonance imaging (MRI) scan is classed as 'full resection' (Weathers, 2019). Despite the potential to damage healthy brain tissue and reduce quality of life when trying to fully resect a glioblastoma, Sagberg, Solheim, and Jakola (2016) found patients reported a better quality of life after full resection than those receiving a biopsy, only. This could be interpreted as being linked to a better prognosis, however one study reported that full resection (>98%) prolongs survival by just 4.2 months to a median of 13 months compared to resection of less than 98%, which resulted in a median survival of 8.8 months (Lacroix *et al.*, 2001). Surgery is currently the best option to extend patient survival however, because of the invasiveness and aggressive nature of the cancer, peripheral tumour cells left behind after surgery outside of the bulk tumour can genetically and phenotypically adapt to manifest into a new, recurrent glioblastoma (Celiku, Gilbert and Lavi, 2019). Hence, recurrence rates in glioblastoma patients are very high at around 90% (Ostrom *et al.*, 2013).

Radiotherapy is used in combination with chemotherapy after surgery in routine glioblastoma treatment (Weller *et al.*, 2021). Data conclude that radiotherapy in combination with various chemotherapies can increase the chances of survival within one year by 19%, in comparison to chemotherapy alone (reviewed by Laperriere, Zuraw and Cairncross, 2002).

In addition to adjuvant TMZ, a relatively new therapy has been incorporated into the standard of care for the treatment of newly diagnosed glioblastoma in the European Union, China, Japan, and the United States of America. Tumour Treating Fields Therapy (TTFields) describes alternating electric fields of low intensity and intermediate frequency that supress tumour growth and spread through causing mitotic arrest, apoptosis, and impacting DNA repair, autophagy, cancer cell migration, membrane permeability, and immunological response processes. In a recent trial (NCT00916409), patients who had received initial surgery or biopsy and had concomitant radiochemotherapy followed by adjuvant TMZ were compared with those who received a combination of adjuvant TMZ and TTFields. Patients

who received TTFields show an average increase of 2.7 months in progression-free survival, and an increased overall survival of 4.9 months (Nishikawa *et al.*, 2023). Overall, TTFields show promise in the treatment of newly diagnosed glioblastoma.

However, TTFields therapy is expensive and currently only privately available in the United Kingdom. Advancements in surgery and radiotherapy do improve the survival of glioblastoma patients, but these improvements are modest and do not suggest that the future of glioblastoma treatment lies in these approaches. Similarly, TMZ resistance is unacceptably high and points to the need for new, more potent targeted therapies for glioblastoma.

1.2. CIZ1 regulates the cell cycle and epigenetic landscape

A novel $p21^{Cip1/Waf1}$-interacting protein was identified by Mitsui et al. (1999) in a modified yeast two hybrid screen. Cip1/Waf1 interacting zinc finger protein (CIZ1) was also concluded to bind the cyclin dependent kinase (CDK) 2 binding region of p21 and affect its localisation. CIZ1 was observed in various human and mouse cell lines. Structural analysis found it to contain polyglutamine repeats, a glutamine-rich region, three zinc finger motifs, and a matrin 3-homologous domain 3 (MH3). Later, CIZ1 expression was identified in many tissues, and it was found to recognise and bind specific DNA sequences (Warder and Keherly, 2003).

1.2.1. CIZ1 regulates the cell cycle

CIZ1 has several roles including epigenetic maintenance, X chromosome inactivation, and cell cycle regulation (Pauzaite *et al.*, 2016; Stewart *et al.*, 2019; Dobbs *et al.*, 2023). CIZ1 promotes the initiation of DNA replication and localises to minichromosome maintenance (MCM) complex and proliferating cell nuclear antigen (PCNA) – proteins both involved in replication licencing (Coverley, Marr and Ainscough, 2005). CIZ1 was identified to be present at the replication fork due to co-localisation with PCNA – a component of the replisome on the nuclear matrix (Ainscough *et al.*, 2007). Taken together with previous data that N-terminal sequences control DNA replication, these data suggested that CIZ1 links the nuclear

matrix to the replisome, through cell division cycle 6 (cdc6) binding (Copeland *et al.*, 2015). The functionality of this localisation revealed CIZ1 to control the recruitment of cyclin A/CDK2 to the replisome to promote initiation of DNA replication (Coverley, Laman and Laskey, 2002) by initially binding cyclin E, which is displaced by cyclin A (Copeland *et al.*, 2010). Recently, CIZ1 has been further implicated in cell cycle control showing a decreased G1 and cell cycle length post quiescence, in its absence (Tollitt *et al.*, 2024). This is associated with elevated cyclin E1, E2 and A2, and increased retinoblastoma (Rb) phosphorylation contributing to early restriction point bypass. Also, the CDK activity threshold required for initiation of DNA replication was increased in CIZ1-deficient cells relative to wild type cells, further indicating the role of CIZ1 in recruiting and modulating CDK activity to regulate the G1/S transition and the initiation of DNA replication. Importantly, this process is regulated by a negative feedback loop where cyclin A-CDK2 interacts with CIZ1, leading to initiation of DNA replication. Subsequently, cyclin A-CDK2 phosphorylates CIZ1, inactivating its DNA replication activity and providing an additional level of cell cycle control (Copeland *et al.*, 2015).

1.2.2. CIZ1 interaction partners

CIZ1 has many interaction partners and thus is implicated in many processes. Figure 1.3 shows the primary structure of CIZ1, overlayed with the regions that bind to each of its interaction partners.

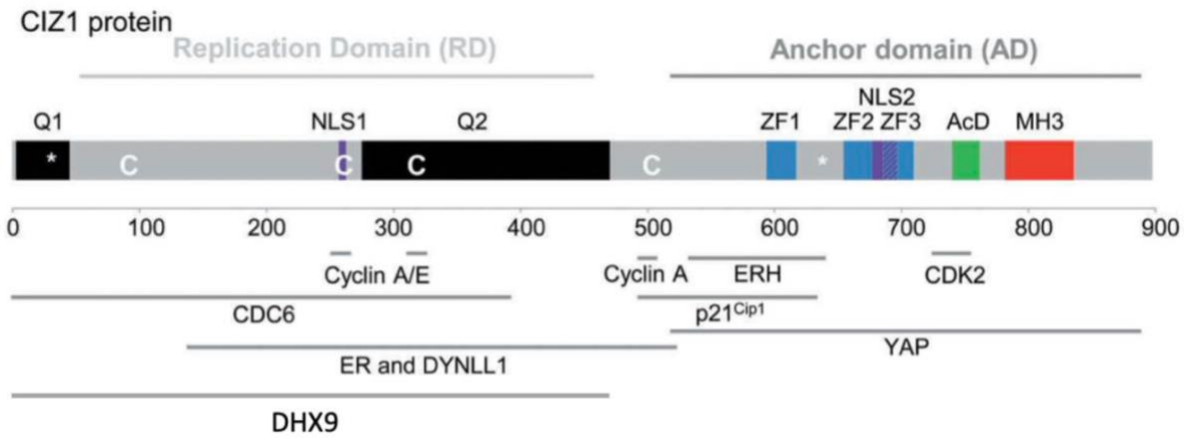

Figure 1. 3. The primary structure of CIZ1 overlayed by interacting molecules and the regions they bind adapted from Swarts et al. (2018) and Thacker at al. (2020). Four alternative exons (C) are displayed with protein domains including glutamine-rich regions

(Q), nuclear localisation signals (NLS), zinc finger domains (ZF), matrin-3 domains (MH3) and an acidic domain (AcD).

Enhancer of rudimentary homolog (ERH) is a highly conserved, small nuclear protein with an array of functions, some being species-specific (reviewed by Kozlowski, 2023). Since ERH was first characterised (Wojcik *et al.*, 1994), it has been implicated in nucleic acid metabolism, transcription of DNA damage and DNA metabolism genes, regulation of cell cycle genes, and heterochromatin formation, consistent with a role in maintaining genome integrity. Human CIZ1 binds ERH (Lukasik *et al.*, 2008) and forms a 2:2 heterotetramer (Wang *et al.*, 2023) at replication foci in HeLa cells (Lukasik et al., 2008; Banko *et al.*, 2013). This suggests CIZ1 promotes progression of the cell cycle through recruiting and localising ERH activity, as well as assisting in genome stability.

CIZ1 has also been identified as a binding partner of DHX9 (Thacker *et al.*, 2020). DHX9 is a DNA/RNA helicase and part of the DExH-box family of helicases, with roles in DNA replication, transcription, translation, genome stability, RNA processing (reviewed by Lee and Pelletier, 2016), and activation of DNA replication origins (Lee *et al.*, 2014). DHX9 has also been implicated in the resolution of R-loops, DNA-RNA hybrids that can promote DNA replication stress and genome instability (Yang *et al.*, 2024). This association further implicates CIZ1 as a recruitment factor/scaffold for other replication/genome stability factors.

In female mammals, the quantity of gene products from the X chromosomes is regulated through epigenetic silencing of one of the X chromosomes (Lyon, 1961). The X-inactivation centre (Xic) produces X inactive specific transcript (Xist), which is a long non-coding RNA that localises to the cis X chromosome and controls the process of its silencing (Brown *et al.*, 1991). CIZ1 was found to bind Xist (Ridings-Figueroa *et al.*, 2017) at the highly repetitive E motif within exon 7 of Xist (Sunwoo *et al.*, 2017) by both N and C-terminal domains of CIZ1 (Sofi *et al.*, 2022). This interaction is modulated by prion-like domains (PLD) 1 and 2 (Sofi *et al.*, 2022), and under (Ridings-Figueroa *et al.*, 2017; Sunwoo *et al.*, 2017) or overexpression (Sunwoo *et al.*, 2017) of CIZ1 leads to Xist mislocalisation. As well as silencing, replication of the inactive X chromosome (Xi) is dependent on CIZ1 as it moves from the nuclear periphery

towards the centre when replicating, in a CIZ1-dependent manner (Stewart *et al.*, 2019). Other work shows a further role of CIZ1 in epigenetics where it controls the epigenetic state of cells during quiescence (Dobbs *et al.*, 2023). These data link cell cycle regulation and epigenetic regulation, suggesting that CIZ1 contributes to genome acessability and genetic stability.

1.2.3. CIZ1 has a role in cancer

CIZ1 has been implicated in promoting tumourigenesis in breast cancer, Ewing sarcoma, pancreatic cancer, lung cancer, colorectal cancer, colon cancer, prostate carcinoma, gallbladder cancer, hepatocellular carcinoma, bladder cancer, and gastric cancer (den Hollander *et al.*, 2006; Rahman *et al.*, 2007; Thalappilly *et al.*, 2008; Rahman, Aziz and Coverley, 2010; Higgins *et al.*, 2012; Yin *et al.*, 2013; Nishibe *et al.*, 2013; Wang *et al.*, 2014; Liu *et al.*, 2015b; Zhang *et al.*, 2015; Wu *et al.*, 2016; Lei *et al.*, 2016; Coverley *et al.*, 2017; Zhou *et al.*, 2018; Swarts *et al.*, 2018; Chen *et al.*, 2019; Chen *et al.*, 2020; Li *et al.*, 2020; Wan *et al.*, 2023). CIZ1 has been found to promote tumourigenesis through either overexpression, underexpression, oncogenic transcription, or alternative splicing. Interestingly, CIZ1 can promote tumourigenesis at high levels and act as a tumour suppressor at normal levels. Deletion of CIZ1 promotes DNA replication stress (Dobbs *et al.*, 2023; Tollitt *et al.*, 2024; Nishibe *et al.*, 2013) and predisposes to lymphoproliferative disorders and leukaemia (Nishibe *et al.*, 2013).

1.2.3.1 Differential splicing

Studies have found differentially spliced CIZ1 variants in Ewing sarcoma (Rahman *et al.*, 2007; Rahman, Aziz and Coverley, 2010), lung cancer (Higgins *et al.*, 2012; Coverley *et al.*, 2017), colon cancer and breast cancer (Swarts *et al.*, 2018). Alternatively spliced CIZ1 variants are stable and specific to cancer, as opposed to normal tissue, in that they show promise as biomarkers for detection of early-stage cancers. Higgins *et al.* (2012) identified a splice variant of CIZ1 as a driver of tumourigenesis and its removal reduced tumour growth in xenograft models. This was the first demonstration that CIZ1, and specifically a splice

variant, was promoting tumour growth. There are also splice variants that have been reported as associated with tumours but not required for growth (Swarts *et al.*, 2018).

1.2.3.2 Oncogenic transcription

CIZ1 is a multifaceted regulator of DNA replication and transcription. The role of CIZ1 in transcriptional regulation is seen in X chromosome inactivation and in oncogenic transcription programmes. CIZ1 has been suggested to play a role in breast cancer through its interaction with ERH and the oestrogen receptor (ER). Oestrogen plays a role in mammary epithelial cell growth and breast cancer development. Oestrogen activates the nuclear proteins: ERα and ERβ, which in turn promote transcription through binding oestrogen-response elements (EREs) on gene promoters or indirectly through binding other transcription factors (Shiau *et al.*, 1998; Klein-Hitpass *et al.*, 1986). CIZ1 has been implicated in a positive feedback loop of oestrogen-dependent proliferation in breast cancer cells. The *CIZ1* gene has been found to contain EREs, allowing oestrogen-dependent expression in ER-positive cells. Increased CIZ1 expression increases the oestrogen sensitivity in mammary epithelial cells by interacting with and coactivating the ER, facilitating its recruitment to promoter regions on chromatin. Additionally, CIZ1 overexpression promotes a cancerous phenotype by increasing anchorage independence, growth rate, and tumourigenesis of breast cancer cells (den Hollander *et al.*, 2006). Dynein light chain 1 (DLC1 or DYNLL1) has also been found to regulate the ER pathway (Rayala *et al.*, 2005) and confer hypersensitivity to oestrogen (den Hollander and Kumar, 2006), although initially identified as a motor protein (Dick *et al.*, 1996). DLC1 promotes cell cycle progression in breast cancer cells by accelerating progression past the G1/S transition through binding and increasing the activity of CDK2. As DLC1 also binds CIZ1, an interesting model by den Hollander and Kumar (2006) proposed that DLC1 localises CIZ1 to the nucleus where it binds CDK2 and p21, however translocation of DLC1-CIZ1 to the cytoplasm sequesters p21 and allows DNA replication licencing. Finally, CIZ1's association with ERH at replication foci also implicate it in breast cancer. ERH overexpression in breast cancer tissue has been shown (Zafrakas *et al.*, 2008) and suggested to play a role in tumour progression. The localisation of ERH to replication foci by CIZ1 (Lukasik et al., 2008; Banko *et al.*, 2013) further implicate it in breast cancer.

The Hippo pathway has a fundamental role in organ development and regeneration. Yes-associated protein (YAP) and transcriptional activator with PDZ-binding motif (TAZ) form a complex with transcriptional enhancer associated domain (TEAD) transcription factors to act as effectors for the Hippo pathway. These complexes express or repress target gene expression through binding to gene enhancers, interacting with chromatin-remodelling complexes, and affecting the transcriptional activity of RNA polymerase II. The main groups of effected genes from this pathway include cell cycle, cell migration, and cell fate regulators. YAP/TAZ hyperactivation is well-documented in promoting cancer development (Moya and Halder, 2019). CIZ1 was identified as a binding partner of YAP (Wu *et al.*, 2016) where it interacts with its anchor domain (Lei *et al.*, 2016), as shown in Figure 1.3. CIZ1 was found to activate and increase the transcriptional activity of YAP, likely through enhancing the YAP-TEAD interaction in hepatocellular carcinoma (HCC). CIZ1 is highly expressed in HCC, which correlates with increased tumour growth, migration, and metastasis.

1.2.3.3 CIZ1 overexpression promotes tumour growth

CIZ1 overexpression has been identified in many cancer types and linked with a pro-cancerous phenotype. CIZ1 overexpression has been observed in seven different types of cancer (Table 1.1). Reduction through direct genetic approaches (e.g. siRNA) causes reductions in tumourigenesis, whereas further increasing CIZ1 causes further progression of the cancer. Table 1.1 shows cancers in which CIZ1 overexpression has been identified, the nature of the alteration to CIZ1, the intervention taken to reduce CIZ1, and the observed phenotypic effects.

Table 1. 1. CIZ1 overexpression promotes tumourigenesis in many types of cancer, adapted from Pauzaite et al. (2016). Studies of cancer types where CIZ1 is overexpressed were investigated and the mode of intervention to reduce CIZ1 noted, with the results of these interventions. Abbreviations: small interfering RNA, siRNA; short hairpin RNA, shRNA; micro RNA, miRNA.

Cancer	Cancer-specific CIZ1 alteration	Mode of intervention	Result of intervention	Source
Colorectal carcinoma	Overexpression	siRNA	Reduced proliferation, and colony formation *in vitro*.	(Yin *et al.*, 2013)
Gall bladder carcinoma	Overexpression	siRNA	Reduced xenograft tumour growth. Reduced tumour migration *in vivo*.	(Zhang *et al.*, 2015)
Prostate cancer	Overexpression	siRNA	Reduced tumourigenesis in xenograft models, reduced proliferation, G1 checkpoint activation.	(Liu *et al.*, 2015b)
Breast cancer	Overexpression	siRNA	Reduced tumourigenesis, proliferation, and anchorage independence.	(den Hollander and Kumar, 2006; den Hollander et al., 2006)
Breast cancer	Overexpression of CIZ1 increases oestrogen sensitivity	CIZ1 overexpression	Increased oestrogen sensitivity and increased tumour size in xenograft models.	(den Hollander *et al.*, 2006)
Hepatocellular carcinoma	Overexpression	CIZ1 overexpression	Increased proliferation and migration.	(Lei *et al.*, 2016; Wu et al., 2016)
		siRNA	Reduced growth, tumourigenesis, and metastasis.	
Bladder cancer	Overexpression	shRNA	Reduced proliferation, increased apoptosis.	(Chen *et al.*, 2019)
Gastric Cancer	Overexpression	miRNA	Reduced proliferation, migration, invasiveness, and increased apoptosis.	(Wan *et al.*, 2023)

1.2.3.4 CIZ1 is overexpressed and mislocalised in glioblastoma

Multiple primary patient-derived glioblastoma tissue samples have shown an increase in CIZ1 expression within the tumour compared to outside the tumour margins (Falkingham, 2021). Taken together with data from other cancers in Table 1.1, this implies that targeting CIZ1 for reduction when overexpressed in glioblastoma may bring about a reduction in cancerous phenotypes. Furthermore, Figure 1.4 C shows that glioblastoma patients with a higher CIZ1 mRNA expression have a poorer prognosis, potentially suggesting CIZ1 is driving cancer progression and presents as an attractive target. In addition to this, a high CIZ1 expression in brain biopsies may indicate the presence of a glioblastoma and could be used as an early detection biomarker, similarly to alternatively spliced CIZ1 variants discussed in Section 1.2.3.1. Figure 1.4 shows CIZ1 overexpression has been observed in glioblastoma and this is linked to poorer patient survival.

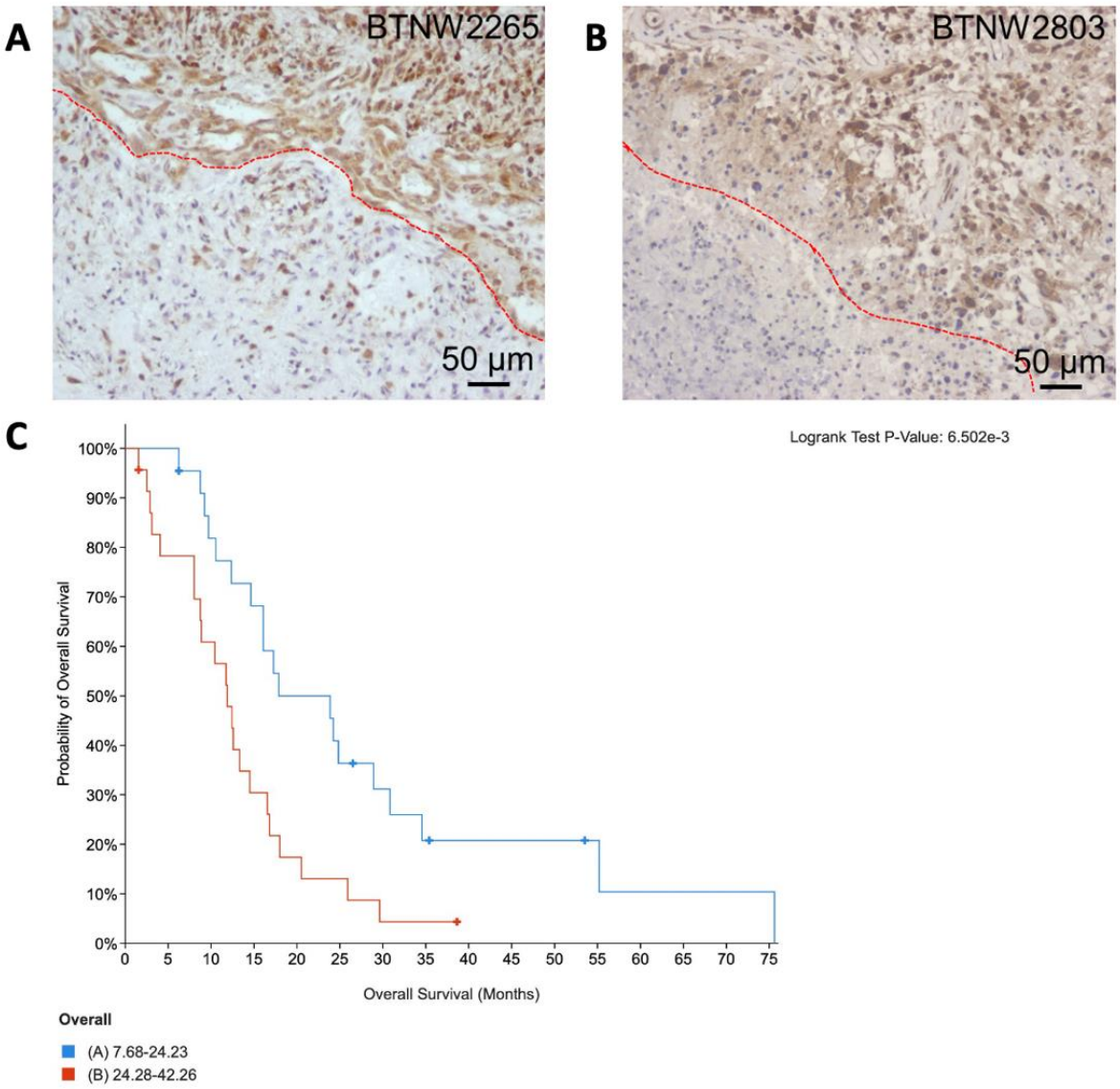

Figure 1. 4. CIZ1 is overexpressed in glioblastoma and associated with poorer patient survival. A, B) Formalin-Fixed Paraffin-Embedded (FFPE) glioblastoma tissue samples labelled with haematoxylin, eosin and immunopurified anti-CIZ1 antibody show higher CIZ1 expression inside the tumour (Falkingham, 2021). Tumour margins are shown by the red line. **C)** Kaplan-Meier plot showing median overall survival for Glioblastoma (Brennan et al., 2013), where n=520, showing significantly (p=0.0413) lower survival for high CIZ1 copy-number 12.60 (95 % CI 11.10 - 13.90) and 15.30 (95 % CI 14.20 - 16.90) months respectively. CI, confidence interval.

These data suggest that CIZ1 is overexpressed in glioblastoma. Other works have demonstrated that reducing CIZ1 levels has resulted in reduced tumour growth, suggesting that it may be a viable drug target. Reduction of CIZ1 levels in glioblastoma may result in anticancer effects, such as those observed in other cancers in Table 1.1.

1.3. CIZ1 is controlled by opposing CDK and UPS activity

Through assaying mouse embryonic fibroblasts with CDK inhibitors and assessing CIZ1 phosphorylation and stability, it has been shown that CDK2 activity correlates to CIZ1 phosphorylation and accumulation prior to the initiation of DNA replication (Pauzaite, 2019). CDK2 and DBF4-dependent kinase (DDK; also known as cell division cycle 7 – cdc7) activity also stabilises CIZ1 post-restriction point in late G1 phase whereas CDK4/6 inhibition has little effect, likely due to the limited activity of these kinases at this point in the cell cycle. Pauzaite (2019) proposes a model describing how CIZ1 levels are controlled throughout the cell cycle (Figure 1.5). Cyclin A/CDK2 activity and CIZ1 phosphorylation closely followed the abundance of CIZ1, suggesting that CDK2 phosphorylation of CIZ1 stabilises it allowing for more efficient S phase entry. On CDK inhibition, the ubiquitin proteosome system (UPS) degraded CIZ1 whilst UPS inhibition recovered CIZ1 levels.

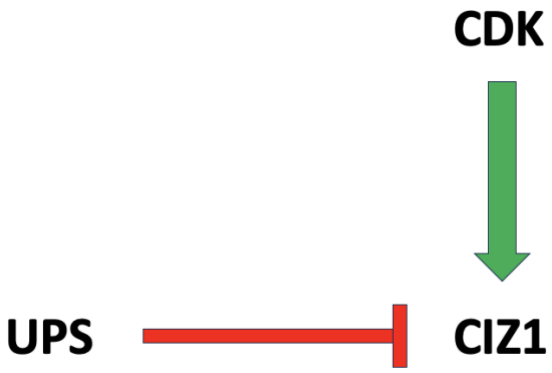

Figure 1. 5. CIZ1 protein levels are controlled by opposing CDK and UPS activities. CDK2-mediated phosphorylation of CIZ1 positively correlates to its expression levels during late G1 phase. In the absence of CDK activity the UPS degrades CIZ1, which can be recovered through UPS inhibition.

This model suggests that CIZ1 levels could be reduced in glioblastoma through CDK inhibition, bringing about anticancer effects such as those in Table 1.1. A panel of six CDK inhibitors were selected to assay on glioblastoma cell lines *in vitro*. The selected inhibitors included: milciclib, abemaciclib, dinaciclib, palbociclib, CVT-313, and PHA-767491.

1.4. CDK inhibitors in cancer therapy

CDKs control progression of the cell cycle, making CDK inhibitors attractive molecules to use in cancer therapy. Small molecule kinase inhibitors have been the focus of treating a range of cancers in many clinical trials, where they have showed promise. Palbociclib, ribociclib, and abemaciclib are small molecules that target CDK4/6 and were FDA approved for clinical use in 2015, 2017, and 2018, respectively. Additionally, there are more CDK inhibitors that show efficacy in cancer, and specifically glioblastoma, therapy.

1.4.1. CDK4/6 inhibitors

Abemaciclib (LY2835219) is a licenced drug for the treatment of hormone receptor positive (HR+) and human epidermal growth factor receptor negative (HER2-) breast cancer (Goetz *et al.*, 2017). It is a CDK4/6 inhibitor with IC_{50} values of 2 nM and 10 nM, respectively in cell-free assays (Gelbert *et al.*, 2014). Abemaciclib has also be clinically trialled for other cancers including: melanoma, lymphoma, neoplasm, solid tumour, and glioblastoma (reviewed by Wander *et al.*, 2022) and is permeable to the blood-brain barrier (BBB; Raub *et al.*, 2015).

One phase I study has completed in 2023 investigating the use of abemaciclib in diffuse intrinsic pontine glioma (DIPG), however results have not yet been published (NCT02644460). Abemaciclib was taken in varying doses, twice daily, for a cycle of 28 days and a maximum treatment duration of two years, with or without radiotherapy. Another trial in progress is investigating the use of abemaciclib with LY3214996 (an extracellular-regulated kinase (ERK) pathway inhibitor – *Bhagwat et al., 2020*) in glioblastoma (NCT04391595). Abemaciclib is also being tested in combination with TMZ, compared to TMZ alone in glioma (NCT06413706); and abemaciclib localisation in glioma is being investigated using intratumoural microdialysis (NCT05413304). A phase I dose escalation trial saw three glioblastoma patients reach stable disease, with two continuing to receive 19 and 23 abemaciclib cycles (Patnaik *et al.*, 2016). Abemaciclib is also being investigated in two further stage I (NCT04074785) and II (NCT02981940) clinical trials.

Palbociclib (PD-0332991) is a licenced breast cancer drug for oestrogen receptor positive (ER+) and HER2- types (Turner *et al.*, 2015). Like abemaciclib, it is a CDK4/6 inhibitor with respective IC_{50} values of 11 nM and 16 nM in cell-free assays (Fry *et al.*, 2004).

Palbociclib can pass the BBB (Raub *et al.*, 2015), so was trialled in a phase II study in treating patients with recurrent Rb positive glioblastoma (NCT01227434). However, this study was terminated early due to insufficient efficacy as 95% of patients progressed within six months (Taylor *et al.*, 2018). Despite this, it was included in a phase I/II study (NCT03158389) using targeted compounds to treat unmethylated MGMT promoter (TMZ resistant) glioblastoma. Palbociclib was orally administered at 75/100/125 mg on 21 days of a 28-day cycle, followed by 4 weeks break and ultimately as maintenance. These results are not yet available. Another ongoing early phase I trial (NCT05432518) aims to assess the efficacy of a daily dose of 125 mg palbociclib in patients with CDK4 and CDK6 amplification in their glioblastoma.

1.4.2. CDK2 inhibitors

Milciclib (PHA-848125) is a phase II CDK2 (IC_{50} of 45 nM) and tropomyosin receptor kinase A (TRKA, IC_{50} of 53 nM) inhibitor, with inhibitory effects towards CDK1, 4, 5 and 7, also (Brasca *et al.*, 2009). TRKA is a receptor for nerve growth factor (NGF) and plays a role in the development of cancer (reviewed by Fan *et al.*, 2024). Phase II clinical trials have explored the use of milciclib in the treatment of metastatic HCC, malignant thymoma, thymic carcinoma, recurrent malignant glioma, and malignant pleural mesothelioma. The most recent trial, in 2017, assessed 31 patients with unresectable, metastatic HCC that were not taking sorafenib. After 3 months, 45% of patients were still alive and 19.4% were alive after 6 months. The average time to progression (TTP) was 5.9 months (2017-000144-18).

Computational modelling has suggested milciclib is able to cross the BBB (Khanam *et al.*, 2022), thus it has been trialled in the treatment of malignant glioma in a phase I/II study. Milciclib was orally administered for 14 consecutive days every three weeks and this trail was completed in 2012 (2006-003193-10), however the results are not available. Furthermore, one study observed increased apoptosis in medulloblastoma cells from

milciclib treatment, in combination with bromodomain and extraterminal (BET) inhibition (Bolin *et al.*, 2018), suggesting milciclib may show efficacy in treating glioblastoma.

CVT-313 is a CDK2 inhibitor with an IC_{50} value of 0.5 µM *in vitro* (Brooks *et al.*, 1997), which has also been identified as an inhibitor of phosphodiesterase (PDE) 4 and 5 (Liu *et al.*, 2023). CVT-313 has not been investigated in clinical trials, but laboratory studies have demonstrated its anticancer effects in an array of diseases including ovarian cancer (Pan *et al.*, 2023), HCC (Yang *et al.*, 2021), breast cancer (Okur and Yerlikaya, 2019; Hwang *et al.*, 2012), diffuse large B-cell lymphoma (Faber and Chiles, 2007), colorectal cancer (Somarelli *et al.*, 2020), lung carcinoma (Talapati *et al.*, 2020), and HeLa cells (Hwang *et al.*, 2012). Interestingly, CVT-313 was identified as ineffective in prostate cancer models (Kanbur, Baykal and Yerlikaya, 2021). The effect of CVT-313 in glioblastoma has not yet been investigated.

1.4.3. CDK2 and DDK inhibitors

PHA-767491 HCl (NMS-1116354) is a cdc7 and CDK9 inhibitor with biochemical IC_{50} values of 10 and 34 nM, respectively. There is ~20-fold selectivity over CDK1/2 and glycogen synthase kinase 3 beta (GSK3-β); 50-fold selectivity over CDK5 and mitogen activated protein kinase-activated protein kinase 2 (MK2); and 100-fold selectivity over polo-like kinase 1 (PL1) and checkpoint kinase 2 (CH2; Montagnoli *et al.*, 2008). Recently, PHA-767491 has also showed CDK2 inhibitory effects (Pauzaite *et al.*, 2022). Like CVT-313, PHA-767491 has not yet been trialled clinically but has shown efficacy against colorectal and prostate cancer (Pauzaite *et al.*, 2022), HCC (Li *et al.*, 2015), multiple myeloma (Liu *et al.*, 2018a; Natoni *et al.*, 2013), chronic lymphocytic leukemia (Natoni *et al.*, 2011), and pancreatic adenocarcinoma (Huggett *et al.*, 2016). Dual cdc7 and CDK9 inhibition by PHA-767491 has also showed to resensitise triple negative breast cancer (TNBC) cells to EGFR-tyrosine kinase inhibitors (EGFR-TKIs) that have developed resistance. Synergistic effects of PHA-767491 and EGFR-TKIs resulted in reduced proliferation, increased apoptosis, G2/M arrest, and inhibited DNA replication in TNBC cells (McLaughlin *et al.*, 2019). PHA-767491 has also progressed to clinical trials for solid tumours (NCT01016327, NCT01092052).

In vitro, the use of PHA-767491 was tested for glioblastoma. Results showed reduced cell viability, reduced proliferation, increased apoptosis, and reduced migration and invasion (Erbayraktar *et al.*, 2016). Whilst PHA-767491 has poor BBB penetrance, a recent study has developed a nanoparticle capable of delivering it to the brain (Rojas-Prats *et al.*, 2021) meaning it may still be used to treat neurological diseases.

1.4.4. Pan-CDK inhibitors

Dinaciclib (SCH727965) is a pan-CDK inhibitor for CDK2, 5, 1, and 9 with IC_{50} values of 1, 1, 3 and 4 nM, respectively in cell-free assays. It also prevents thymidine DNA incorporation (Parry *et al.*, 2010). The BBB penetrance of dinaciclib has not yet been determined, however its permanent dipole (Figure 1.6) may make the molecule too polar to pass the membrane.

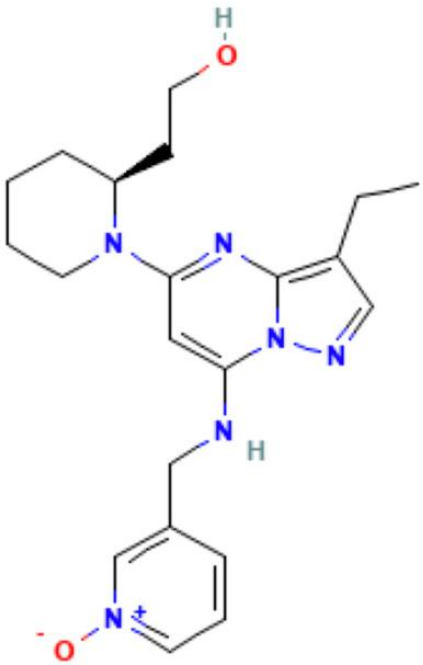

Figure 1. 6. The molecular structure of dinaciclib (NCBI, 2024). Dinaciclib is a pyrazolo[1,5-a]pyridine with antitumour activity through its CDK inhibitory effects.

Clinical trials testing the efficacy and safety of dinaciclib in relapsed/refractory (rr) multiple myeloma, rr chronic lymphocytic leukemia, rr diffuse large B cell lymphoma, solid tumours, solid neoplasm, and others (NCBI, 2024). In 2017, dinaciclib was enrolled in phase III trial comparing it to ofatumumab (the only available treatment in this case) in patients with

refractory chronic lymphocytic leukemia (NCT01580228). Dinaciclib was shown to be well tolerated and proves to treat cancer as it increased overall survival by 4.5 months and progression-free survival by 7.8 months compared to ofatumumab (Ghia *et al.*, 2017). Dinaciclib has not yet been assessed clinically but shows promise in treating glioblastoma *in vitro* (Riess *et al.*, 2021; Xu *et al.*, 2022; Riess *et al.*, 2020; Jackson *et al.*, 2024; Riess *et al.*, 2022) and *in vivo* (Zhang *et al.*, 2019).

1.5. Aims

As shown, CIZ1 overexpression is linked to tumourigenesis in various cancers and reduction alleviates this phenotype. Similarly, CIZ1 overexpression is observed in primary patient-derived glioblastoma tissue samples and high CIZ1 mRNA expression correlates to poorer patient survival in patient cohorts. CDKs have been evidenced to stabilise CIZ1 levels and inhibition causes CIZ1 reduction in mouse embryonic fibroblasts. Given this, and the previous efficacy shown by CDK inhibitors in cancer therapy, this work aims to establish a link between the anticancer effects of a panel of six CDK inhibitors in glioblastoma tissue samples and their ability to reduce CIZ1 protein levels. This will be assessed through monitoring of proliferation, cell death, and cell cycle arrest, whilst data are compared to an immortalised cell line representative of normal glia. These objectives will be assessed as follows:

1. Measure the viability of patient-derived and immortalised 2D glioblastoma cultures in response to a 72-hour incubation with varying concentrations of CDK inhibitors and compare the IC_{50} values to those in normal glia.
2. Assay the effect of varying concentrations of CDK inhibitors on immortalised 3D glioblastoma spheroids following a one-week incubation.
    a. Measure the reduction of spheroid diameter in response to each CDK inhibitor and compare potency.
    b. Determine the extent of cell death using a live/dead stain in response to each CDK inhibitor and compare toxicity.
3. Monitor cell cycle phase hourly of 2D immortalised glioblastoma culture when treated with 10 µM, 5 µM CDK inhibitors or a vehicle control over a 16-hour incubation.
4. Western immunoblotting analysis of CIZ1 protein expression in 2D patient-derived and immortalised glioblastoma tissue samples, following 72-hour incubation with CDK inhibitors at 10 µM.

2. Materials and Methods

2.1 Tissue culture

SVG p12 and U-87 MG immortalised cell lines were purchased from the American Type Culture Collection (ATCC) and patient-derived BTNW914 cells were provided by the Brain Tumour North West (BTNW) tissue bank at Royal Preston Hospital, with full ethical approval. These stocks were generated from the biopsy of a human glioblastoma of a female 67-year-old, patient who had provided informed consent. Cells were stored in liquid nitrogen in the appropriate media (Table 2.1) with 10% (v/v) dimethylsulfoxide (DMSO; Sigma-Aldrich) and thawed in a 37°C water bath before culturing.

All cell lines were cultured on 15 cm petri dishes (Nunclon delta tissue culture coated, Thermo Scientific) using 30 mL of the appropriate base media (Table 2.1) supplemented with 10% (v/v) foetal calf serum (Gibco) and 1% (v/v) Penicillin-Streptomycin-Glutamine antibiotic solution (Gibco). Large petri dishes were used to maintain a larger number of stock cells compared with flasks. FUCCI and QuCCI U-87 MG cells were cultured using the same media as U-87 MG cells with additional 1 µg/mL puromycin (Gibco). Generally, confluence was maintained at 20-80% for all cell lines. Passaging was done by removing media, washing with 10 mL Dulbecco's phosphate-buffered saline (DPBS, Gibco), adding 10% (v/v) trypsin (5%, with EDTA), no phenol red (Gibco) diluted with DPBS, incubating at 37°C for 3 minutes to dissociate the cells, then removing some of the solution and adding fresh media. Incubation conditions were 37°C at 5% CO_2 with 100% humidity.

Table 2. 1. Media used for SVG p12, U-87 MG, and BTNW914 cell lines. Abbreviations: Dulbecco's Modified Eagle Medium (DMEM).

Cell line	Media	Manufacturer
SVG p12	DMEM, high glucose	Gibco
U-87 MG	DMEM, high glucose	Gibco
BTNW914	Ham's F-10 Nutrient Mix	Gibco

One of the effects of CDK inhibition in glioblastoma is thought to be cell cycle arrest; to further assess the mechanism of each of the panel of six CDK inhibitors, cell cycle

information is needed. The FUCCI(CA)2 construct (Sakaue-Sawano *et al.*, 2017) provides cell cycle information through expression of fluorescently labelled chromatin licencing and DNA replication factor 1/Cdc10-dependent transcript 1 (Cdt1) and Geminin cell cycle indicators.

Cdt1 mediates replication licensing and progression into S phase. It is inhibited by Geminin binding and ubiquitin-mediated proteolysis. After S phase and replication licencing, Geminin binds the middle domain of Cdt1 and the NTD is targeted for degradation by two E3 ligases: Cullin 4, damage-specific DNA binding protein 1 ($CUL4^{Ddb1}$) and Skp1-Cullin-1-F-box (SCF) Cullin-Ring E3 Ubiquitin Ligase complex containing Skp2 (SCF^{Skp2}). $CUL4^{Ddb1}$ recognises the PCNA interaction protein motif (PIP box) of Cdt1 only in S phase as $CUL4^{Ddb1}$ only targets proteins bound to PCNA. Cdt1 degradation by SCF^{Skp2} is dependent on cyclin A-dependent kinase phosphorylation of the cyclin binding sequence (Cy) motif within Cdt1. The Cdt1 inhibitor: Geminin is also degraded by an E3 ligase – anaphase-promoting complex, Hct1/srw1/fizzy-related cdc20 homologue 1 (APC^{Cdh1}). Throughout the cell cycle the activities of $CUL4^{Ddb1}$/SCF^{Skp2} and APC^{Cdh1} oscillate reciprocally, which affects the expression of Cdt1 and Geminin (Figure 2.1 A and B).

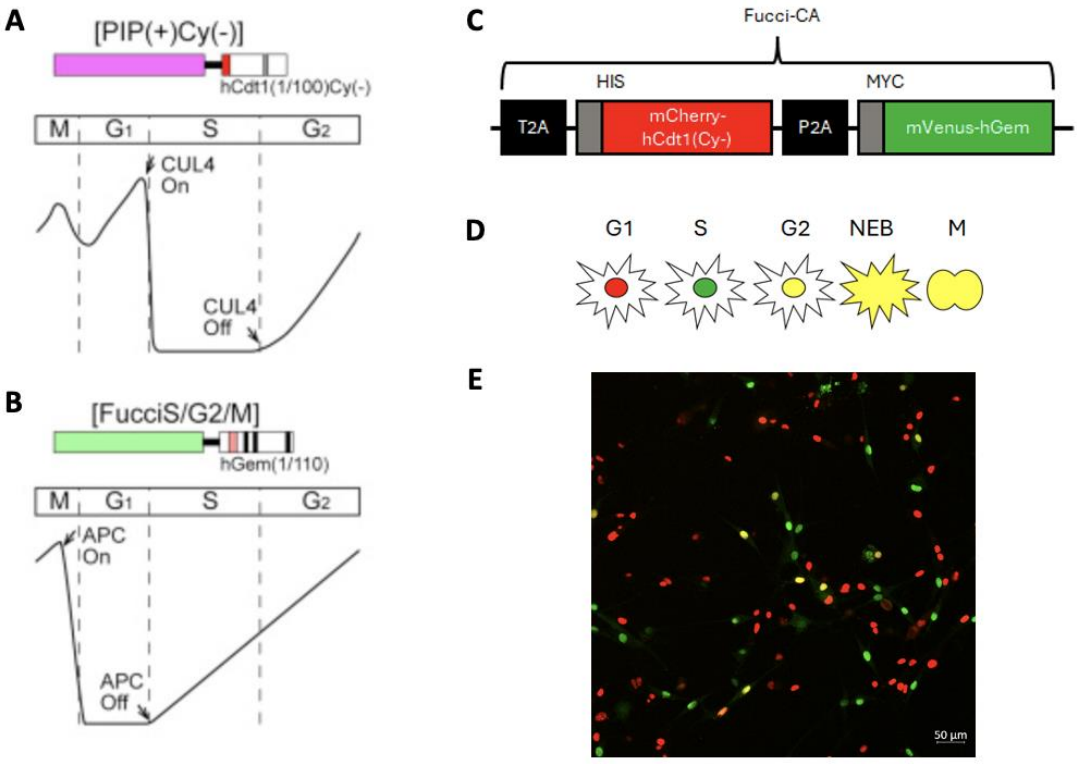

Figure 2. 1. The FUCCI(CA)2 construct allows U-87 MG cells to fluoresce differentially based on cell cycle phase. A, B) The reciprocal activity of CUL4 and APC result in reverse-mirrored expression of the hCdt1(1/100)Cy(–) and hGem(1/110) probes (Sakaue-Sawano et al., 2017). **C)** A cartoon of the FUCCI(CA)2 construct shows mCherry-hCdt1(1/100)Cy(–) and mVenus-hGem(1/110) probes downstream of T2A and P2A self-cleaving peptide linkers. **D)** A cartoon showing the fluorescence colour of cells at different stages of the cell cycle and **E)** a microscope image of FUCCI U87-MG cells treated with 5 µM palbociclib for 8 hours (Figure 3.12). Abbreviations: T2A, Thosea asigna virus 2A; P2A, porcine teschovirus-1 2A; NEB, nuclear envelope breakdown; M, mitosis.

The FUCCI(CA)2 construct (Figure 2.1 C) contains the (human) hCdt1(1/100)Cy(–) probe. This is not targeted by SCF^{Skp2} as it does not contain the Cy motif but is targeted by $CUL4^{Ddb1}$, resulting in a sharper reduction in S phase. This is combined with the hGem(1/110). Cdt1 and Geminin probes are conjugated to fluorescent mCherry and mVenus proteins, respectively to allow fluorescent detection when they are differentially expressed in cells. Conjugated probes are regulated under a ubiquitous promoter and self-cleaved through *Thosea asigna* virus 2A (T2A) and porcine teschovirus 2A (P2A) peptide linkers after being integrated into a cell's DNA, producing a 1:1 stoichiometry of each protein. $CUL4^{Ddb1}$ activity in S phase allows mCherry-hCdt1(1/100)Cy(–) levels to increase during G2/M/G1 phase (Figure 2.1 A) and cells to fluoresce red during G1 phase (Figure 2.1 D) when there is also

low green fluorescence. APC^{Cdh1} activity during G1 phase allows mVenus-hGem(1/110) levels to steadily build throughout S, G2, and M phase (Figure 2.1 B). This results in green fluorescent cells in S phase and yellow fluorescence around late G2 and M phase when red fluorescence is also high (Figure 2.1 D). During live cell imaging, the combination of red and green fluorescence is largely dominated by the mCherry signal, so cells appear yellow for only a short time.

2.2. Cell viability assay

The ability of CDK inhibitors to reduce the viability of glioblastoma cells is essential to assess their potential clinical use. Inhibitors must be potent in reducing the viability of glioblastoma to ensure a safe dose can be administered to patients. To be effective as a targeted therapy, inhibitors must also selectively reduce the viability of glioblastoma over normal glia – this is to ensure fewer side effects. Prestoblue™ was used here as a measure of cell viability. Prestoblue™ is a resazurin-based, cell permeable molecule; that is converted into a red fluorescent form by the reducing environment of a viable cell. The reducing power correlates to the number of viable cells within the sample, which in turn correlates to the fluorescence intensity produced by the Prestoblue™ reagent.

Cell viability assays were performed with BTNW914, U-87 MG, and SVG p12 cells using black, fluorescence-compatible 96-well plates (Nunclon delta tissue culture coated, Thermo Scientific). Each well was seeded with 2,000 cells per well using 100 µL of a cell dilution containing trypsinised cells, media, and DPBS. Cell number was determined using a haemocytometer for each experiment. Plates were incubated for 24 hours before treatment. CDK inhibitor stock solutions were 10 mM, dissolved in DMSO. 1 in 4 serial dilutions of CDK inhibitors (Selleckchem) were made and added (100 µL) to each well in triplicate (or sixfold – see results) to reach final volumes of 200 µL and final inhibitor concentrations of 100, 25, 6.25, 1.56, 0.391, 0.0975, and 0.0244 µM. The highest concentration of inhibitor was decided to be 100 µM and the lowest 24.4 nM as these resulted in plateaus at either end of the dose dependence curve, giving a sigmoidal shape in most cases. The appropriate media was added (100 µL) to the bottom row of wells as a control. Cells were cultured for 72 hours, which was the optimal time to identify differing

effects between concentrations and across inhibitors. One hour before reading, Prestoblue™ (10 µL, Invitrogen) was added to each well and mixed, then left to incubate. Plates were read on a Tecan infinite M200 PRO using the parameters in Table 2.2.

Table 2. 2. Tecan infinite M200 PRO parameters.

Parameter	Value
Excitation wavelength	560 nm
Emission wavelength	590 nm
Number of flashes	25
Settle time between flashes	0 ms
Gain	100
Integration lag time	0 µs
Integration time	20 µs

Fluorescence from control wells was averaged per plate and this was set as the 100% viable value. Fluorescence measurements from each sample well were then standardised with respect to this, a mean was taken for each inhibitor concentration, and values plotted using GraphPad. Graphs were plotted for each inhibitor, showing response curves for each cell line on each. GraphPad was also used to determine IC_{50} values. Dose dependence curves were fit using the 3-parameter fit in GraphPad for all cell lines and drugs tested. When a predicated IC_{50} value was not within the concentration range used, it was stated as above/below that of the highest/lowest concentration.

2.3. Spheroid assays

For U-87 MG spheroid experiments, 96-well ultra-low attachment plates (Corning) were seeded with 200 U-87 MG cells per well in 100 µL of media. Plates were incubated for 24 hours before treatment to allow spheroid formation. Subsequently, 1 in 4 serial dilutions of inhibitors were made and added (100 µL) to each well to reach final volumes of 200 µL and final inhibitor concentrations of 100, 25, 6.25, 1.56, 0.391, 0.0975, 0.0244, and 0.0061 µM. This concentration range allowed for a sigmoidal response in most cases. The appropriate media was added (100 µL) to six other wells as positive controls. Cells were cultured one week before analysis, which allowed sufficient time for the drugs to penetrate the spheroids and exert their effects, without completely destroying spheroids at every concentration. Cell

viability was determined using the live cell stain: calcein AM (1:2000) and the cell impermeant dead stain: ethidium homodimer (1:500) from the Viability/Cytotoxicity Assay Kit for Animal Live and Dead Cells (proteintech). After addition of live/dead stain, cells were incubated for 3 hours, 37°C, 5% CO_2. Wells were then imaged using the Leica Stellaris 5 Confocal Microscope at 10X magnification and x and y spheroid dimensions measured and recorded, averaging the measurements and plotting values using GraphPad prism and determining IC_{50} values for each drug.

For fluorescence microscopy imaging, lasers were set as according to the parameters in Table 2.3 and data for each fluorophore was collected sequentially. The brightfield image was taken at the same time as the calcein AM image, followed by that of ethidium homodimer. Images were taken on the microscope and processed using Photoshop.

Table 2. 3. Leica Stellaris 5 Confocal Microscope laser parameters to image U-87 MG spheroids stained with calcein AM and ethidium homodimer.

Fluorophore	Excitation Maxima	Emission Maxima	Laser wavelength used	Emission collection	Reference
Calcein AM	494 nm	517 nm	494 nm	510- 570 nm	Proteintech
Ethidium homodimer	528 nm	617 nm	528 nm	> 600 nm	Proteintech

2.4. FUCCI and QuCCI cell cycle live cell imaging

2.4.1. Bacterial transformation, amplification and plasmid purification

FUCCI(CA)2 (Sakaue-Sawano *et al.*, 2017) and QuCCI plasmids (both a gift from Dr. Richard Mort) and followed the addgene Bacterial Transformation protocol (Addgene, 2017) to amplify these plasmids for transfection into U-87 MG cells. Competent *E. coli* BL21 (DE3) were removed from storage (-80°C) and thawed on ice. FUCCI/QuCCI DNA was added (1 µL) to competent cells (50 µL), mixed, then incubated on ice for 30 minutes. Bacteria were heat shocked (42°C, 45 seconds) using a heat block then iced for 2 minutes. SOC media (800 µL; Fisher Scientific) was added to each tube, and both were incubated on a shaking incubator

(37°C, 200 rpm, 45 minutes). FUCCI (600 µL) and QuCCI (200 µL) transformed cells were transferred to four LB (Melford) agar plates each, spread evenly, and incubated overnight (37°C) along with a negative control plate of untransformed *E. coli*.

Five colonies (for each plasmid) were transferred into LB media (10 mL, with 100 mg/mL ampicillin – Gibco) and incubated in a shaking incubator (37°C, 200 rpm, > 12 hours). Plasmids were purified from samples using Protocol 5.1: 'Isolation of transfection-grade plasmid DNA in low throughput (REF 740490)' from the kit: 'Nucleospin Plasmid Transfection-grade, Mini kit for ultra-pure plasmid DNA' (Macherey-Nagel). DNA concentrations were then determined using a Nanodrop 2000 Spectrophotometer by pipetting elution buffer (2 µL) onto the apparatus to calibrate it, then adding each sample (2 µL). Absorbance values were recorded at 260 and 280 nm and purity determined by A260/280 of ~1.8-2.

2.4.2. Transfection

To transfect U-87 MG cells, Lonza's 'Cell Line Nucleofactor™ Kit T' protocol was used according to manufacturer's protocol. Five microlitres of each plasmid, and a piggyBac recombination plasmid (Yusa *et al.*, 2011), was added and transfected using programme X-001. A negative control plate was also established. After 48 hours, media containing puromycin (see Section 2.1) was added to both transfected plates and the negative control plate to select for successfully transfected cells. Media was changed on plates daily and photos of cells taken down the microscope eyepiece.

2.4.3. Fluorescence microscopy of fixed FUCCI/QuCCI U-87 MG cells

FUCCI/QuCCI U-87 MG cells were seeded into 24-well plates (Nunclon delta tissue culture coated, Thermo Scientific) with coverslips in the wells. Cells were seeded at 30% density in 2 mL of media. After 72 hours, media was removed from coverslips and washed 3 times with PBS (1 mL). Then, coverslips were incubated with 4% formaldehyde (Fisher Bioreagent) for 10 minutes and washed a further 3 times with DPBS, before mounting onto slides.

The Zeiss LSM 880 with Airyscan Confocal Microscope was used to take images at 40X magnification. Lasers were set up according to Table 2.4. The 458 nm Laser was turned off when imaging the FUCCI U-87 MG cells and data was collected sequentially.

Table 2. 4. Zeiss LSM 880 with Airyscan Confocal Microscope laser parameters used to image FUCCI and QuCCI U-87 MG cells.

Fluorophore	Excitation Maxima	Emission Maxima	Laser used	Emission collection	Reference
mVenus	515 nm	527 nm	514 nm	Optimised using Acquisition Wizard.	(FPbase, 2024c)
mCherry	587 nm	610 nm	594 nm	Optimised using Acquisition Wizard.	(FPbase, 2024b)
mCerulean	433 nm	475 nm	458 nm	Optimised using Acquisition Wizard.	(FPbase, 2024a)

2.4.4. FUCCI U-87 MG live cell imaging

FUCCI U-87 MG cells were seeded onto glass bottomed, black walled 24-well plates (CellVis) at 30-40% confluence, with a total volume of 2 mL, and incubated for 24 hours (37°C, 5% CO_2). Cells were then treated with CDK inhibitors (10 µM and 5 µM), a vehicle control (1% DMSO) or no treatment. These concentrations were on the upper end of the IC_{50} values identified for the inhibitors (Table 3.1), so were selected to ensure an effect was observed. The plate was set up on the Zeiss LSM 880 with Airyscan Confocal Microscope (37°C, 5% CO_2) and an automatically focused image of each well taken each hour over 16 hours. As the doubling time for U-87 MG cells is approximately 34 hours according to their product sheet (ATCC HTB-14, USA), it was thought that a 16-hour incubation should reveal characteristics of any cell cycle arrest, if this was indeed an effect. Lasers were set up according to Table 2.4, excluding the 458 nm laser as the mCerulean fluorophore is not present within the FUCCI(CA)2 system.

2.5. Quantitative analysis of CIZ1 protein levels

2.5.1. Protein Harvesting

U-87 MG and BTNW914 cells were seeded onto 6-well plates (Nunc) at 30-40% confluence, and incubated for 24 hours (37°C, 5% CO_2). Inhibitors were added (10 µM) to treatment wells, whilst DMSO (1%) was added as a vehicle control. Each well and mixed and plates were incubated for a further 72 hours. 72 hours has previously been reported by the lab as sufficient to identify changes in CIZ1 levels. Cells were harvested by removing media, then washing with 1X Tris-buffered saline (TBS; Sigma-Aldrich) and removing. 4X SDS-PAGE loading buffer (0.2 M Tris-HCl (Thermo Fisher), 0.4 M dithiothreitol (DTT; Melford), 8% (w/v) sodium dodecyl sulfate (SDS; Melford), 6 mM bromophenol blue (Sigma-Aldrich), 4.3 M glycerol (Fisher-Scientific)) was diluted 1:2 and DTT (100 mM) and phenylmethylsulfonyl fluoride (PMSF, 2 mM; Sigma-Aldrich) were added and heated to boiling point. 100 µL was added to each well and a cell scraper was used to harvest cells. Samples were heated to 95˚C (10 minutes) and stored at -20 ˚C until analysis. Samples were heated to 95 ˚C (10 minutes) prior to loading on a SDS-PAGE gel for western blotting.

2.5.2. SDS-PAGE

10% polyacrylamide gels were made using resolving gel (10% acrylamide (National Diagnostics), 325 mM Tris-HCl pH 8.8, 0.1% (w/v) SDS, 0.06 (w/v) APS (Sigma-Aldrich), 0.002% (w/v) TEMED (Thermo Scientific), Milli-Q water) and stacking gel (5% acrylamide, 125 mM Tris-HCl pH 6.8, 0.1% (w/v) SDS, 0.05% (w/v) APS, 0.0025% (w/v) TEMED, Milli-Q water).

Gels were placed into a gel tank (BioRad), which was filled with 1X Tris-glycine SDS gel running buffer – diluted from a 10X stock (Fisher Bioreagents) with Milli-Q water. Samples (10 µL) and PageRuler™ Prestained Protein Ladder (5 µL; Thermo Scientific) were loaded into gels and run (100 V for 15 minutes, then 200 V until completion).

2.5.3. Transfer of protein to PVDF membranes

Gels were removed and the wells and below the dye front removed before briefly soaking in transfer buffer (0.3 M Tris Base (Fisher Bioreagent), 10 mM CAPS (Sigma-Aldrich), 10% (v/v) ethanol (Fisher Bioreagent), 0.0002% (w/v) SDS). Blotting paper (Cytiva) was briefly soaked in transfer buffer and four pieces placed on a flat electrode. PVDF membrane (Cytiva) was briefly soaked in ethanol to hydrate and subsequently soaked in transfer buffer (5 minutes), then placed on top of the blotting paper. The gel was then placed and finally four more pieces of transfer buffer-saturated blotting paper placed on top of the gel. The top electrode was placed on top of the stack and run (90 minutes, 1 mA per cm^2 of paper area).

2.5.4. Western Blotting

Membranes were blocked with blocking buffer for 1 hour at room temperature (10 mL; 1X TBS, 1% (w/v) BSA (Fisher Bioreagents), 0.1% (v/v) Tween 20 (Sigma-Aldrich)) to prevent non-specific interactions, then buffer removed. Appropriate antibodies were used to detect actin and CIZ1 protein. An anti-ß-actin monoclonal antibody (Sigma-Aldrich, A1978) was diluted 1:10000 in blocking buffer and added to membranes, then an anti-CIZ1 antibody (Covalab; Copeland, 2015) was diluted 1:1000 and added. Membranes were incubated on a roller (4°C, > 12 hours). Primary antibodies were removed, and membranes were washed with 5 mL blocking buffer briefly, removed, then 3 further washes for 5 minutes. Horse radish peroxidase-conjugated secondary antibodies were added for actin monoclonal: anti-mouse (Abcam, AB6789), and CIZ1 polyclonal primary antibodies: anti-rabbit (Abcam, AB6721). These were diluted 1:5000 in blocking buffer and added to membranes on a roller for 1 hour at room temperature. Secondary antibodies were removed, and membranes washed with 5 mL wash buffer (1X TBS, 0.1% (v/v) Tween 20) briefly to remove excess antibody, removed, then three further washes for 5 minutes.

SuperSignal™ West Pico PLUS Chemiluminescent Substrate kit (Thermo Scientific) reagents were mixed and pipetted onto membranes (1 mL per membrane) before imaging using the iBright™ CL1500 Imaging System.

2.5.5. Protein quantitation

Analysis reports were downloaded from the iBright™ CL1500 Imaging System and intensities for actin and CIZ1 bands recorded. Standardised CIZ1 bands were calculated by dividing the CIZ1 signal by the actin signal of the same sample. Each standardised CIZ1 signal was then divided by its respective standardised CIZ1 signal from the vehicle control to obtain the signal as a percentage of the control (as some gels had multiple lanes with the same control, averages of the repeats were taken here and used). These values were calculated per repeat and plotted, for each CIZ1 band, individually using Excel and on the same bar chart using GraphPad prism. Statistical analysis was done on GraphPad prism using an ANOVA followed by a Dunnett's multiple comparison.

3. Results

3.1. CDK inhibitors reduce proliferation in glioblastoma cells

To assess the effect of CDK inhibition on the viability of glioblastoma cells, a primary patient-derived glioblastoma cell line (BTNW914) was compared with an established glioblastoma cell line (U-87 MG) and a representative normal glia cell line (SVG p12). Cells were seeded and treated with a dilution series of each CDK inhibitor for 72 hours. Cell viability was determined using Prestoblue™ and standardised according to vehicle controls (Figure 3.1).

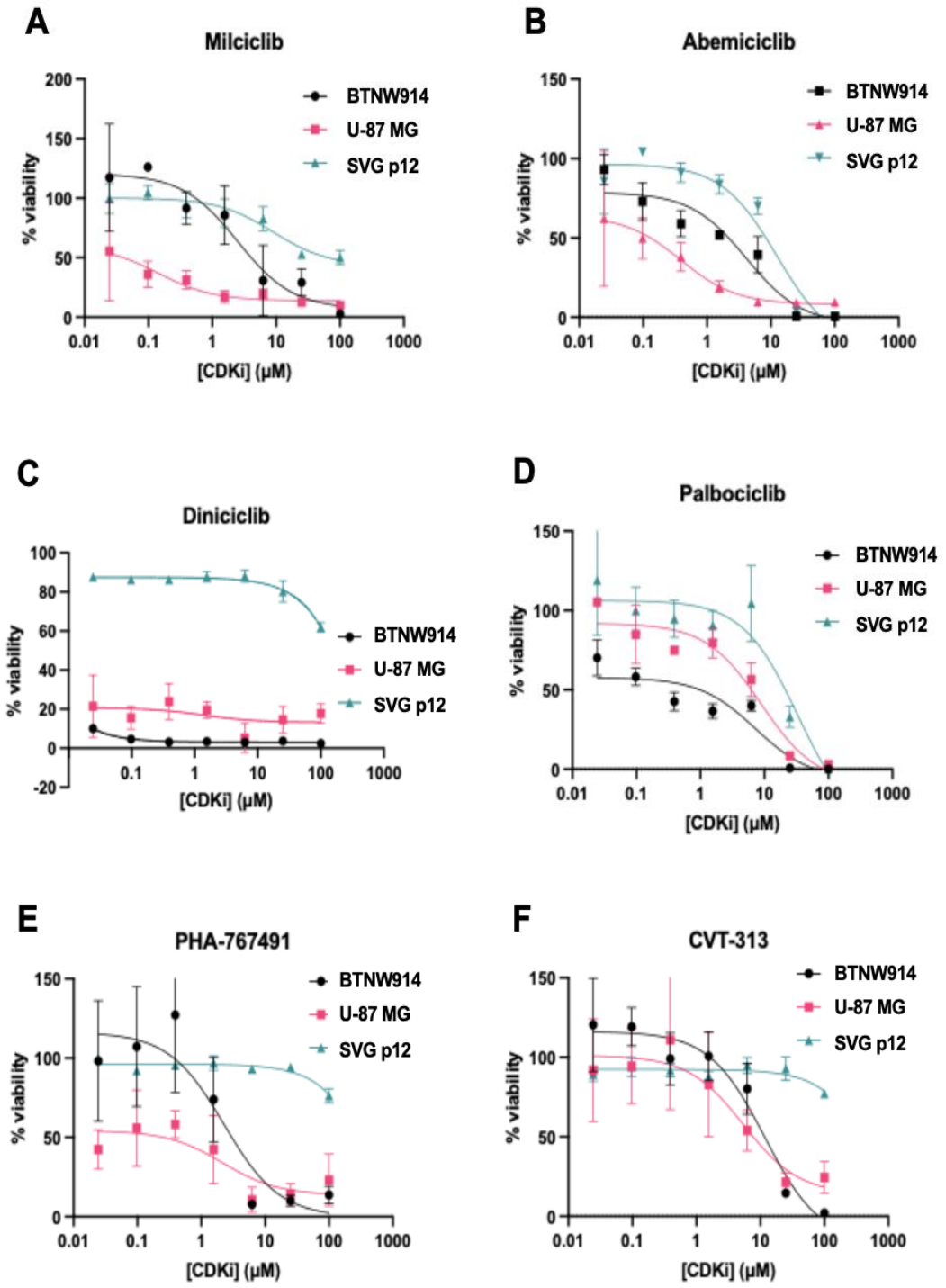

Figure 3. 1. CDK inhibition reduces glioblastoma cell viability and is selective for glioblastoma. Cell viability was determined for BTNW914, U-87 MG, and SVG p12 cell lines when treated with a dilution series of CDK inhibitors. Treatments were n=3, except for CVT-313 and PHA-767491 for BTNW914 and U-87 MG cells where n=6. Fluorescence values were standardised and plotted as percentage viabilities with respect to the averaged control fluorescence for each plate used. Data show mean ± standard deviation and were fit with a 3-parameter dose dependent curve using GraphPad.

IC_{50} values for each inhibitor and cell line were determined from the response curve using GraphPad (Table 3.1).

Table 3. 1. IC_{50} values of CDK inhibitors for BTNW914, U-87 MG and SVG p12 in 2D culture. IC_{50} values determined for each inhibitor from 2D viability assays using GraphPad. Values were stated as </> when the predicted value by GraphPad was outside of the concentration range used.

	Milciclib (µM)	Abemaciclib (µM)	Dinaciclib (µM)	Palbociclib (µM)	CVT-313 (µM)	PHA-767491 (µM)
BTNW914	2.495	4.126	< 0.0244	11.21	7.240	2.287
U-87 MG	< 0.0244	0.3884	< 0.0244	8.900	5.479	2.171
SVG p12	8.908	12.44	> 100	33.74	>100	>100

Milciclib showed potent antiproliferative effects in BTNW914 (2.495 µM) and U-87 MG (< 0.0244 µM) cells. U-87 MG cells were particularly sensitive with ~50% viability at the lowest concentration tested, preventing accurate determination of the IC_{50} value. The response of BTNW914 showed a sigmoid shape, allowing an accurate IC_{50} determination. This contrasts with the U-87 MG dose dependence curve that did not reach a concentration where it did not reduce viability and barely reaches 50% viability at the lowest concentration tested (Figure 3.1 A), suggesting that the concentration range used was too high to see a sigmoidal response and therefore accurately determine an IC_{50} value. Comparison with the normal glia cell line: SVG p12 shows a selective effect, with > 50% of cells viable at 100 µM, suggesting that there is an increased sensitivity in glioblastoma cells. U-87 MG are the most sensitive cell type to milciclib, and there is > 3.5-fold selectivity for BTNW914 over SVG p12. This selectivity may be higher as the concentration required to fully inhibit SVG p12 growth was not reached (Figure 3.1 A), and the use of higher concentrations is not possible due to limited solubility in DMSO.

The effect of the CDK4/6 inhibitor abemaciclib on cellular proliferation identified that U-87 MG is the most sensitive cell line (0.3884 µM) with ~10-fold higher potency than in BTNW914 (4.126 µM) and SVG p12 cells are the least sensitive to the CDK4/6 inhibitor (12.44 µM, Figure 3.1 B). The first licenced CDK4/6 inhibitor palbociclib shows similar responses but with higher IC_{50} values. It was the weakest inhibitor tested despite its broad clinical assessment in many cancer types (Zeverijn *et al.*, 2023). The IC_{50} values for

palbociclib (Figure 3.1 D) were 11.21 µM (BTNW914) and 8.9 µM (U-87 MG). However, palbociclib has over 3-fold selectivity for glioblastoma cells relative to normal glia where the IC_{50} value for SVG p12 was 33.74 µM.

Both PHA-767491 (Figure 3.1 E) and CVT-313 (Figure 3.1 F) show potent, anti-proliferative effects in glioblastoma cells. The IC_{50} values for PHA-767491 were similar in both BTNW914 (2.287 µM) and U-87 MG (2.171 µM). Despite this, the viability of U-87 MG cells only reaches ~50%, indicating that these cells are more sensitive to PHA-767491 than BTNW914. A broader titration of concentrations may identify a more accurate IC_{50} value, but this was not performed. Similarly, CVT-313 treatment results in similar responses in BTNW914 (7.240 µM) and U-87 MG (5.479 µM). For both PHA-767491 and CVT-313 there are marked differences in the response of normal glia. SVG p12 show little sensitivity to either inhibitor, suggesting that the IC_{50} values are greater than 100 µM. Collectively the data suggest that glioblastoma cells display > 40-fold greater sensitivity to PHA-767491 and 14-fold sensitivity to CVT-313.

Dinaciclib (Figure 3.1 C) is the most potent inhibitor tested here and the IC_{50} values could not be calculated for any glioblastoma cell line when treated with 100 – 0.0244 µM. BTNW914 and U-87 MG cells showed less than 25% viability for all concentrations, highlighting the sensitivity of these cells to dinaciclib. This contrasts with SVG p12 cells as these were very resistant to its activity and only show reductions in viability at 25 and 100 µM (Figure 3.1C). Much higher concentrations would be needed to determine an accurate IC_{50} value, but at these concentrations the levels of DMSO would confound results. These data suggest that dinaciclib is the most potent drug towards glioblastoma (BTNW914 and U-87 MG) and the least towards normal glia (SVG p12) making it the most selective for cancer with a fold selectivity that cannot be calculated (due to indeterminable IC_{50} values) but is at least 4000-fold.

The effects of CDK inhibition in the glioblastoma cells used here can be summarised into two groups. In the first group milciclib, abemaciclib, and palbociclib show effective inhibition of proliferation in U-87 MG cells and a slightly weaker effect on the primary glioblastoma cell line: BTNW914 (Table 3.1). In each case there is also a further reduction in potency against

the normal glial cell line: SVG p12. For milciclib, abemaciclib, and palbociclib there is an approximate 3-fold higher IC_{50} concentration for normal glia relative to the glioblastoma cell lines, suggesting a weak selectivity for each inhibitor. The second group containing PHA-767491, CVT-313, and dinaciclib show potent anti-proliferative effects in glioblastoma cells and weak effects on normal glia *in vitro*. These data suggest that CDK inhibition may be a potent, selective, and therefore potentially effective approach to prevent proliferation in glioblastoma and further analysis of their mechanism of action is required.

3.2. CDK inhibition reduces glioblastoma spheroid size

Pre-clinical drug testing aims to screen inhibitors for potency. Monolayer (2D) tissue culture-based assays are convenient and still useful in predicting the response of cancer cells to treatments. However, 3D glioblastoma models more accurately mimic the cell-cell and cell-environment interactions that take place within a tumour and contain dividing, quiescent, and necrotic cells, consistent with the layers of cells considered to be present within an active tumour (reviewed by Manikandan and Jaiswal, 2023).

To further assess the potential of CDK inhibition in more representative *in vitro* models, U-87 MG spheroids were produced on ultra-low attachment plates 24 hours before inhibitor treatment. This allows for efficient spheroid formation before the addition of CDK inhibitor. A range of inhibitor concentrations were added to spheroids (1 in 4 dilutions of 100 – 0.0061 µM) for each inhibitor and spheroids were incubated for one week without further addition of drug. Spheroids were then imaged, diameter measured, and plot against drug concentration (Figure 3.2).

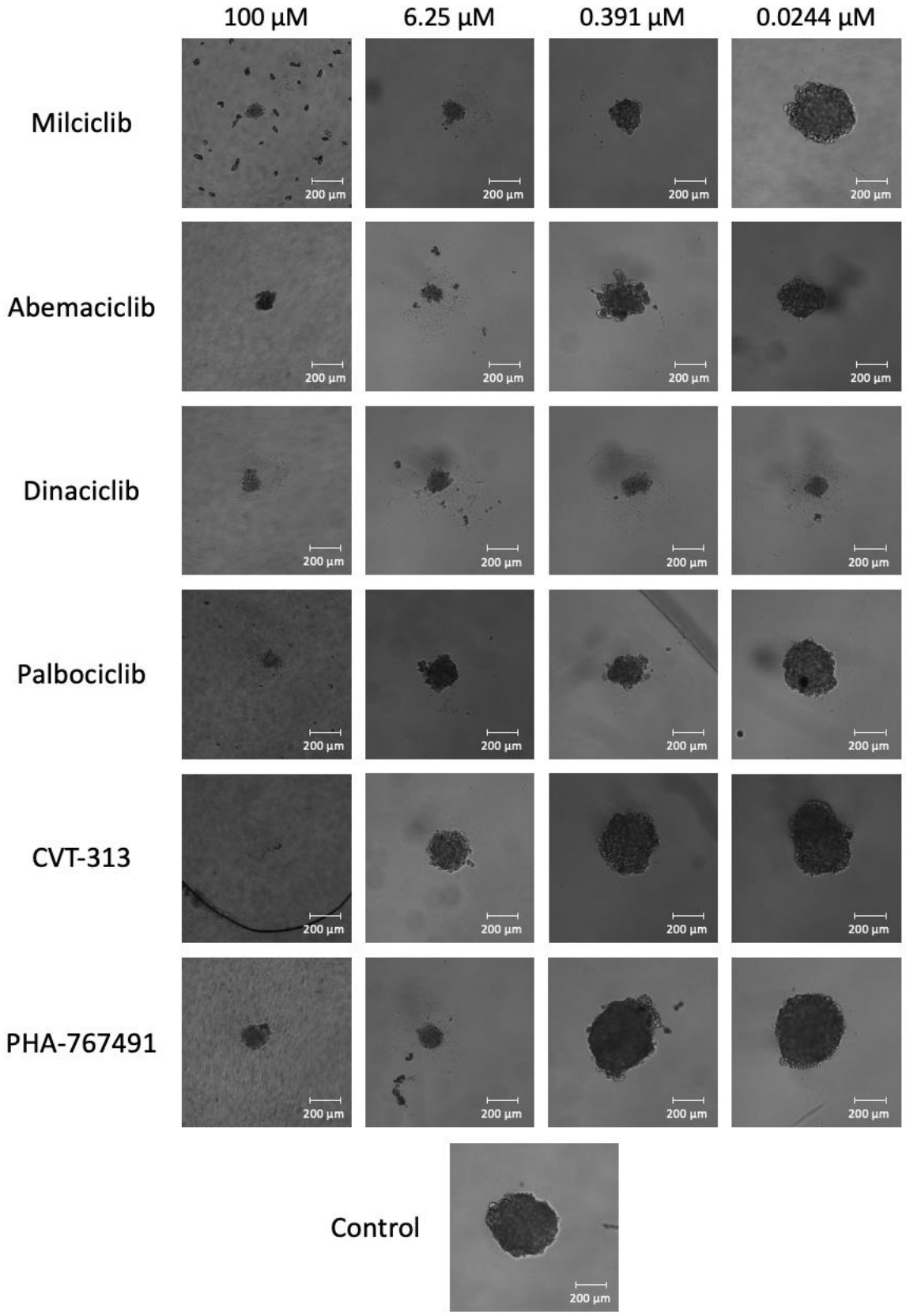

Figure 3. 2. CDK inhibition causes reduction in U-87 MG spheroid size. Representative images of CDK inhibitor-treated spheroids at 100, 6.25, 0.391, and 0.0244 µM. A control spheroid is shown where no CDK inhibitor was added. U-87 MG cells were seeded 24 hours

before treatment and spheroids were incubated for one week before image acquisition at 10X magnification using the Leica Stellaris 5 Confocal Microscope.

For each inhibitor, spheroid size decreased with increasing CDK inhibitor concentration. X and y dimensions were measured and averaged for each spheroid. The spheroid size was plotted against drug concentration and fit with a 3-parameter dose dependence equation using GraphPad (Figure 3.3).

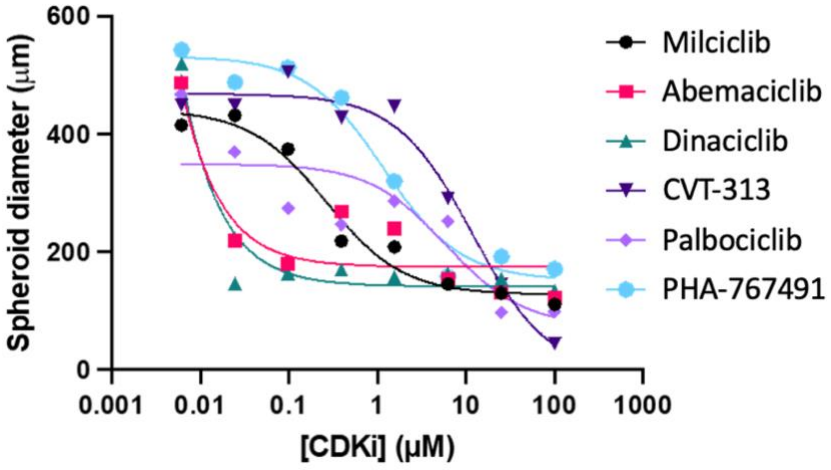

Figure 3. 3. CDK inhibition reduces U-87 MG spheroid size. U-87 MG cells were seeded 24 hours prior to seven-day incubation with CDK inhibitors (100 – 0.0061 µM). Spheroids were imaged at 10X magnification where x and y dimensions were measured. Dimensions were averaged for each spheroid and means were plotted using a 3-parameter dose dependence curve in GraphPad.

Using these measurements, IC_{50} values were determined by fitting a 3-parameter dose dependence curve in GraphPad (Table 3.2).

Table 3. 2. IC_{50} values of CDK inhibitors on U-87 MG 3D spheroids. IC_{50} values were determined from spheroid dimensions using GraphPad.

	Milciclib (µM)	Abemaciclib (µM)	Dinaciclib (µM)	Palbociclib (µM)	CVT-313 (µM)	PHA-767491 (µM)
U-87 MG	0.2651	< 0.0244	< 0.0244	5.934	11.93	1.168

Evaluation of the effect of CDK inhibition in 3D spheroids showed that all were effective at reducing spheroid size. However, there were a range of effects. The most potent inhibitors tested were the CDK4/6 inhibitor abemaciclib and the pan-CDK inhibitor dinaciclib. Both

show similar trends where a steep reduction in spheroid size between 0.0244 and 0.0975 µM is followed by spheroids all of a similar size as concentrations increase. At 0.0244 µM, the abemaciclib-treated spheroid was similar in size to the control spheroids at around 400 µm in diameter, whereas the dinaciclib-treated spheroid was just 100 µm. To accurately determine the IC_{50} value, more than one data point should be close to 0 and 100% viability to detect the upper and lower limits of the sigmoidal relationship. Due to limitations in the concentrations used, the IC_{50} value was not determined for the most potent CDK inhibitors in 3D culture abemaciclib or dinaciclib, but the IC_{50} value would be in the low nanomolar range. Similarly, milciclib was found to have a nanomolar IC_{50} value at 265.1 nM in 3D models.

PHA-767491 was a potent inhibitor with an IC_{50} estimated at 1.168 µM. The full response curve can be seen within the concentration range used with upper and low plateaus both visible. 100 µM PHA-767491 treatment was slightly less effective in reducing spheroid size (with averaged x and y dimensions at 170.85 µm), however it still proves to be a potent inhibitor.

The data collected for palbociclib did not fit with the 3-parameter sigmoid-shaped curve that the software has attempted to fit. Palbociclib treatments have caused the spheroid sizes to plateau around the median concentrations used, with another plateau at high concentrations (Figure 3.3). This shaped response curve potentially indicates a more complex effect, perhaps indicating that palbociclib is targeting different kinases at different concentrations leading to a non-sigmoid relationship; therefore, the prediction of 5.934 µM as the IC_{50} is potentially inaccurate.

The CDK2 inhibitor CVT-313 is the least potent inhibitor on 3D U-87 MG spheroids with an estimated IC_{50} of 11.93 µM. The upper plateau and middle of the sigmoid shape is visible within the concentration range. The curve appears to plateau at 100 µM, but higher concentrations would allow for a more accurate IC_{50} calculation. For inhibitors above this value, there are issues with drug solubility and the toxic effect of DMSO that can become apparent at higher levels.

To summarise, milciclib (TRKA and CDK2, 1, 4, 5, 7 inhibitor), abemaciclib (CDK4/6 inhibitor), and dinaciclib (CDK1, 2, 5, 9 inhibitor) were the most potent inhibitors in 3D with nanomolar IC_{50} values. Data show that CDK inhibitors are effective in reducing glioblastoma spheroid size *in vitro*.

3.3. CDK inhibition promotes cell death in 3D spheroids

Data presented in Figure 3.3 and Table 3.2 indicate that CDK inhibition can reduce spheroid size. This supports data from 2D culture that CDK inhibition can reduce proliferation. However, these data do not distinguish between cytostatic effects such as cell cycle arrest, that could prevent growth without inducing cell death, or whether CDK inhibitors can promote cell death *in vitro*. To determine if CDK inhibition promotes cell death, a live/dead stain was used. Calcein AM is a cell-permeable viability stain that passes across the membranes of live cells and is metabolised into a charged, fluorescent molecule that is membrane-impermeable. This was co-incubated with ethidium homodimer I, which is cell-impermeable and can only pass through the leaky membranes of dead or apoptotic cells where it intercalates with double stranded DNA and fluoresces. Calcein AM and ethidium homodimer were used to determine if CDK inhibitors induced cell death through labelling of live, viable cells and dead cells (Figure 3.4).

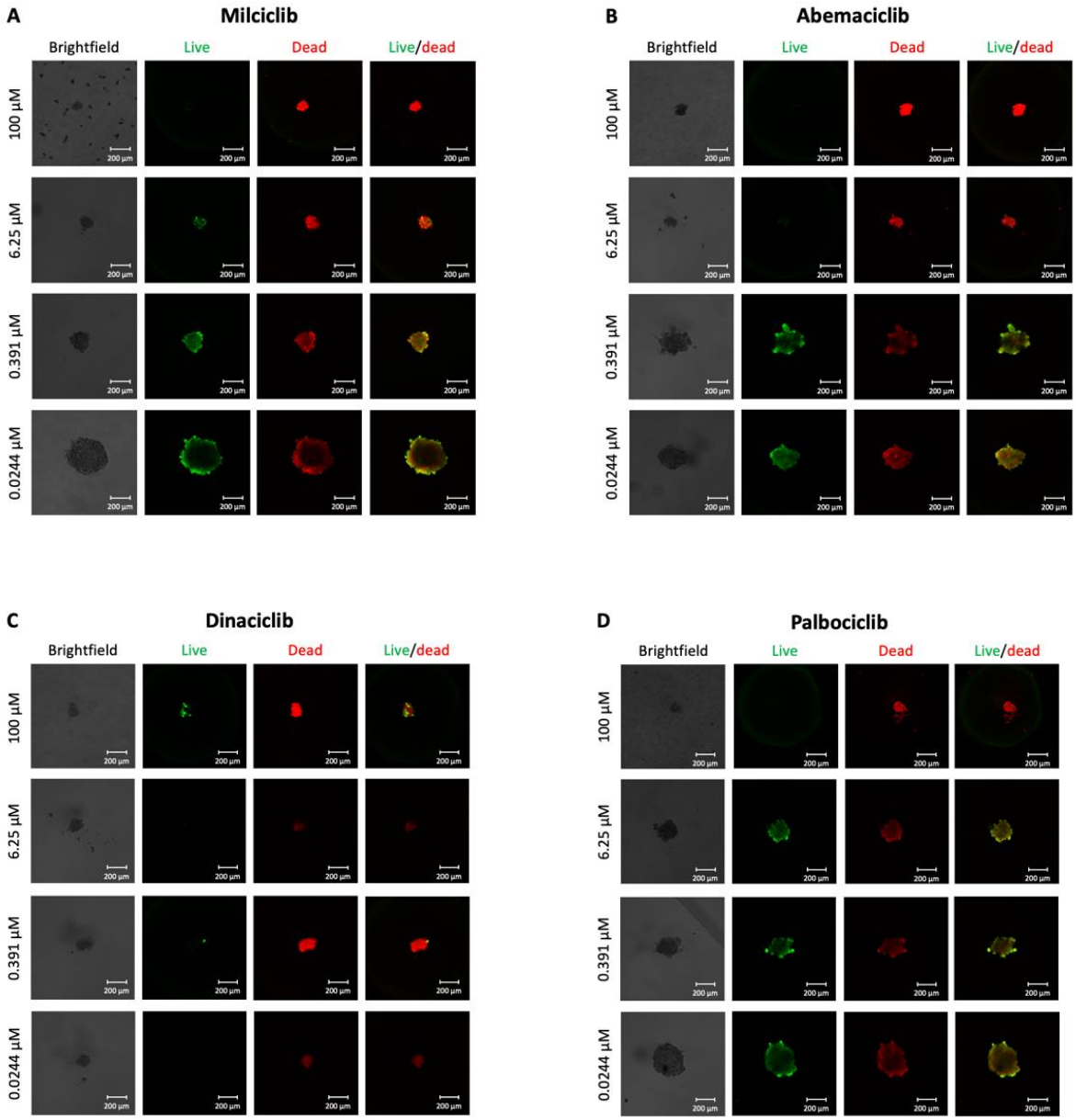
A
Milciclib
Brightfield
Live
Dead
Live/dead
100 µM
6.25 µM
0.391 µM
0.0244 µM
B
Abemaciclib
C
Dinaciclib
D
Palbociclib
200 µm

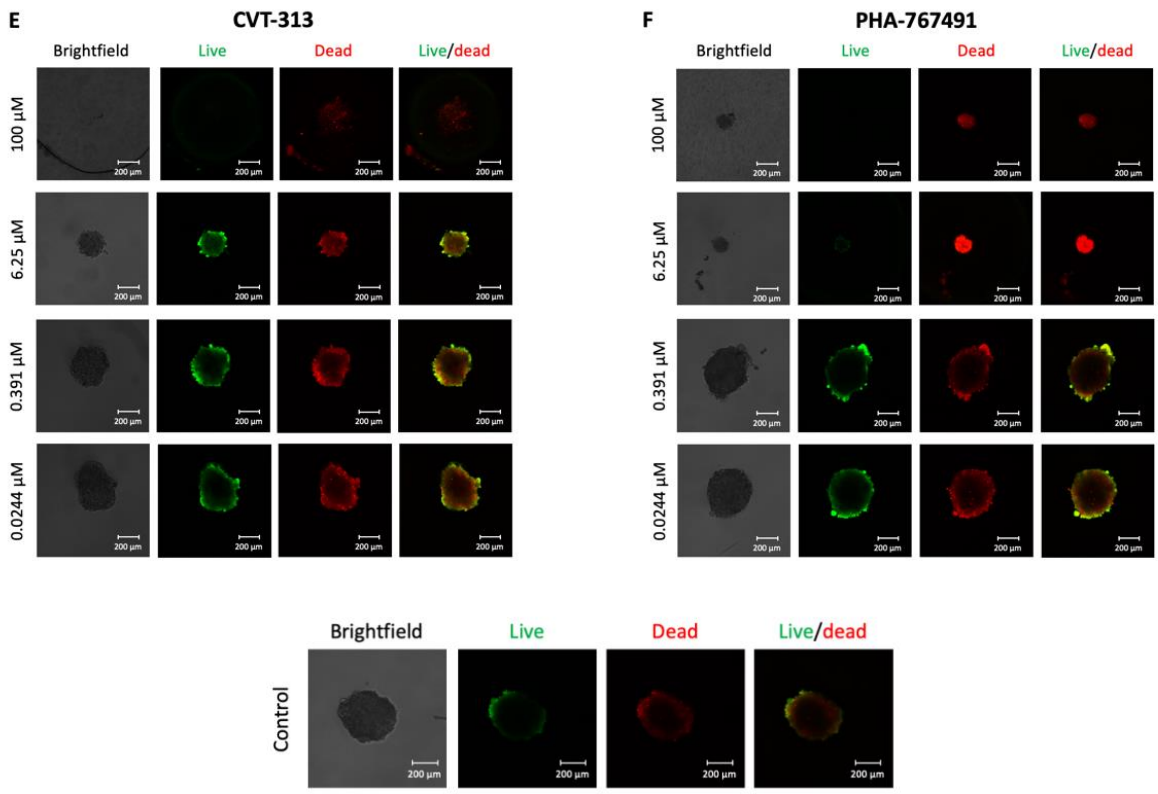

Figure 3. 4. CDK inhibition causes cell death in fluorescent U-87 MG spheroids. U-87 MG cells were seeded 24 hours prior to seven-day incubation with CDK inhibitors (100 – 0.0061 µM). Spheroids were incubated with calcein AM (green) and ethidium homodimer (red) three hours before imaging. Images were taken on the Leica Stellaris 5 Confocal Microscope at 10X magnification.

Figure 3.4 shows inhibitor-treated spheroids at 100, 6.25, 0.391, and 0.0244 µM, displaying brightfield, live, dead, and live-dead merged channels. The brightfield images at 100 µM show very small spheroids. The live and dead channels reveal that these spheroids contain only dead cells, revealing a cytotoxic effect mediated by CDK inhibitor treatment. At lower concentrations of drug, the brightfield images show larger spheroids with green, fluorescent live cells around the periphery, as well as dead cells that are present in every case. When the drug concentration nears its 3D IC_{50} value (Table 3.2), it proves effective at killing U-87 MG cells within the spheroid. As the concentration decreases below this value, more viable cells are observed within the treated spheroid.

Dinaciclib, PHA-767491, and milciclib display the strongest cytotoxic effects in 3D culture, however all CDK inhibitors tested result in cell death. These data show that CDK inhibition is cytotoxic to glioblastoma in 3D culture and not merely cytostatic.

3.4. Validation of FUCCI and QuCCI U-87 MG transfection

U-87 MG cells were transfected with the FUCCI(CA)2 construct (and QuCCI construct, although these cells were not assayed) and later analysed using live-cell imaging following CDK inhibitor treatment. After transfection of FUCCI/QuCCI plasmids into U-87 MG cells, puromycin was added to cells' media to select for those successfully transfected. Images were taken using a camera down the eye piece of a light microscope for 16 days after selection was introduced (Figure 3.5).

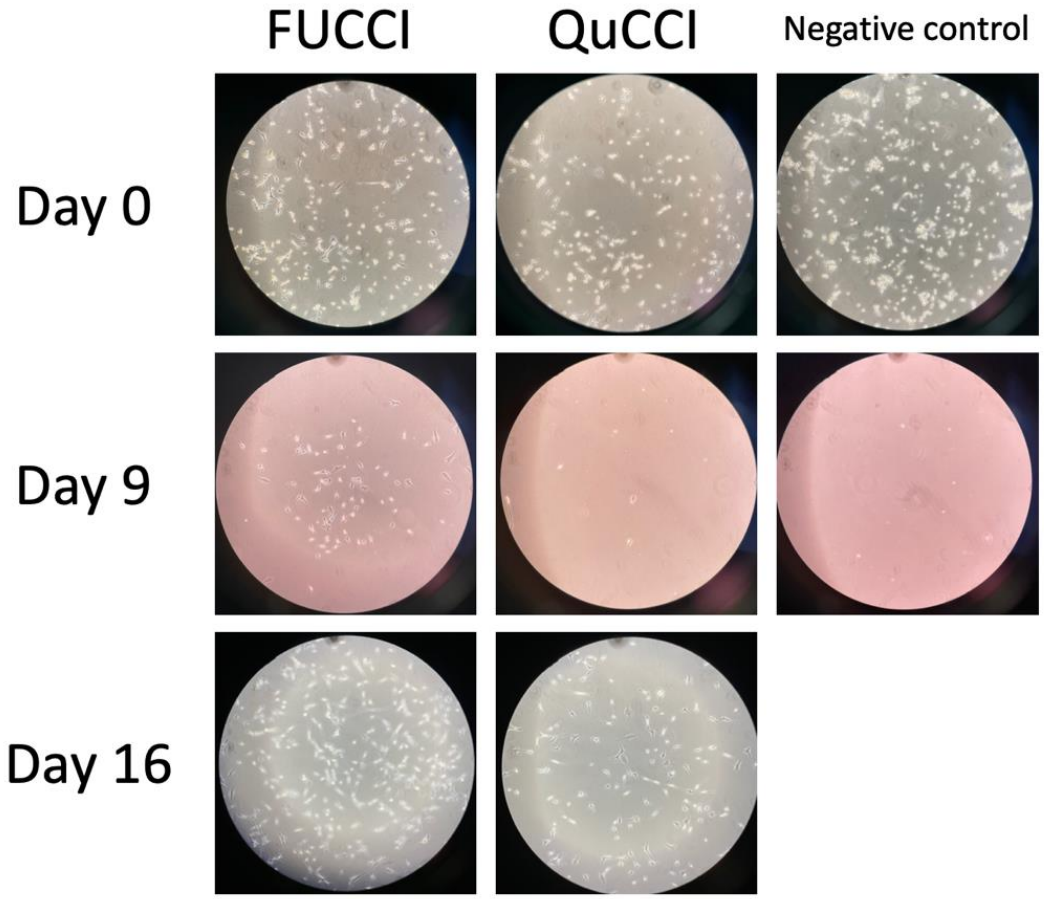

Figure 3. 5. Representative images taken of FUCCI, QuCCI, and negative control U-87 MG cells during selection for those successfully transfected. U-87 MG cells were transfected with FUCCI/QuCCI and a piggyBac recombination plasmid and puromycin added 48 hours later to select for transfected cells. Images were taken each time the media was changed for 16 days at 20X magnification using a light microscope. The negative control plate was discarded after day 9 of selection.

U-87 cells on all plates had a high density: around 40% for FUCCI and negative control plates and 30% for the QuCCI plate on day 0, these densities heavily dropped 9 days into selection and there were very few cells on the FUCCI plate and even fewer on the QuCCI plate. The negative control plate had only dead cells, which was expected as parental cells were not resistant to puromycin. After 16 days of selection, FUCCI cells had increased to around 70% confluence and QuCCI cells to around 40% confluence. No more images were taken after day 16. To confirm that the transfections were successful, FUCCI and QuCCI U-87 MG cells were fixed with formaldehyde and imaged using confocal microscopy (Figure 3.6).

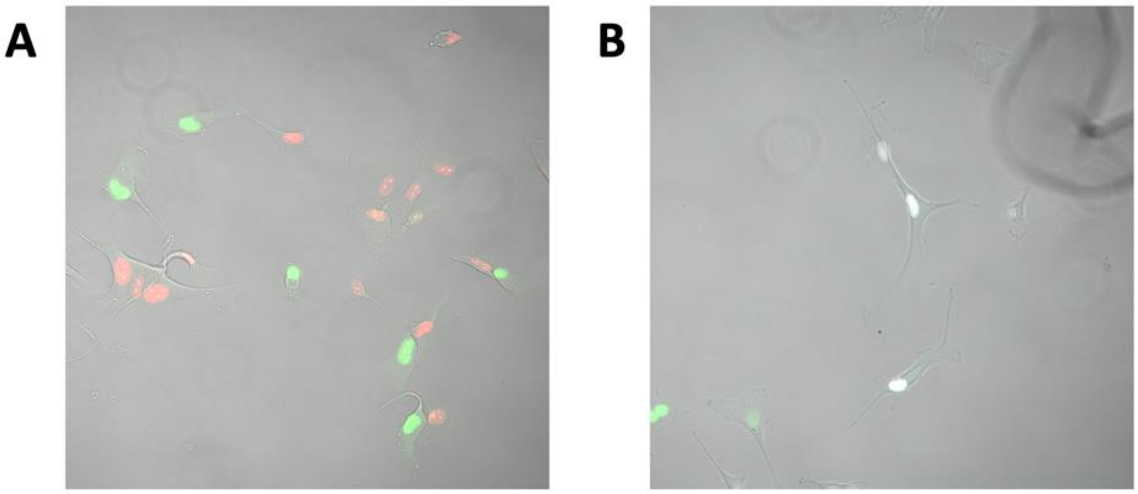

Figure 3. 6. Fixed FUCCI and QuCCI U-87 MG cell images. Cells were grown on coverslips, fixed with formaldehyde, and imaged at 40X magnification merging the brightfield and fluorescence channels.

3.5. CDK inhibition causes cell cycle arrest in FUCCI U-87 MG cells

FUCCI U-87 MG cells were seeded at 30-40% confluence and treated with CDK inhibitors. Images of cells were taken every hour for 16 hours post-CDK inhibitor treatment and cell cycle phase monitored. Figures 3.7 – 3.13 show fluorescent images taken of cells at 0, 8, and 16 hours following incubation with 10/5 µM CDK inhibitor, or control, treatment. Proportions of G1 (red) and S/G2 (green) cells were plotted as line graphs for each treatment. Yellow cells were excluded from the graphs so that cells could be divided into G1 or S/G2 only to identify any cell cycle arrest/accumulation. A line graph for each treatment is also shown with total cell number to quantify cell death.

Figure 3.7 A and B show progression of FUCCI U-87 MG cells through the cell cycle as they change from red to green, divide, and turn red again. Graphs D and F show cell number increases as cells progress through the cell cycle during the experiment, and C and E show fluctuation of cell cycle phase (red/green) as cells divide normally with no treatment/DMSO. However, samples have a higher number of cells in G1 (red) than S/G2 (green), which is a common observation across almost every treatment from this experiment.

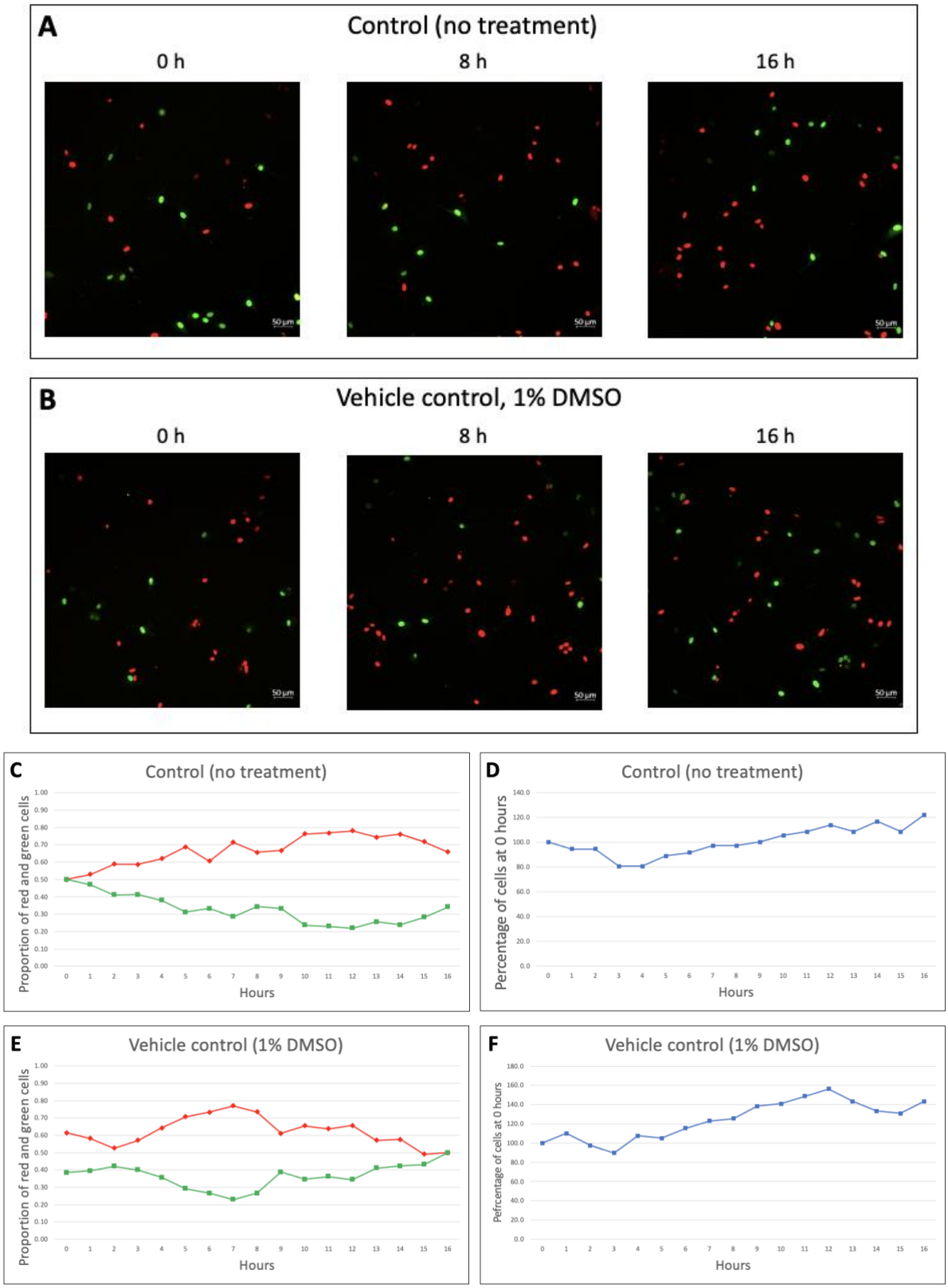

Figure 3. 7. Untreated and DMSO-treated FUCCI U-87 MG cells progress through the cell cycle and divide. Samples were incubated with **A)** no treatment (n=1) or **B)** vehicle control (1% DMSO, n=1) and images taken every hour for 16 hours – images at 0, 8, and 16 hours are shown. **C, E)** Proportions of FUCCI U-87 MG cells in G1 (red) and S/G2 phase (green) were counted and plotted as line graphs, alongside **D, F)** line graphs showing total cell number.

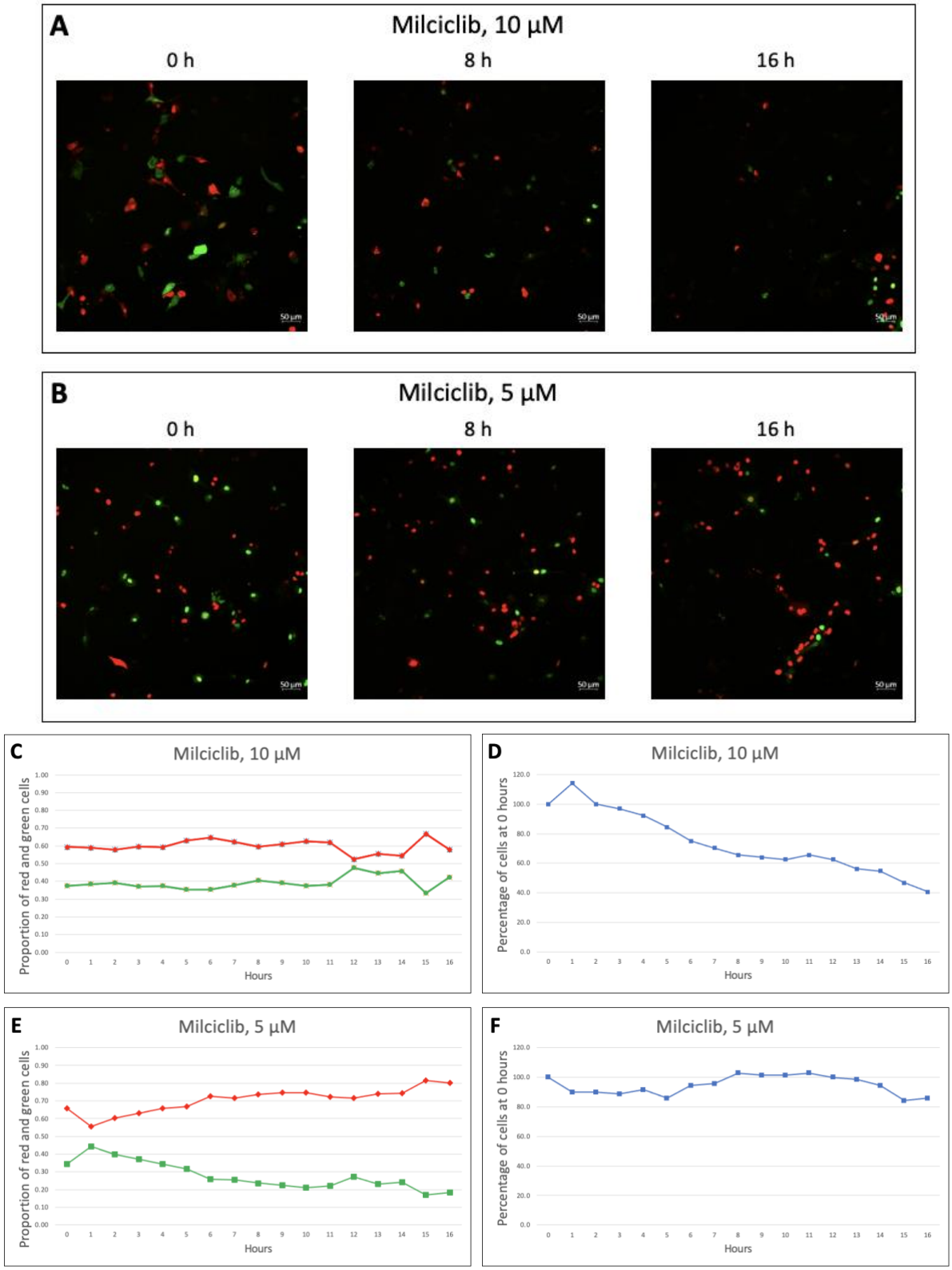

Figure 3. 8. Milciclib kills FUCCI U-87 MG cells at high concentrations and causes G1 accumulation at lower concentrations. Samples were incubated with **A)** 10 µM (n=1) or **B)** 5 µM (n=1) milciclib and images taken every hour for 16 hours – images at 0, 8, and 16 hours are shown. **C, E)** Proportions of FUCCI U-87 MG cells in G1 (red) and S/G2 phase (green) were counted and plotted as line graphs, alongside **D, F)** line graphs showing total cell number.

Milciclib treatment at 10 µM results in proportions of G1 and S/G2 cells to remain consistent across the entire duration of the experiment (Figure 3.8 C), but cell number steadily decreases throughout the experiment to around 40%. This implies that milciclib causes cell death at 10 µM irrespective of cell cycle phase (Figure 3.8 D). This contrasts with results seen with 5 µM milciclib that show only a slight decrease in cell number to ~85% of the initial number (Figure 3.8 B, F) but results in cell cycle arrest with 80% of cells in G1 phase (Figure 3.8 B, E). These data suggest that milciclib is cytostatic at 5 µM and cytotoxic at 10 µM.

Live-cell imaging of abemaciclib-treated samples found few cells in the microscope's field of view (Figure 3.9 A, B), unfortunately reducing the sample size and making comparison of cell numbers to the control impossible, due to the large increase in cell number after abemaciclib treatment (Figure 3.9 D). Abemaciclib treatment at 5 µM also resulted in an increase in cell number (Figure 3.9 B, F) but only maximally to ~160% at 12 hours before reducing again towards the end of the incubation. Despite low cell number, G1 accumulation is observed at both 10 and 5 µM (Figure 3.9 C, E) with over 80% of cells reporting as in G1 phase by the end of the experiment at both 10 and 5 µM, consistent with cytostatic effects for acute abemaciclib treatment.

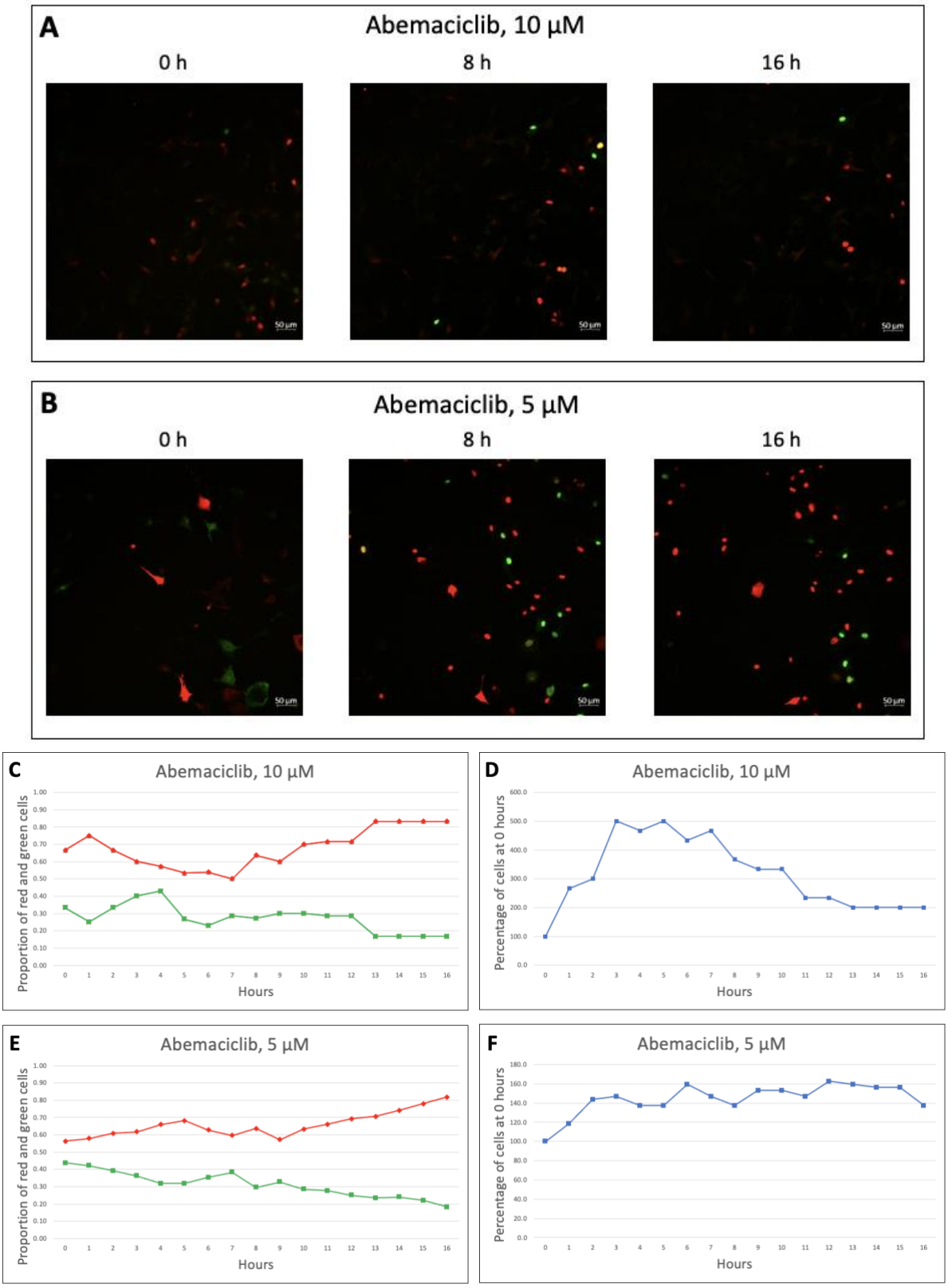

Figure 3. 9. Abemaciclib causes G1 accumulation at multiple concentrations in FUCCI U-87 MG cells. Samples were incubated with **A)** 10 µM (n=1) or **B)** 5 µM (n=1) abemaciclib and images taken every hour for 16 hours – images at 0, 8, and 16 hours are shown. **C, E)** Proportions of FUCCI U-87 MG cells in G1 (red) and S/G2 phase (green) were counted and plotted as line graphs, alongside **D, F)** line graphs showing total cell number.

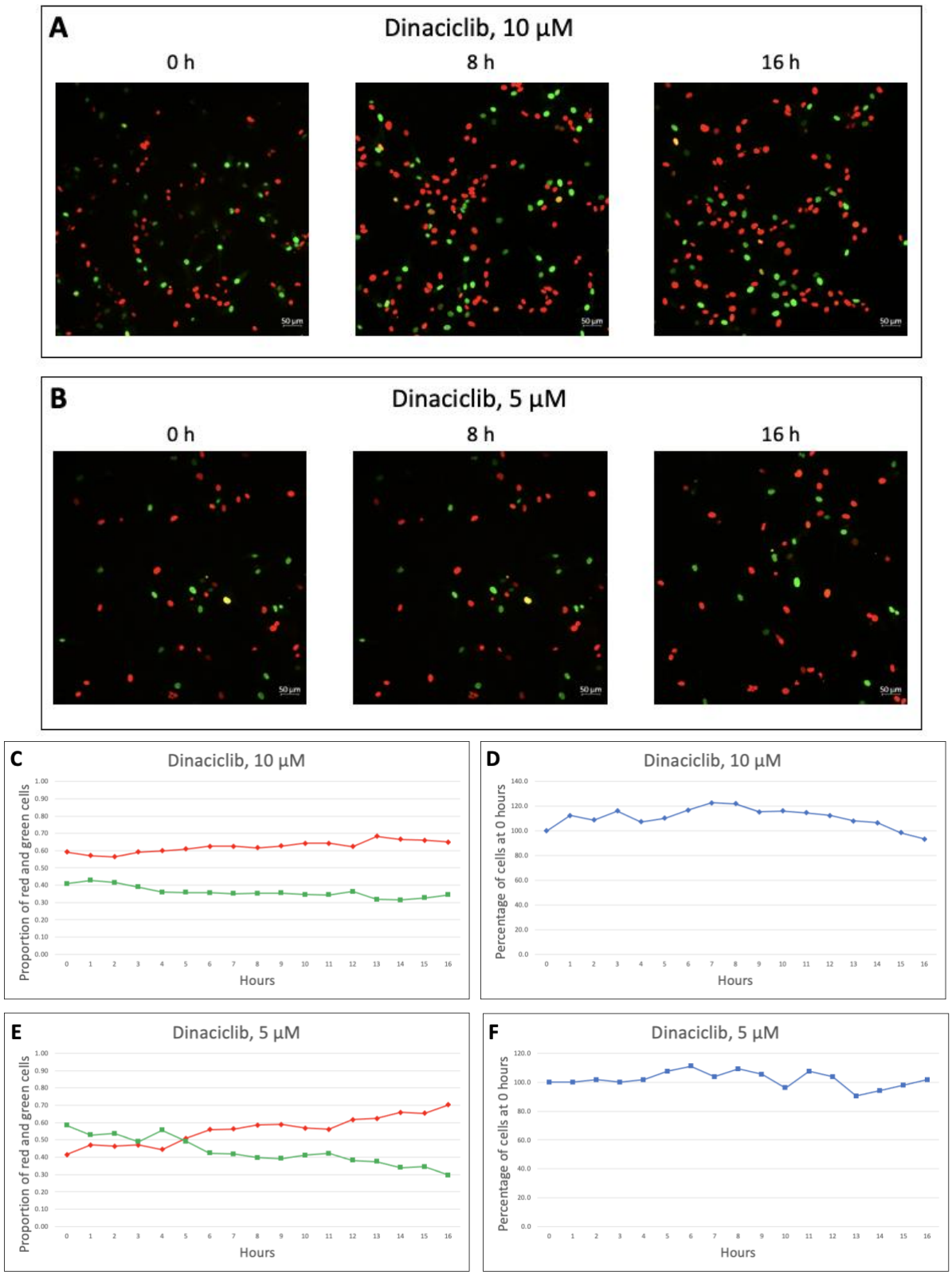

Figure 3. 10. Dinaciclib appears to cause cell death at high concentrations in FUCCI U-87 MG cells. Samples were incubated with **A)** 10 µM (n=1) or **B)** 5 µM (n=1) dinaciclib and images taken every hour for 16 hours – images at 0, 8, and 16 hours are shown. **C, E)** Proportions of FUCCI U-87 MG cells in G1 (red) and S/G2 phase (green) were counted and plotted as line graphs, alongside **D, F)** line graphs showing total cell number.

Dinaciclib shows no cell cycle phase-specific effects in FUCCI U-87 MG cells at 10 or 5 µM (Figure 3.10 A, B, C, E). When treated with 10 µM, around 60% of cells remain in G1 phase and 40% in S/G2 phase throughout the entire incubation. Following 5 µM treatment, the number of cells in G1 phase appears to increase from 11-16 hours incubation to around 70%, however this could be random fluctuation. Cell number remains consistent following 5 µM treatment (Figure 3.10 F) and only begins to show a gradual decrease after 8 hours of incubation with 10 µM dinaciclib (Figure 3.10 D). The data from both 2D and 3D experiments found dinaciclib to be the most potent, making the small change in cell number here a surprising result. Differences in incubation time of 16 hours here compared to 72/144 hours for 2D viability/3D assays, respectively may have led to the differences in results. In shorter treatments there appears to be a cytostatic effect with an enrichment in G1 phase for both concentrations tested.

Palbociclib treatment at 10 µM results in no change in the proportions of cells in either G1 or S/G2 phase, suggesting there is no cell cycle arrest at this concentration. However, it does reduce cell number (Figure 3.11 A, D) suggesting palbociclib is inducing cell death. At 5 µM, palbociclib induced death and caused a reduction in total cell number of ~20% (Figure 3.11 F). In addition, 5 µM palbociclib treatment causes cell cycle arrest in G1 phase resulting in almost 80% of cells in G1 phase at 16 hours and 20% in S/G2 phase (Figure 3.11 E).

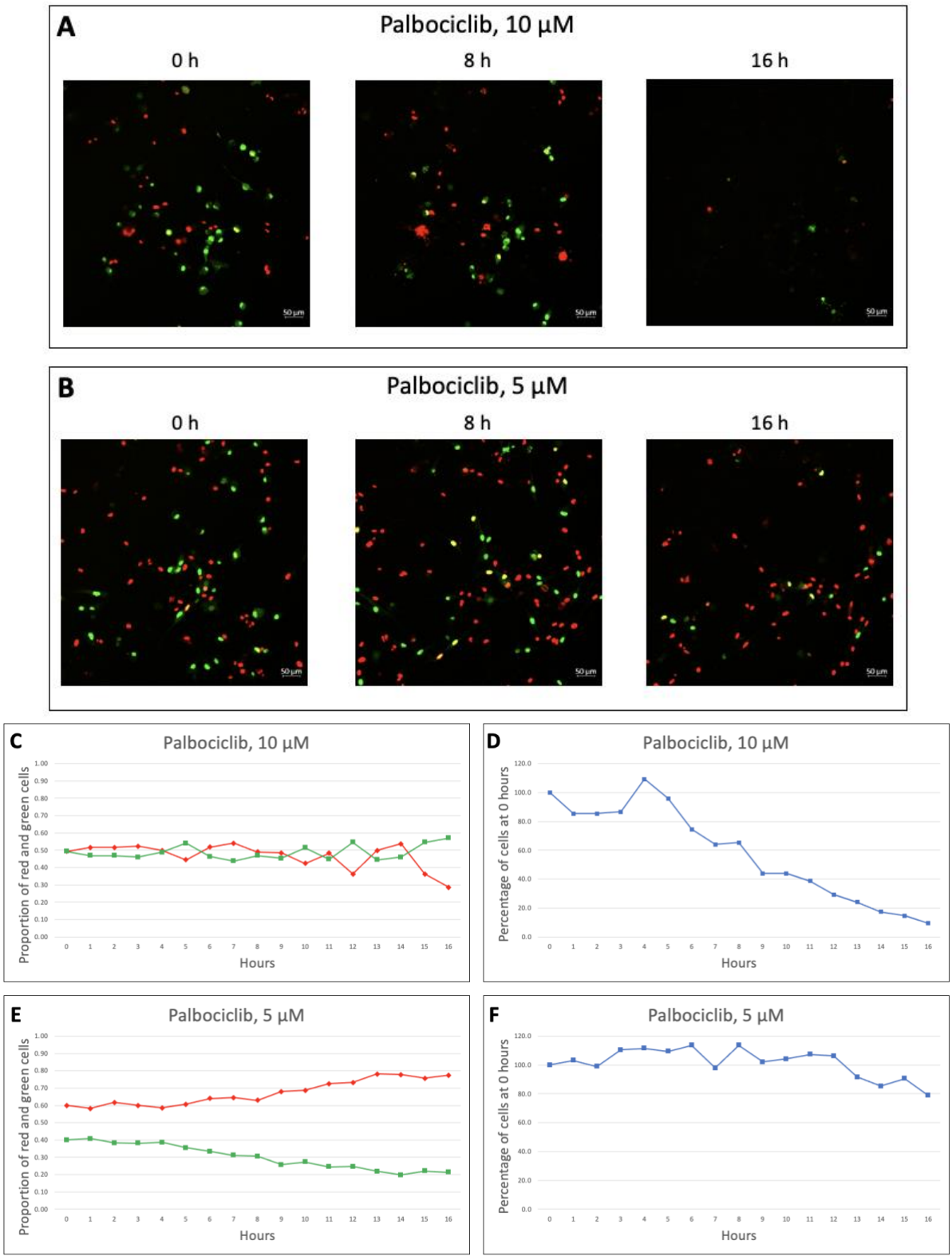

Figure 3. 11. Palbociclib shows concentration dependent cytotoxic and cytostatic effects in FUCCI U-87 MG cells. Samples were incubated with **A)** 10 µM (n=1) or **B)** 5 µM (n=1) palbociclib and images taken every hour for 16 hours – images at 0, 8, and 16 hours are shown. **C, E)** Proportions of FUCCI U-87 MG cells in G1 (red) and S/G2 phase (green) were counted and plotted as line graphs, alongside **D, F)** line graphs showing total cell number.

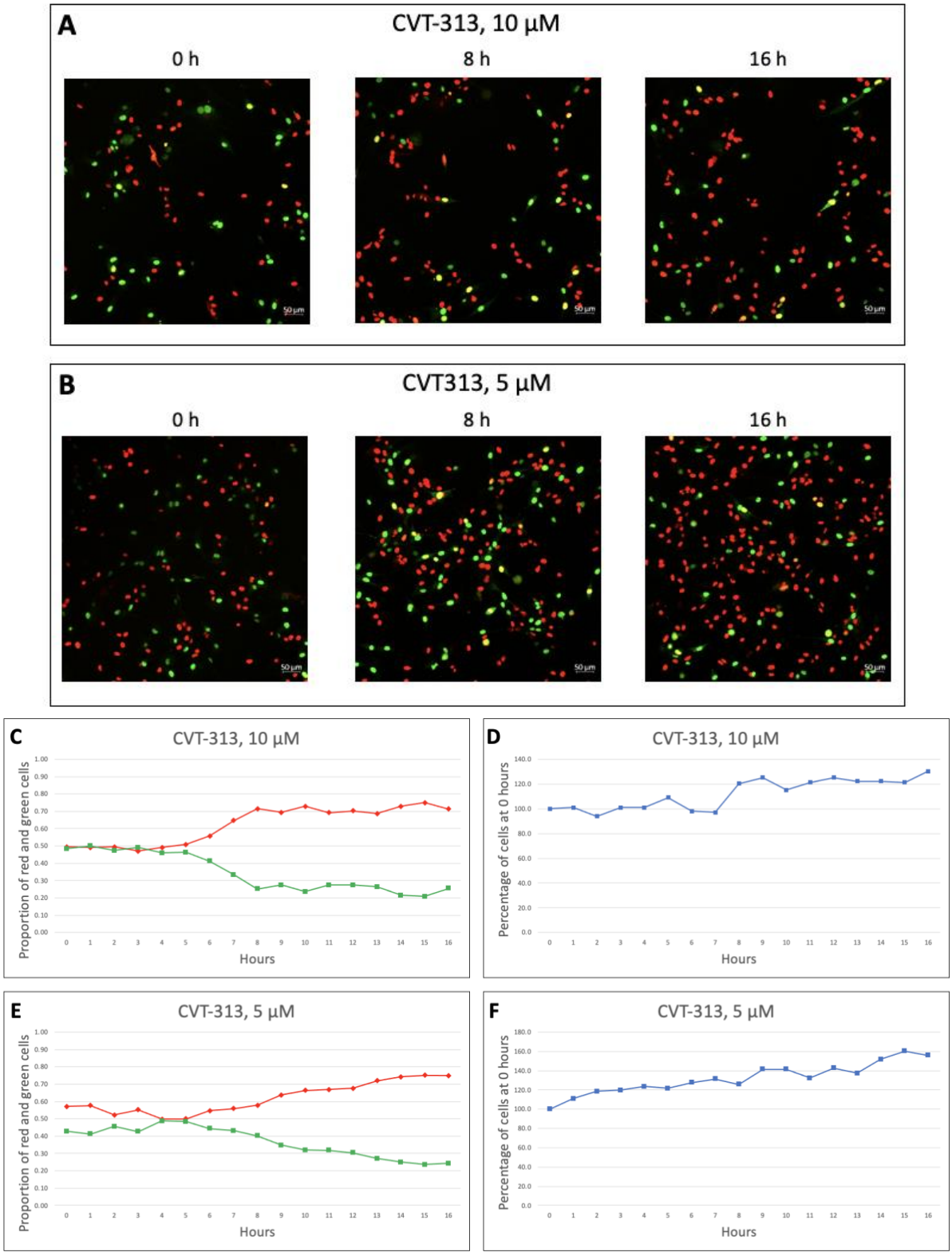

Figure 3. 12. CVT-313 causes G1 accumulation in FUCCI U-87 MG cells at high and low concentrations. Samples were incubated with **A)** 10 µM (n=1) or **B)** 5 µM (n=1) CVT-313 and images taken every hour for 16 hours – images at 0, 8, and 16 hours are shown. **C, E)** Proportions of FUCCI U-87 MG cells in G1 (red) and S/G2 phase (green) were counted and plotted as line graphs, alongside **D, F)** line graphs showing total cell number.

CVT-313 treatment at both 10 and 5 µM resulted in increased cell proliferation over 16 hours (Figure 3.12 D, F) and an increase in the proportion of G1 cells (Figure 3.12 C, E). Around 70% of cells are arrested in G1 by the end of the experiment when treated with 10 µM CVT-313, and around 75% of cells are G1-arrested after a 16-hour incubation with 5 µM CVT-313. These data suggest that CVT-313 promotes cell cycle arrest in G1 phase after acute treatment, with limited cell death, suggesting a cytostatic mechanism.

Following treatment with PHA-767491, cells appear to stop dividing after 10 and 5 µM treatment incubations as the number of cells stays close to 100% of the number at the start of the experiment (Figure 3.13 D and F). Proportions of cells in G1 and S/G2 also appear to remain almost consistent across the entire incubation with a similar number of red and green cells observed in all the images in Figure 3.13 A and B. Although, the proportion of cells in G1 does appear to increase slightly (to 0.6) after both 10 (Figure 3.13 C) and 5 µM (Figure 3.13 E) incubations, suggesting cell cycle arrest and a cytostatic effect.

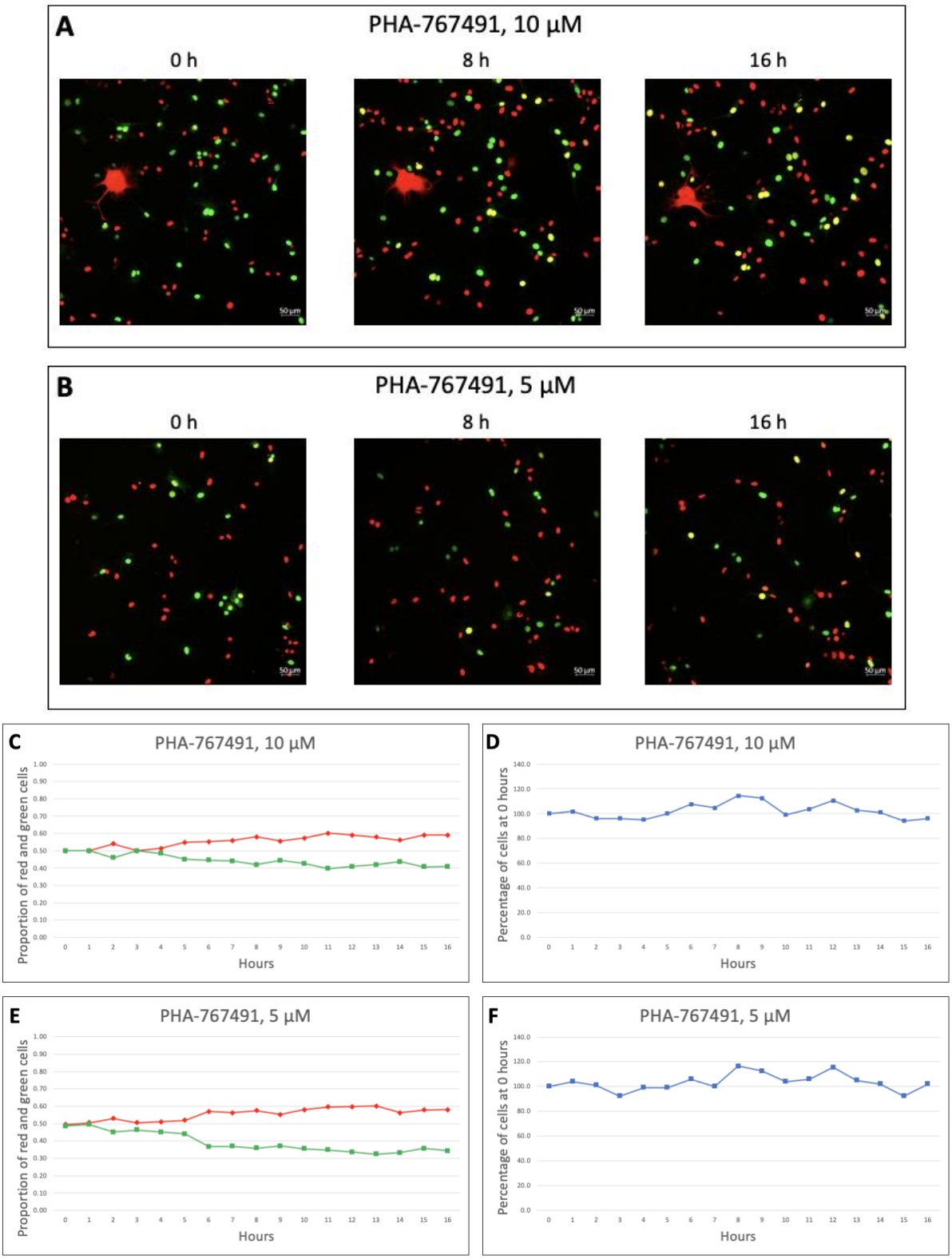

Figure 3. 13. PHA-767491 elicits weak cell cycle arrest in G1 phase in FUCCI U-87 MG. Samples were incubated with **A)** 10 µM (n=1) or **B)** 5 µM (n=1) PHA-767491 and images taken every hour for 16 hours – images at 0, 8, and 16 hours are shown. **C, E)** Proportions of FUCCI U-87 MG cells in G1 (red) and S/G2 phase (green) were counted and plotted as line graphs, alongside **D, F)** line graphs showing total cell number.

3.6. CDK inhibition has inconsistent effects on CIZ1 levels

U-87 MG and BTNW914 cells were treated with the CDK inhibitor panel (72 hours) and a vehicle control (1% DMSO, 72 hours). Cells were harvested and protein extracted and assessed by western blotting (Figure 3.14, 3.16). Figures 3.14 and 3.16 show actin and CIZ1 protein levels from U-87 MG and BTNW914 samples and bar charts showing relative CIZ1 levels standardised to the DMSO control for each replicate.

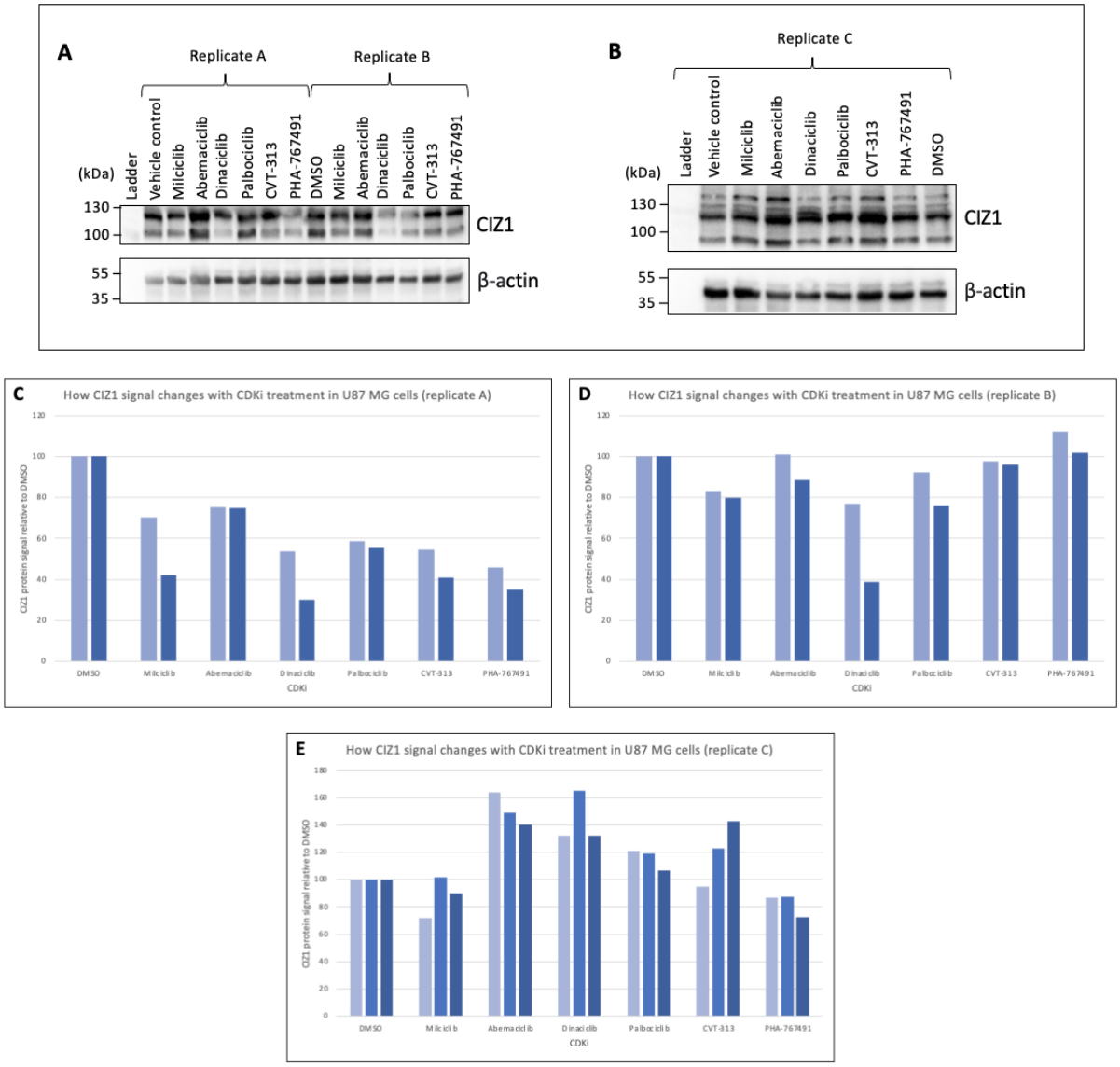

Figure 3. 14. CDK inhibition shows varied effects on CIZ1 levels in U-87 MG. U-87 MG samples were treated with a vehicle control (1% DMSO) or 10 µM CDK inhibitors for 72 hours. Cells were harvested, then protein was extracted and analysed by western blotting using CIZ1 and actin primary antibodies. Image analysis and quantitation was performed on the iBright™ CL1500 Imaging System. **A, B)** Annotated membrane images are shown with **C, D, E)** standardised CIZ1 signals as a percentage of the vehicle control for each replicate. The anti-CIZ1 antibody detected at least two bands in U-87 MG samples, and all were quantified. The first bar of each pair is the upper CIZ1 band and the second is the lower band – replicate C has three bars which correspond to the upper, middle, and lower CIZ1 bands on the image.

In replicate A, CDK inhibition reduced CIZ1 levels in every sample (Figure 3.14 A, C). CIZ1 has multiple bands that are cell line specific and likely represent splice variants of CIZ1. Abemaciclib reduced the upper and lower CIZ1 bands by the least amount (over 20%),

whereas dinaciclib and PHA-767491 reduced CIZ1 levels by the highest amount (~50% for upper bands and 70% for lower bands). Similarly, replicate B showed a CIZ1 reduction for most inhibitors and only a slight increase for the upper CIZ1 band after 10 µM abemaciclib treatment and both bands after PHA-767491 incubation.

Replicate C shows three CIZ1 bands (Figure 3.14 B) with an additional lower band to replicate A and B. These bands were present on the other membrane but were excluded from analysis as they were very weak. Figure 3.14 E has three bars for each replicate to represent these three CIZ1 bands. Replicate C is an outlier compared to the other U-87 MG replicates. Every inhibitor treatment resulted in an increase in CIZ1 protein except for PHA-767491. Some CIZ1 bands were significantly increased by 80%. Replicate C is also different to the others in that there is no consistency in the relative reductions of the CIZ1 bands within each sample, whereas in replicate A and B the upper band has a relatively higher intensity and is reduced by less than the lower band in every sample. It is not clear why this replicate showed a different band pattern or CIZ1 level in response to CDK inhibition. Further replicates are required to fully assess the efficacy of CDK inhibitors to reduce CIZ1 levels.

There is also some variation in the effect of the inhibitors across the replicates. For example, PHA-767491 shows one of the largest reductions in CIZ1 for replicate A and C, but shows the largest increase in replicate B. In contrast, abemaciclib incubation shows a modest reduction in replicates A and B and a large increase in replicate C, suggesting it is less effective at reducing CIZ1 levels than some of the other inhibitors.

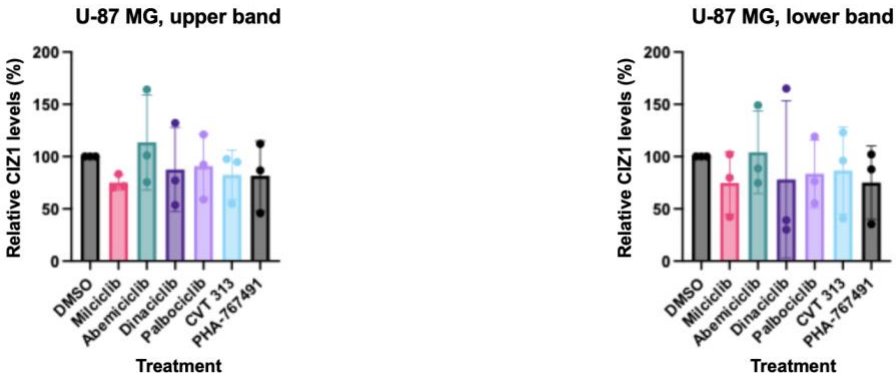

Figure 3. 15. CDK inhibition slightly reduces CIZ1 protein levels in U-87 MG. U-87 MG samples were treated with a vehicle control (1% DMSO) or CDK inhibitors for 72 hours. Cells were harvested then protein was extracted and analysed by western blotting using CIZ1 and actin primary antibodies. Image analysis and quantitation was performed on the iBright™ CL1500 Imaging System. CIZ1 signals were standardised against actin bands and converted to a percentage of the DMSO sample for each replicate. Percentages for each replicate were averaged and plotted with ± standard deviation.

Figure 3.15 shows average values from each replicate of relative CIZ1 levels compared to the vehicle control average. Figure 3.15 shows that none of the CDK inhibitors tested were able to significantly reduce CIZ1 levels in U-87 MG cells for either band/isoform of CIZ1. Some promising reductions were observed for individual replicates; however, these have been averaged out by multiple replicates and there was no significant change for any treatment compared to the vehicle control. Additional repeats are required to determine whether there lies a relationship between CDK activity and CIZ1 levels in glioblastoma cells.

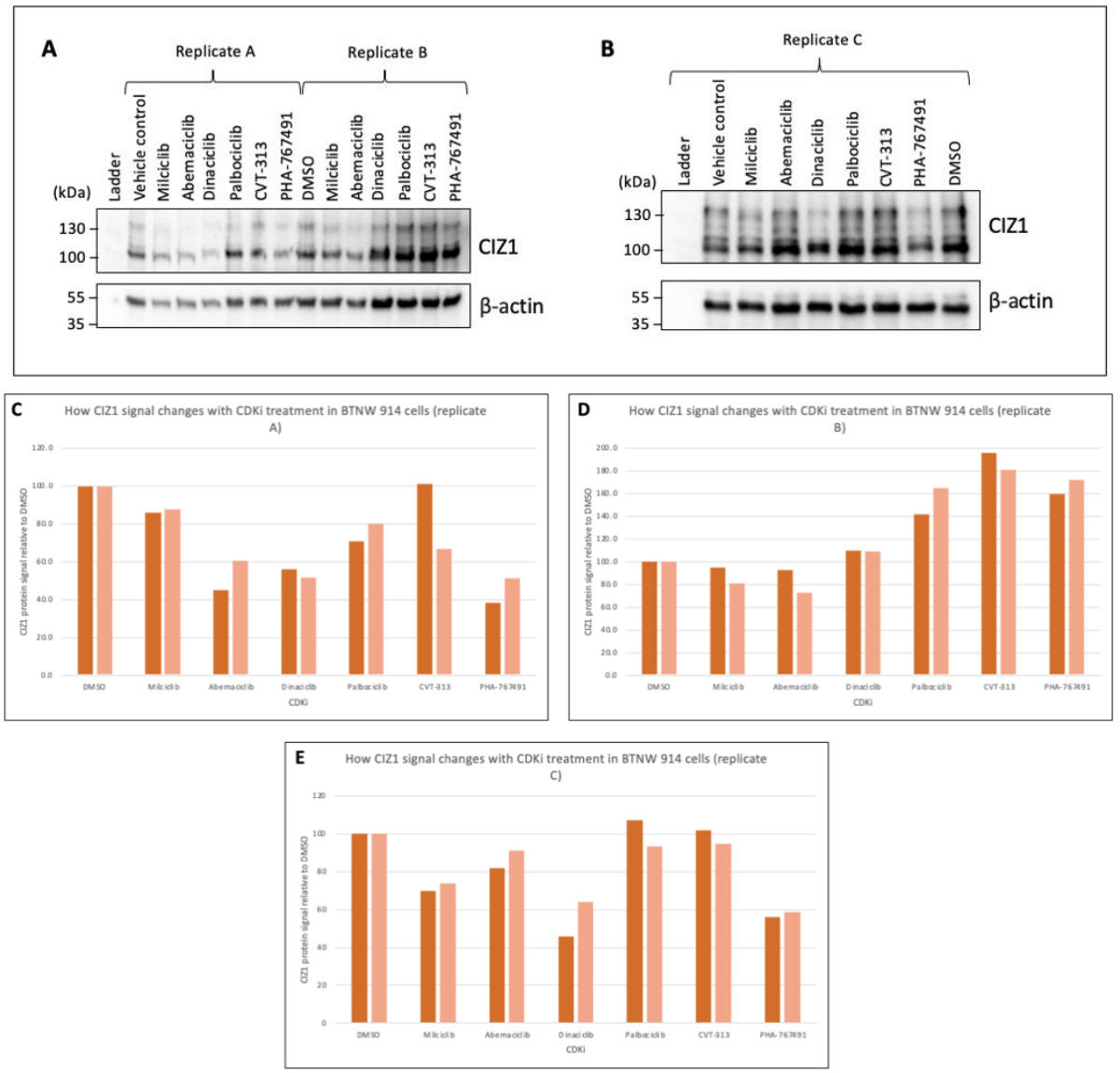

Figure 3. 16. CDK inhibition shows varied effects on CIZ1 levels in BTNW914. BTNW914 samples were treated with a vehicle control (1% DMSO) or 10 µM CDK inhibitors for 72 hours. Cells were harvested, then protein was extracted and analysed by western blotting using CIZ1 and actin primary antibodies. Image analysis and quantitation was performed on the iBright™ CL1500 Imaging System. **A, B)** Annotated membrane images are shown with **C, D, E)** standardised CIZ1 signals as a percentage of the vehicle control for each replicate. The anti-CIZ1 antibody detected at least two bands in U-87 MG samples, and all were quantified. The first bar of each pair is the upper CIZ1 band and the second is the lower band – replicate C has three bars which correspond to the upper, middle, and lower CIZ1 bands on the image.

CIZ1 reduction from CDK inhibition in BTNW914 is observed in the most part in replicates A and C, however replicate B appears to be an outlier and shows differing results.

Replicates A and C show a reduction in CIZ1 levels following incubation for most CDK inhibitors, except for the upper band in the CVT-313-treated sample in replicate A and the upper bands following palbociclib and CVT-313 treatments in replicate C (Figure 3.16 C, E). Dinaciclib and PHA-767491 appear to be the most effective inhibitors in reducing CIZ1 levels in BTNW914. They result in one of the most significant reductions in CIZ1 protein band intensity, which is consistent across replicate A and C. CVT-313 is perhaps the least effective inhibitor in inducing CIZ1 reduction as it shows a slight increase in band intensity in replicates A and C.

As in replicate C for U-87 MG, replicate B for BTNW914 appears to be an outlier and shows different results to the other replicates. A small reduction in CIZ1 is observed for milciclib and abemaciclib-treated samples whereas the other samples show an increase in response to CDK inhibition, as significant as almost 200% of the CIZ1 signal from the DMSO-treated sample (Figure 3.16 D). These data are inconsistent with what was observed in the other replicates.

Although the upper CIZ1 band signal is less intense than the lower band in every sample (Figure 3.16 A, B), there appears to be no pattern as to which band is more reduced by CDK inhibition – this is different to U-87 MG samples. Although where CIZ1 levels are increased/decreased, all bands are broadly in agreement suggesting they are isoforms of CIZ1.

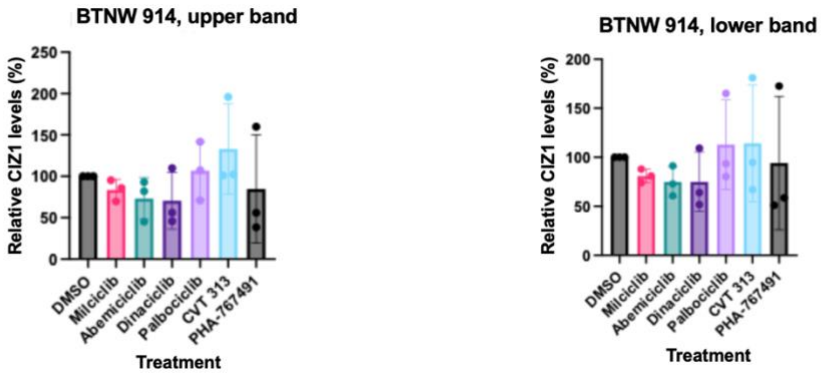

Figure 3. 17. CDK inhibition slightly reduces CIZ1 protein levels in BTNW914. BTNW914 samples were treated with a vehicle control (1% DMSO) or CDK inhibitors for 72 hours. Cells were harvested then protein was extracted and analysed by western blotting using CIZ1 and actin primary antibodies. Image analysis and quantitation was performed on the iBright™ CL1500 Imaging System. CIZ1 signals were standardised against actin bands and converted to a percentage of the DMSO sample for each replicate. Percentages for each replicate were averaged and plotted with ± standard deviation.

BTNW914 samples show a similar trend to U-87 MG. Some promising reductions were observed but these have been averaged out in the mean data (Figure 3.17), showing no significant reductions. CDK inhibition had no significant increasing or decreasing effect on CIZ1 in this cell line. The differences observed in experimental replicates suggest that repeats are required to elucidate whether CDK inhibition does indeed reduce CIZ1 levels in glioblastoma cells.

Overall, our data show these CDK inhibitors are potent antiproliferative agents in glioblastoma cultures, showing large selectivity over normal glia. High potency has also been observed in 3D cultures and cytotoxicity demonstrated in 2D and 3D models, through live cell imaging and live/dead staining, respectively. As well as cell death, cell cycle arrest was also observed from live cell imaging experiments. These effects could not be linked to a reduction in CIZ1 protein expression, however the potent effects of CDK inhibition on immortalised and patient-derived glioblastoma cultures is indisputable.

4. Discussion

4.1. CDK inhibitors have potent antiproliferative effects in 2D and 3D glioblastoma culture

CDK inhibition is a clinically relevant approach for cancer therapy (Finn *et al.*, 2015; Finn *et al.*, 2016; Hortobagyi *et al.*, 2016; Goetz *et al.*, 2017; Im *et al.*, 2019; Hortobagyi *et al.*, 2018; Slamon *et al.*, 2020). To assess the effect of CDK inhibition on the proliferative potential of glioblastoma cells Prestoblue™ was used to determine cell viability. All CDK inhibitors tested showed a high potency in reducing cellular proliferation in 2D and 3D glioblastoma cultures. Milciclib, abemaciclib, and dinaciclib had nanomolar IC_{50} values in U-87 MG 2D and 3D culture and milciclib and abemaciclib had low micromolar IC_{50} values in 2D BTNW914 assays, with dinaciclib remaining at 388 nM. Potency was slightly lower for palbociclib, CVT-313, and PHA-767491 but IC_{50} values were still in the low micromolar range (Table 3.1 and 3.2). Surprisingly, palbociclib was effective at reducing proliferation in glioblastoma cells but showed the poorest overall performance despite its broad clinical use. In every case, U-87 MG cells were more susceptible to CDK inhibition than BTNW914. When comparing the potency of each inhibitor on U-87 MG in 2D and 3D assays, milciclib and CVT-313 were more potent in 2D whereas abemaciclib, palbociclib and PHA-767491 were more potent in 3D. Due to the high potency of dinaciclib in both cultures, its IC_{50} value could not be determined in either case. The differential effects in 2D culture may reflect the cell permeability of the inhibitors tested here, and these assays may be useful to identify CDK inhibitors for further testing in preclinical animal models.

The high potency of CDK inhibitors has been confirmed in other work. Milciclib has demonstrated a high potency in other glioblastoma cell lines: SF268, SF539, U-251, as well as U-87 MG (Albanese *et al.*, 2013). IC_{50} values were determined as 2.5, 1.4, and 2.1 µM for SF268, SF539 and U-251, respectively. A higher IC_{50} value was determined in 2D U-87 MG culture (1.6 µM) than here (<24.4 nM), but still demonstrates the high potency of milciclib in this cell line. The IC_{50} value determined for milciclib in BTNW914 (2.495 µM) lies within the range of those determined in the other cell lines in this study (1.4 – 2.5 µM). No other work has assessed the potential for CVT-313 to induce anticancer effects in glioblastoma *in vitro*,

however we identify it to be as potent as other inhibitors that have been investigated elsewhere, however slightly less effective in 3D.

Palbociclib has a much lower potency in U-87 MG and BTNW914 with IC_{50} values of 8.9 and 11.21 µM. A similar value of 12 µM was determined in the glioblastoma patient-derived cell line: HW1 (Whittaker *et al.*, 2017). It was also less potent than abemaciclib and dinaciclib in 2D and 3D culture (Riess *et al.*, 2021). Palbociclib treatment at 10 µM only reduced 2D viability by ~25% on average across five cell lines. In 3D culture, it did not reduce viability in glioma stem-like cells (GSCs) but did in neural stem/progenitor cells (NSCs). GSCs are a subpopulation of glioblastoma cells that are partly responsible for tumour behaviour, whereas NSCs represent normal tissue (Gong *et al.*, 2011). Therefore, the responses of GSCs and NSCs are distinct from those determined here with U-87 MG spheroids. Also, incubation of palbociclib at 10 µM required a long incubation of 14 days to reduce the viability of almost the entire sample of patient-derived glioma stem cell-enriched cell lines (GSC-ECLs), hinting to its lower efficacy. Another study found that 2 µM palbociclib incubation for 72 hours reduced U-87 MG 2D viability by around 40% (Liu *et al.*, 2018b), which was just slightly lower than 6.25 µM palbociclib for 72 hours reducing U-87 MG viability by ~45%, here. However, palbociclib has demonstrated higher potency with IC_{50} values of 1 and 0.5 µM in TMZ resistant and sensitive cells, respectively (Li *et al.*, 2019). A variation in potency across cell lines suggests their responses to palbociclib treatment are specific in each case.

Determination of 2D IC_{50} values for dinaciclib as <24.4 nM and PHA-767491 concentrations of 2.287 and 2.171 µM for BTNW914 and U-87 MG, respectively are consistent with other studies. For U-87 MG and U-251 MG, the determined IC_{50} of PHA-767491 was ~2.5 µM for both (Erbayraktar *et al.*, 2016). EC_{50} values for dinaciclib are all below 24 nM at 7, 8, and 9 nM for U-87 MG, PC40, and SC40 cells, respectively (Xu *et al.*, 2022). These values indicate that PHA-767491 and dinaciclib are both extremely potent across multiple glioblastoma cell lines in 2D culture. Dinaciclib has been investigated in other studies, reducing 2D viability in nanomolar concentrations after 72 hours incubation by 40-45% in three glioblastoma cell lines (HROG02, HROG05, and HGOG63) and by 40% in five glioblastoma cell lines (HROG02, 05, 52, 63, 75), on separate occasions (Riess *et al.*, 2022; Riess *et al.*, 2021). Dinaciclib also displayed efficacy in spheroid models, showing 50% reductions in viability at nanomolar

concentrations in 3D GSCs and NSCs (Riess *et al.*, 2021), as well as a viability reduction over 50% in HROG02/63 3D spheroids (Riess *et al.*, 2022). A stronger effect was observed in 3D cultures as opposed to 2D cultures, but our work could not confirm this as the IC_{50} value was lower than the lowest concentration used in each case (24.4 nM).

Abemaciclib gives similar data to dinaciclib in that it is extremely potent *in vitro* and more potent in 3D models (Riess *et al.*, 2022; Riess *et al.*, 2021). One study reported an IC_{50} value of 48.1 nM for abemaciclib in 2D culture (Yin *et al.*, 2018). This is much lower than the values reported here: 4.126 µM for BTNW914 and 388.4 nM in U-87 MG. However, the variation in responses of different cell lines to abemaciclib is well documented. 1 µM treatment was found to reduce viability by 25, 20, 5, and 50% in GBM03, 06, 14, and 15 cell lines (Freitag *et al.*, 2024), and showed over 2-fold difference in potency between U-87 MG/MO59K and T98G cells (Hsieh *et al.*, 2021). Even within this study, abemaciclib shows over a 10-fold difference in potency between U-87 MG and BTNW914 cells (Table 3.1). Despite this, it is a clear conclusion that abemaciclib shows promise in glioblastoma treatment from these *in vitro* studies. Understanding which cell lines or tumours respond to abemaciclib requires identification of biomarkers that may indicate the potential effect and requires further investigation.

Spheroid cultures display a more complex environment than 2D cultures. Their depth creates nutrient, oxygen, drug, and metabolism gradients from the outer to inner layers. Oxygen and nutrient gradients cause the inner cells to be less metabolically active and have a lower proliferation rate than the outer cells, this reduces the efficacy of cell cycle inhibitors. The hydrophobicity of these CDK inhibitors may also affect their penetrance into the spheroid and their efficacy. On the contrary, 2D cultures have a large, exposed surface where cells are more heterogenous and respond similarly to drugs. Therefore, CDK inhibitors would be expected to be more potent in 2D culture, however this is not always the case here.

Perhaps the most significant observation in this study is the selective effect CDK inhibition has on glioblastoma cells relative to normal glia. Dinaciclib is the most potent inhibitor in glioblastoma and the most selective with an > 4000-fold selectivity for glioblastoma over

normal glia (Table 3.1). PHA-767491 and CVT-313 also display weak effects on the normal glial cell line: SVG p12, and strong antiproliferative effects on the glioblastoma cell lines. Milciclib, abemaciclib, and palbociclib exert a small selectivity for glioblastoma of around 3-fold. Some of these findings are corroborated by Riess et al. (2022) as they compared the viabilities of glioblastoma with normal cells following dinaciclib and abemaciclib treatments, using L929 (murine fibroblasts), NHDF (normal human dermal fibroblasts), and h-MSC (human mesenchymal stem cells) for comparative analysis. Whilst dinaciclib reduced viability of glioblastoma by 40-45%, L929, NHDF, and h-MSC viabilities were reduced by 0-15%. Abemaciclib demonstrates slightly lower selectivity as it reduces glioblastoma viability by 40-50% at 10 µM and L929, NHDF, and h-MSC viability by 20, 40, and 10%, respectively. Our data are potentially more relevant as we investigated the effect of CDK inhibition on normal glia, a more representative cell type within the brain. Taken together these data are supportive of preclinical studies using orthotopic animal models to determine the effect of CDK inhibition.

4.2. CDK inhibition arrests the cell cycle of glioblastoma cells

To determine if the reduction in proliferation was associated with cell cycle arrest, FUCCI live cell imaging was performed. This revealed that cell cycle arrest was observed in glioblastoma cultures following incubation with CDK inhibitors.

The CDK2 inhibitors milciclib and CVT-313 both promote G1 accumulation at 5 µM, yet at 10 µM milciclib enhances cell death revealing cytotoxic effects whereas CVT-313 is cytostatic, promoting G1 accumulation. These differential concentration dependent effects may reflect differences in the IC_{50} values of < 24.4 nm and 0.2651 µM (milciclib) and 5.479 and 11.93 µM (CVT-313) in 2D and 3D models respectfully. The study showed cytotoxic and cytostatic mechanisms for two CDK2 inhibitors.

PHA-767491 is a cdc7 and CDK9 inhibitor with recently shown CDK2 inhibitory effects (Pauzaite *et al.*, 2022). As a CDK2 inhibitor, cells would be expected to arrest in G1 following PHA-767491 incubation, like milciclib and CVT-313. However, at both 10 and 5 µM, total cell number stays constant and G1 phase cells only slightly accumulate to ~60% of the sample

(Figure 3.8). Cdc7 and CDK2 control progression through the G1/S transition, so inhibition of these proteins would cause G1 accumulation. However, PHA-767491 also inhibits CDK9, which does not have cell cycle phase-specific activity. Inhibition of this transcriptional CDK, along with CDK2 and cdc7, causes the G1 accumulation to be less obvious as this inhibitor is targeting other proteins aside from those controlling the G1/S transition. This causes G1 accumulation in FUCCI U-87 MG cells, but to a lesser extent than those treated with milciclib and CVT-313.

Dinaciclib treatment does not largely reduce cell number or affect the proportions of cell cycle phases of FUCCI U-87 MG cells (Figure 3.10). Dinaciclib acts as a pan-CDK inhibitor, inhibiting different points of the cell cycle and non-cell cycle specific CDKs alike. This does not cause accumulation at any cell cycle phase as the multiple targets produce a more complex picture within cells.

CDK4/6 are active in early G1 phase, and CDK4/6 inhibitors are routinely used to synchronise cells in G1 phase. Abemaciclib promotes accumulation in G1 phase following 10 and 5 µM treatments (Figure 3.9). This was expected as CDK4/6 inhibition prevents cells from being able to progress to S phase. Palbociclib is also a CDK4/6 inhibitor and showed G1 accumulation in cells treated with 5 µM, with almost 80% of cells in G1 phase after 16 hours (Figure 3.11). Despite palbociclib having a less potent effect on U-87 MG viability (IC_{50}: 8.9 µM), a huge reduction in cell number was observed during live cell imaging of 10 µM palbociclib-treated FUCCI U-87 MG cells, suggesting a high amount of cell death. This revealed to be independent of cell cycle phase as proportions of cells in G1 and S/G2 phase remained consistent in this experiment. The large amount of cell death here was unexpected and suggests palbociclib is a potent inhibitor in U-87 MG cells.

Other work has also identified palbociclib to cause cell cycle arrest in G1 phase. One study revealed that a 48-hour incubation caused the percentage of cells in G1 phase to increase to 25.3% of the sample, compared to 8.83% in a DMSO control (Shi *et al.*, 2020). Whilst the percentage of cells accumulating in G1 was much higher in our data (77%) and the incubation time was shorter (16 hours), the concentration of palbociclib used by Shi et al. was not stated, so may have been much lower than 5 µM to give a weaker effect. Very

similar results to here were found by Whittaker et al. (2017), where 4 µM palbociclib treatment for 24 hours increased the percentage of G0/G1 HW1 cells from 53 to 81%. In comparison, our data show 5 µM palbociclib treatment for 16 hours increased the percentage of G1 cells from 60 to 77%, indicating a very similar response.

4.3. CDK inhibition is cytotoxic in 2D and 3D glioblastoma cultures

By the nature of their activity, CDK inhibitors can induce cell cycle arrest. Whilst this may slow tumour growth, inhibitors that induce cell death would be more potent in reducing tumour growth. As some FUCCI live cell imaging data indicates these inhibitors may cause cell death, the extent of their cytotoxic effects was investigated. Data presented here found, perhaps unexpectedly, that cell death occurs in response to every CDK inhibitor in 3D and in some cases in 2D culture in glioblastoma cells. Every inhibitor causes cell death in 3D culture, which is observed through the red fluorescence of ethidium homodimer, a cell impermeant dye that intercalates into DNA when cell membranes lack integrity (Figure 3.4). Dinaciclib induces the most cell death as few live cells remain after treatment with any concentration. Milciclib, abemaciclib and PHA-767491 also induce a large amount of cell death, evident through intense ethidium homodimer staining even as concentrations decrease. Palbociclib and CVT-313 are still cytotoxic but allow for growth of much larger spheroids.

Cell death can also be assessed in 2D culture by the total cell number counts during the FUCCI U-87 MG live cell imaging. Through monitoring cell number in live cell imaging experiments, milciclib and palbociclib cause total cell number to drop throughout the experiment, suggesting they cause cell death in 2D culture. Cell death is not observed following incubation with abemaciclib, dinaciclib, CVT-313, or PHA-767491 – this is especially unexpected considering the high potency of dinaciclib suggested by other data. These findings could be because some of the CDK inhibitors are more potent in 3D culture – as seen from the viability data – or that cytotoxic effects only manifest after a longer incubation time, as 3D spheroids were incubated with inhibitors for seven days, whereas live cell imaging experiments inhibitors were only incubated for 16 hours.

Other data also suggest CDK inhibitors induce cell death in glioblastoma cells. Firstly, palbociclib incubation at 12 µM was found to increase the percentage of apoptotic cells in a sample from 4 to 83% (Whittaker *et al.*, 2017). FUCCI U-87 MG live-cell imaging data shows similarly that total cell number decreased by 91% following incubation at 10 µM, suggesting this percentage of cells have died. Here, total cell number reduced by 20% following 5 µM palbociclib incubation. Another study found that just 0.5 µM palbociclib induced apoptosis in 20% of cells during a 24-hour incubation. Data here show palbociclib is cytotoxic even at low concentrations. In addition, abemaciclib was found to induce early apoptosis and dinaciclib to induce necrosis (Riess *et al.*, 2021), despite our findings that dinaciclib was not cytotoxic in 2D. In this experiment inhibitors were incubated for 72 hours, further supporting the theory that glioblastoma cells need to be exposed to CDK inhibition for an extended time (> 16 hours) to experience the cytotoxic effects. Cell death was not observed following abemaciclib treatment in 2D either, however this is likely due to the low number of visible cells in the field of view of the microscope (Figure 3.9 A, B). Finally, PHA-767491 also induced apoptosis in U-87 MG and U-251 MG cell lines at 10 µM (Erbayraktar *et al.*, 2016). To conclude, CDK inhibitors are cytotoxic in 2D and 3D glioblastoma culture, but data suggest they require extended incubation to elicit these effects.

4.4. CDK inhibition gives mixed results in reducing CIZ1 levels

CIZ1 overexpression in cancer has been well documented and has been shown to promote tumourigenesis. Significantly, this tumourigenic effect is reduced through siRNA, shRNA, or miRNA mediated CIZ1 depletion (Table 1.1). CIZ1 overexpression has also been implicated in poor prognoses for glioblastoma patients and shown to be overexpressed in tumour tissue relative to surrounding, healthy tissue (Figure 1.4). Here, we assessed a model proposed by Pauzaite (2019) that suggests CDK phosphorylation of CIZ1 stabilises it throughout the cell cycle, through prevention of UPS mediated degradation of CIZ1. This observation was determined using murine fibroblasts and suggests that CIZ1 levels in glioblastoma cells should respond similarly, where the specific ubiquitin ligase activity is present. Two glioblastoma cell lines were assessed: U-87 MG and BTNW914, using six different CDK inhibitors. In U-87 MG cells, two replicates out of three showed CIZ1 reduction in response to every CDK inhibitor, on average (Figure 3.14). The final replicate showed anomalous

results, where almost every inhibitor caused a CIZ1 increase (Figure 3.14 B, E). A similar trend for BTNW914 saw two replicates revealing a CIZ1 reduction in response to inhibitor treatment, and one showing an increase (Figure 3.16). The inconsistent data are inconclusive, and more analyses of the effects of CDK inhibition on CIZ1 levels are required. More replicates would potentially identify the statistical differences before and after treatment.

CIZ1 levels have been assessed in response to CDK inhibition previously. Of those studied, PHA-767491 and CVT-313 show the most convincing data in reducing CIZ1. Both have shown to significantly ($p<0.05$) reduce CIZ1 in PC-3 (prostatic adenocarcinoma) and SW480 (colorectal cancer) cell lines (Pauzaite, 2019). Also, both show an insignificant CIZ1 reduction in NIH/3T3 (mouse embryonic fibroblasts) cells (Caprani, 2022). When assessed in glioblastoma, Falkingham (2021) suggested a CIZ1 reduction in BTNW914 following PHA-767491 treatment, but provided no statistical analysis, and observed no effect in U-87 MG cells. CVT-313 also showed no effect on CIZ1 in BTNW914 or U-87 MG. Another study demonstrated an insignificant reduction in CIZ1 following PHA-767491 and CVT-313 treatments (Iwanowytsch, 2023). Here, PHA-767491 caused an insignificant CIZ1 reduction in BTNW914 and U-87 MG, whereas CVT-313 resulted in a CIZ1 increase in cell lines. These inhibitors have generated an array of conflicting data.

Palbociclib also resulted in an insignificant CIZ1 reduction in NIH/3T3 fibroblasts (Caprani, 2022) and in BTNW914 (Iwanowytsch, 2023; Falkingham, 2021), but showed no effect in U-87 MG (Falkingham, 2021). Here, palbociclib produced differential effects in U-87 MG and BTNW914 cells. Palbociclib treatment led to an insignificant increase in CIZ1 levels in BTNW914 and decrease in U-87 MG.

These studies also investigated the effect of other CDK inhibitors: roscovitine (Cdc2, CDK2, CDK5 inhibitor), Ro3306 (CDK2 inhibitor), and CDK2-IN-73 (cyclin A/CDK2 inhibitor) that all showed insignificant reductions or no effect on CIZ1 in glioblastoma. The mixed data in this area (increases, reductions, no effects) suggest a more complex relationship, potentially dependent on specific CDKs and/or cell cycle phase. Interestingly, Pauzaite (2019) showed the effects of CDK inhibitors in cell cycle synchronised NIH/3T3 cells. In this context there

were significant effects on CIZ1 levels that correlated with cell cycle phase where CDK2 inhibition with CVT-313, PHA-767491, and roscovitine effectively reduced CIZ1 levels. This was also supported by siRNA targeting cyclin E1 and cyclin E2 or cyclin A2 alone that effectively reduced CIZ1 levels. Importantly this was reversed by proteosome inhibition with MG132, consistent with proteosome mediated degradation. The data presented here suggest that the effects are either more inconsistent in glioblastoma cells, or perhaps there are alterations to the expression of either phosphatases that have been shown to regulate CIZ1 phosphorylation status (Pauzaite, 2019), modulation of E3 ligase activity or potentially deubiquitinase (DUB) activity. Further work in genetically distinct cell lines may resolve some of these questions.

Further development of the methodology within this thesis would prove insightful. For example, using multiple dosing throughout an incubation compared to one single dose at the start may show distinct effects. Extending the incubation of FUCCI U-87 MG live cell imaging experiments may also reveal an optimal incubation and concentration for each inhibitor to observe cell cycle effects. Also, using these newly developed FUCCI U-87 MG cells to create 3D spheroid cultures would allow similar assessment of cell cycle effects in 3D, which could be compared with 2D data. A mass spectrometry experiment assessing the phosphorylation status of CIZ1 in untreated and CDK inhibitor treated glioblastoma samples may reveal more information of the proposed model of CIZ1 regulation in glioblastoma.

Investigating how CDK inhibition complemented other standard glioblastoma treatments (TMZ, radiotherapy, TTFields) would be insightful. CDK inhibition may slow/arrest the cell cycle of glioblastoma cells, allowing other therapies more opportunity to exert cytotoxic effects. A future direction of this work could be to identify synergy between CDK inhibition and the new TTFields therapy.

Limitations of this work include the absence of a patient-derived 3D model. Immortalised and patient-derived 2D cultures show differing responses to CDK inhibition, so not being able to compare these in 3D is a weakness, here. Also, measuring the potency of CDK inhibitors in 3D culture through measurement of spheroid diameters was perhaps an

inaccurate method. After live/dead staining, it was apparent that some dead cells were being part of the measurements, resulting in falsely high IC_{50} estimations by GraphPad.

Here, we show that a panel of CDK inhibitors are effective at treating glioblastoma *in vitro*. This efficacy should now be investigated in preclinical animal models to further the advancement of this therapy to the clinic. Also, variation in the effects of CDK inhibitors across cell lines has been demonstrated here and elsewhere. Screening a panel of patient-derived glioblastoma cell lines for relative CIZ1 expression and relating this to their response to CDK inhibition may reveal the reasons for the variations in responses and also determine the relationship between CDK activity, CIZ1 expression, and tumourigenesis in glioblastoma.

5. Conclusion

In summary, the link between CIZ1 expression and CDK inhibition in glioblastoma is unclear and needs further investigation. However, CDK inhibitors are potent inhibitors of cellular proliferation and induce cytotoxic and cytostatic effects. These data support further investigation of CDK inhibition in glioblastoma in pre-clinical animal models to determine its efficacy in more sophisticated models.

6. Bibliography

Addgene (2017) *Bacterial Transformation*. Protocols. Available at: https://www.addgene.org/protocols/bacterial-transformation/ (Accessed: 24th August 2024).

Agnihotri, S., Gajadhar, A. S., Ternamian, C., Gorlia, T., Diefes, K. L., Mischel, P. S., Kelly, J., McGown, G., Thorncroft, M., Carlson, B. L., Sarkaria, J. N., Margison, G. P., Aldape, K., Hawkins, C., Hegi, M. and Guha, A. (2012) 'Alkylpurine-DNA-N-glycosylase confers resistance to temozolomide in xenograft models of glioblastoma multiforme and is associated with poor survival in patients', *J Clin Invest,* 122(1), pp. 253-66.

Ainscough, J. F., Rahman, F. A., Sercombe, H., Sedo, A., Gerlach, B. and Coverley, D. (2007) 'C-terminal domains deliver the DNA replication factor Ciz1 to the nuclear matrix', *J Cell Sci,* 120(Pt 1), pp. 115-24.

Albanese, C., Alzani, R., Amboldi, N., Degrassi, A., Festuccia, C., Fiorentini, F., Gravina, G., Mercurio, C., Pastori, W., Brasca, M., Pesenti, E., Galvani, A. and Ciomei, M. (2013) 'Anti-tumour efficacy on glioma models of PHA-848125, a multi-kinase inhibitor able to cross the blood-brain barrier', *Br J Pharmacol,* 169(1), pp. 156-66.

Alifieris, C. and Trafalis, D. T. (2015) 'Glioblastoma multiforme: Pathogenesis and treatment', *Pharmacol Ther,* 152, pp. 63-82.

Auffinger, B., Tobias, A. L., Han, Y., Lee, G., Guo, D., Dey, M., Lesniak, M. S. and Ahmed, A. U. (2014) 'Conversion of differentiated cancer cells into cancer stem-like cells in a glioblastoma model after primary chemotherapy', *Cell Death Differ,* 21(7), pp. 1119-31.

Banko, M. I., Krzyzanowski, M. K., Turcza, P., Maniecka, Z., Kulis, M. and Kozlowski, P. (2013) 'Identification of amino acid residues of ERH required for its recruitment to nuclear speckles and replication foci in HeLa cells', *PLoS One,* 8(8), pp. e74885.

Bhagwat, S. V., McMillen, W. T., Cai, S., Zhao, B., Whitesell, M., Shen, W., Kindler, L., Flack, R. S., Wu, W., Anderson, B., Zhai, Y., Yuan, X. J., Pogue, M., Van Horn, R. D., Rao, X., McCann, D., Dropsey, A. J., Manro, J., Walgren, J., Yuen, E., Rodriguez, M. J., Plowman, G. D., Tiu, R. V., Joseph, S. and Peng, S. B. (2020) 'ERK Inhibitor LY3214996 Targets ERK Pathway-Driven Cancers: A Therapeutic Approach Toward Precision Medicine', *Mol Cancer Ther,* 19(2), pp. 325-336.

Bolin, S., Borgenvik, A., Persson, C. U., Sundström, A., Qi, J., Bradner, J. E., Weiss, W. A., Cho, Y. J., Weishaupt, H. and Swartling, F. J. (2018) 'Combined BET bromodomain and CDK2 inhibition in MYC-driven medulloblastoma', *Oncogene,* 37(21), pp. 2850-2862.

Brasca, M. G., Amboldi, N., Ballinari, D., Cameron, A., Casale, E., Cervi, G., Colombo, M., Colotta, F., Croci, V., D'Alessio, R., Fiorentini, F., Isacchi, A., Mercurio, C., Moretti, W., Panzeri, A., Pastori, W., Pevarello, P., Quartieri, F., Roletto, F., Traquandi, G., Vianello, P., Vulpetti, A. and Ciomei, M. (2009) 'Identification of N,1,4,4-tetramethyl-8-{[4-(4-

methylpiperazin-1-yl)phenyl]amino}-4,5-dihydro-1H-pyrazolo[4,3-h]quinazoline-3-carboxamide (PHA-848125), a potent, orally available cyclin dependent kinase inhibitor', *J Med Chem,* 52(16), pp. 5152-63.

Brennan, C. W., Verhaak, R. G., McKenna, A., Campos, B., Noushmehr, H., Salama, S. R., Zheng, S., Chakravarty, D., Sanborn, J. Z., Berman, S. H., Beroukhim, R., Bernard, B., Wu, C. J., Genovese, G., Shmulevich, I., Barnholtz-Sloan, J., Zou, L., Vegesna, R., Shukla, S. A., Ciriello, G., Yung, W. K., Zhang, W., Sougnez, C., Mikkelsen, T., Aldape, K., Bigner, D. D., Van Meir, E. G., Prados, M., Sloan, A., Black, K. L., Eschbacher, J., Finocchiaro, G., Friedman, W., Andrews, D. W., Guha, A., Iacocca, M., O'Neill, B. P., Foltz, G., Myers, J., Weisenberger, D. J., Penny, R., Kucherlapati, R., Perou, C. M., Hayes, D. N., Gibbs, R., Marra, M., Mills, G. B., Lander, E., Spellman, P., Wilson, R., Sander, C., Weinstein, J., Meyerson, M., Gabriel, S., Laird, P. W., Haussler, D., Getz, G. and Chin, L. (2013) 'The somatic genomic landscape of glioblastoma', *Cell,* 155(2), pp. 462-77.

Brooks, E. E., Gray, N. S., Joly, A., Kerwar, S. S., Lum, R., Mackman, R. L., Norman, T. C., Rosete, J., Rowe, M., Schow, S. R., Schultz, P. G., Wang, X., Wick, M. M. and Shiffman, D. (1997) 'CVT-313, a specific and potent inhibitor of CDK2 that prevents neointimal proliferation', *J Biol Chem,* 272(46), pp. 29207-11.

Brown, C. J., Ballabio, A., Rupert, J. L., Lafreniere, R. G., Grompe, M., Tonlorenzi, R. and Willard, H. F. (1991) 'A gene from the region of the human X inactivation centre is expressed exclusively from the inactive X chromosome', *Nature,* 349(6304), pp. 38-44.

Cahill, D. P., Levine, K. K., Betensky, R. A., Codd, P. J., Romany, C. A., Reavie, L. B., Batchelor, T. T., Futreal, P. A., Stratton, M. R., Curry, W. T., Iafrate, A. J. and Louis, D. N. (2007) 'Loss of the mismatch repair protein MSH6 in human glioblastomas is associated with tumor progression during temozolomide treatment', *Clin Cancer Res,* 13(7), pp. 2038-45.

Caprani, L. (2022) *Analysis of the role of CDK and ubiquitin E3 ligase activity in regulation of CIZ1 proteostasis.* MSc by Research, Lancaster University.

Celiku, O., Gilbert, M. R. and Lavi, O. (2019) 'Computational modeling demonstrates that glioblastoma cells can survive spatial environmental challenges through exploratory adaptation', *Nat Commun,* 10(1), pp. 5704.

Chakrabarti, I., Cockburn, M., Cozen, W., Wang, Y. P. and Preston-Martin, S. (2005) 'A population-based description of glioblastoma multiforme in Los Angeles County, 1974-1999', *Cancer,* 104(12), pp. 2798-806.

Chen, X., Wang, P., Wang, S., Li, J., Ou, T. and Zeng, X. (2019) 'CIZ1 knockdown suppresses the proliferation of bladder cancer cells by inducing apoptosis', *Gene,* 719, pp. 143946.

Chen, Y. R., Wu, Y. S., Wang, W. S., Zhang, J. S. and Wu, Q. G. (2020) 'Upregulation of lncRNA DANCR functions as an oncogenic role in non-small lung cancer by regulating miR-214-5p/CIZ1 axis', *Eur Rev Med Pharmacol Sci,* 24(5), pp. 2539-2547.

Copeland, N. A., Sercombe, H. E., Ainscough, J. F. and Coverley, D. (2010) 'Ciz1 cooperates with cyclin-A-CDK2 to activate mammalian DNA replication in vitro', *J Cell Sci,* 123(Pt 7), pp. 1108-15.

Copeland, N. A., Sercombe, H. E., Wilson, R. H. and Coverley, D. (2015) 'Cyclin-A-CDK2-mediated phosphorylation of CIZ1 blocks replisome formation and initiation of mammalian DNA replication', *J Cell Sci,* 128(8), pp. 1518-27.

Coverley, D., Higgins, G., West, D., Jackson, O. T., Dowle, A., Haslam, A., Ainscough, E., Chalkley, R. and White, J. (2017) 'A quantitative immunoassay for lung cancer biomarker CIZ1b in patient plasma', *Clin Biochem,* 50(6), pp. 336-343.

Coverley, D., Laman, H. and Laskey, R. A. (2002) 'Distinct roles for cyclins E and A during DNA replication complex assembly and activation', *Nat Cell Biol,* 4(7), pp. 523-8.

Coverley, D., Marr, J. and Ainscough, J. (2005) 'Ciz1 promotes mammalian DNA replication', *J Cell Sci,* 118(Pt 1), pp. 101-12.

den Hollander, P. and Kumar, R. (2006) 'Dynein light chain 1 contributes to cell cycle progression by increasing cyclin-dependent kinase 2 activity in estrogen-stimulated cells', *Cancer Res,* 66(11), pp. 5941-9.

den Hollander, P., Rayala, S. K., Coverley, D. and Kumar, R. (2006) 'Ciz1, a Novel DNA-binding coactivator of the estrogen receptor alpha, confers hypersensitivity to estrogen action', *Cancer Res,* 66(22), pp. 11021-9.

Dick, T., Ray, K., Salz, H. K. and Chia, W. (1996) 'Cytoplasmic dynein (ddlc1) mutations cause morphogenetic defects and apoptotic cell death in Drosophila melanogaster', *Mol Cell Biol,* 16(5), pp. 1966-77.

Dobbs, O. G., Wilson, R. H. C., Newling, K., Ainscough, J. F. and Coverley, D. (2023) 'Epigenetic instability caused by absence of CIZ1 drives transformation during quiescence cycles', *BMC Biol,* 21(1), pp. 175.

Erbayraktar, Z., Alural, B., Erbayraktar, R. S. and Erkan, E. P. (2016) 'Cell division cycle 7-kinase inhibitor PHA-767491 hydrochloride suppresses glioblastoma growth and invasiveness', *Cancer Cell Int,* 16, pp. 88.

Faber, A. C. and Chiles, T. C. (2007) 'Inhibition of cyclin-dependent kinase-2 induces apoptosis in human diffuse large B-cell lymphomas', *Cell Cycle,* 6(23), pp. 2982-9.

Falkingham, N. (2021) *Evaluation of CIZ1 as a biomarker for neurological tumours.* MSc by Research, Lancaster University.

Fan, Y., Zhang, B., Du, X., Wang, B., Yan, Q., Guo, L. and Yao, W. (2024) 'Regulating Tumorigenicity and Cancer Metastasis through TRKA Signaling', *Curr Cancer Drug Targets,* 24(3), pp. 271-287.

Finn, R. S., Crown, J. P., Lang, I., Boer, K., Bondarenko, I. M., Kulyk, S. O., Ettl, J., Patel, R., Pinter, T., Schmidt, M., Shparyk, Y., Thummala, A. R., Voytko, N. L., Fowst, C., Huang, X., Kim, S. T., Randolph, S. and Slamon, D. J. (2015) 'The cyclin-dependent kinase 4/6 inhibitor palbociclib in combination with letrozole versus letrozole alone as first-line treatment of oestrogen receptor-positive, HER2-negative, advanced breast cancer (PALOMA-1/TRIO-18): a randomised phase 2 study', *Lancet Oncol,* 16(1), pp. 25-35.

Finn, R. S., Martin, M., Rugo, H. S., Jones, S., Im, S. A., Gelmon, K., Harbeck, N., Lipatov, O. N., Walshe, J. M., Moulder, S., Gauthier, E., Lu, D. R., Randolph, S., Diéras, V. and Slamon, D. J. (2016) 'Palbociclib and Letrozole in Advanced Breast Cancer', *N Engl J Med,* 375(20), pp. 1925-1936.

Fleury, A., Menegoz, F., Grosclaude, P., Daures, J. P., Henry-Amar, M., Raverdy, N., Schaffer, P., Poisson, M. and Delattre, J. Y. (1997) 'Descriptive epidemiology of cerebral gliomas in France', *Cancer,* 79(6), pp. 1195-202.

FPbase (2024a) *mCerulean*. Available at: https://www.fpbase.org/protein/mcerulean/ (Accessed: 24th August 2024).

FPbase (2024b) *mCherry*. Available at: https://www.fpbase.org/protein/mcherry/ (Accessed: 24th August 2024).

FPbase (2024c) *mVenus*. Available at: https://www.fpbase.org/protein/mvenus/ (Accessed: 24th August 2024).

Freitag, T., Kaps, P., Ramtke, J., Bertels, S., Zunke, E., Schneider, B., Becker, A. S., Koczan, D., Dubinski, D., Freiman, T. M., Wittig, F., Hinz, B., Westhoff, M. A., Strobel, H., Meiners, F., Wolter, D., Engel, N., Troschke-Meurer, S., Bergmann-Ewert, W., Staehlke, S., Wolff, A., Gessler, F., Junghanss, C. and Maletzki, C. (2024) 'Combined inhibition of EZH2 and CDK4/6 perturbs endoplasmic reticulum-mitochondrial homeostasis and increases antitumor activity against glioblastoma', *NPJ Precis Oncol,* 8(1), pp. 156.

Fry, D. W., Harvey, P. J., Keller, P. R., Elliott, W. L., Meade, M., Trachet, E., Albassam, M., Zheng, X., Leopold, W. R., Pryer, N. K. and Toogood, P. L. (2004) 'Specific inhibition of cyclin-dependent kinase 4/6 by PD 0332991 and associated antitumor activity in human tumor xenografts', *Mol Cancer Ther,* 3(11), pp. 1427-38.

Gelbert, L. M., Cai, S., Lin, X., Sanchez-Martinez, C., Del Prado, M., Lallena, M. J., Torres, R., Ajamie, R. T., Wishart, G. N., Flack, R. S., Neubauer, B. L., Young, J., Chan, E. M., Iversen, P., Cronier, D., Kreklau, E. and de Dios, A. (2014) 'Preclinical characterization of the CDK4/6 inhibitor LY2835219: in-vivo cell cycle-dependent/independent anti-tumor activities alone/in combination with gemcitabine', *Invest New Drugs,* 32(5), pp. 825-37.

Ghia, P., Scarfò, L., Perez, S., Pathiraja, K., Derosier, M., Small, K., McCrary Sisk, C. and Patton, N. (2017) 'Efficacy and safety of dinaciclib vs ofatumumab in patients with relapsed/refractory chronic lymphocytic leukemia', *Blood: Vol. 13*. United States, pp. 1876-1878.

Goetz, M. P., Toi, M., Campone, M., Sohn, J., Paluch-Shimon, S., Huober, J., Park, I. H., Trédan, O., Chen, S. C., Manso, L., Freedman, O. C., Garnica Jaliffe, G., Forrester, T., Frenzel, M., Barriga, S., Smith, I. C., Bourayou, N. and Di Leo, A. (2017) 'MONARCH 3: Abemaciclib As Initial Therapy for Advanced Breast Cancer', *J Clin Oncol,* 35(32), pp. 3638-3646.

Gong, X., Schwartz, P. H., Linskey, M. E. and Bota, D. A. (2011) 'Neural stem/progenitors and glioma stem-like cells have differential sensitivity to chemotherapy', *Neurology,* 76(13), pp. 1126-34.

Hegi, M. E., Diserens, A. C., Gorlia, T., Hamou, M. F., de Tribolet, N., Weller, M., Kros, J. M., Hainfellner, J. A., Mason, W., Mariani, L., Bromberg, J. E., Hau, P., Mirimanoff, R. O., Cairncross, J. G., Janzer, R. C. and Stupp, R. (2005) 'MGMT gene silencing and benefit from temozolomide in glioblastoma', *N Engl J Med,* 352(10), pp. 997-1003.

Higgins, G., Roper, K. M., Watson, I. J., Blackhall, F. H., Rom, W. N., Pass, H. I., Ainscough, J. F. and Coverley, D. (2012) 'Variant Ciz1 is a circulating biomarker for early-stage lung cancer', *Proc Natl Acad Sci U S A,* 109(45), pp. E3128-35.

Hodges, L. C., Smith, J. L., Garrett, A. and Tate, S. (1992) 'Prevalence of glioblastoma multiforme in subjects with prior therapeutic radiation', *J Neurosci Nurs,* 24(2), pp. 79-83.

Hortobagyi, G. N., Stemmer, S. M., Burris, H. A., Yap, Y. S., Sonke, G. S., Paluch-Shimon, S., Campone, M., Blackwell, K. L., André, F., Winer, E. P., Janni, W., Verma, S., Conte, P., Arteaga, C. L., Cameron, D. A., Petrakova, K., Hart, L. L., Villanueva, C., Chan, A., Jakobsen, E., Nusch, A., Burdaeva, O., Grischke, E. M., Alba, E., Wist, E., Marschner, N., Favret, A. M., Yardley, D., Bachelot, T., Tseng, L. M., Blau, S., Xuan, F., Souami, F., Miller, M., Germa, C., Hirawat, S. and O'Shaughnessy, J. (2016) 'Ribociclib as First-Line Therapy for HR-Positive, Advanced Breast Cancer', *N Engl J Med,* 375(18), pp. 1738-1748.

Hortobagyi, G. N., Stemmer, S. M., Burris, H. A., Yap, Y. S., Sonke, G. S., Paluch-Shimon, S., Campone, M., Petrakova, K., Blackwell, K. L., Winer, E. P., Janni, W., Verma, S., Conte, P., Arteaga, C. L., Cameron, D. A., Mondal, S., Su, F., Miller, M., Elmeliegy, M., Germa, C. and O'Shaughnessy, J. (2018) 'Updated results from MONALEESA-2, a phase III trial of first-line ribociclib plus letrozole versus placebo plus letrozole in hormone receptor-positive, HER2-negative advanced breast cancer', *Ann Oncol,* 29(7), pp. 1541-1547.

Hsieh, T. H., Liang, M. L., Zheng, J. H., Lin, Y. C., Yang, Y. C., Vo, T. H., Liou, J. P., Yen, Y. and Chen, C. H. (2021) 'Combining an Autophagy Inhibitor, MPT0L145, with Abemaciclib Is a New Therapeutic Strategy in GBM Treatment', *Cancers (Basel),* 13(23).

Huggett, M. T., Tudzarova, S., Proctor, I., Loddo, M., Keane, M. G., Stoeber, K., Williams, G. H. and Pereira, S. P. (2016) 'Cdc7 is a potent anti-cancer target in pancreatic cancer due to abrogation of the DNA origin activation checkpoint', *Oncotarget,* 7(14), pp. 18495-507.

Hwang, C. Y., Lee, S. M., Park, S. S. and Kwon, K. S. (2012) 'CDK2 differentially controls normal cell senescence and cancer cell proliferation upon exposure to reactive oxygen species', *Biochem Biophys Res Commun,* 425(1), pp. 94-9.

Im, S. A., Lu, Y. S., Bardia, A., Harbeck, N., Colleoni, M., Franke, F., Chow, L., Sohn, J., Lee, K. S., Campos-Gomez, S., Villanueva-Vazquez, R., Jung, K. H., Chakravartty, A., Hughes, G., Gounaris, I., Rodriguez-Lorenc, K., Taran, T., Hurvitz, S. and Tripathy, D. (2019) 'Overall Survival with Ribociclib plus Endocrine Therapy in Breast Cancer', *N Engl J Med,* 381(4), pp. 307-316.

Information, N. C. f. B. (2024) *PubChem Compound Summary for CID 5394, Temozolomide*. Available at: https://pubchem.ncbi.nlm.nih.gov/compound/Temozolomide (Accessed: 14th August 2024 2024).

Iwanowytsch, O. (2023) *Ciz1 as a biomarker and drug target in Glioblastoma multiforme.* MSc by Research, Lancaster University.

Jackson, M. R., Richards, A. R., Oladipupo, A. A., Chahal, S. K., Caragher, S., Chalmers, A. J. and Gomez-Roman, N. (2024) 'ClonoScreen3D - A Novel 3-Dimensional Clonogenic Screening Platform for Identification of Radiosensitizers for Glioblastoma', *Int J Radiat Oncol Biol Phys,* 120(1), pp. 162-177.

Kanbur, E., Baykal, A. T. and Yerlikaya, A. (2021) 'Molecular analysis of cell survival and death pathways in the proteasome inhibitor bortezomib-resistant PC3 prostate cancer cell line', *Med Oncol,* 38(9), pp. 112.

Kawaguchi, K., Otani, R., Kikuchi, M., Kushihara, Y., Funata, N., Yamada, R. and Shinoura, N. (2021) 'Genetic Characteristics of Mismatch Repair-deficient Glioblastoma', *NMC Case Rep J: Vol. 1*. Japan: © 2021 The Japan Neurosurgical Society., pp. 565-571.

Khanam, M., Moin, A. T., Ahmed, K. A., Patil, R. B., Ripon Khalipha, A. B., Ahmed, N., Bagchi, R., Ullah, M. A., Ferdoush, J., Islam, S. and Rudra, B. (2022) 'Computational modeling of potential milciclib derivatives inhibitor-CDK2 binding through global docking and accelerated molecular dynamics simulations', *Informatics in Medicine Unlocked,* 33, pp. 101069.

Klein-Hitpass, L., Schorpp, M., Wagner, U. and Ryffel, G. U. (1986) 'An estrogen-responsive element derived from the 5' flanking region of the Xenopus vitellogenin A2 gene functions in transfected human cells', *Cell,* 46(7), pp. 1053-61.

Kozlowski, P. (2023) 'Thirty Years with ERH: An mRNA Splicing and Mitosis Factor Only or Rather a Novel Genome Integrity Protector?', *Cells,* 12(20).

La Starza, R., Pierini, T. and Metro, G. (2019) *MGMT Promoter Methylation in Glioma: ESMO Biomarker Factsheet*. Factsheets on Biomarkers. ESMO OncologyPRO: EMSO. Available at: https://oncologypro.esmo.org/education-library/factsheets-on-biomarkers/mgmt-promoter-methylation-in-glioma (Accessed: 23rd August 2024).

Lacroix, M., Abi-Said, D., Fourney, D. R., Gokaslan, Z. L., Shi, W., DeMonte, F., Lang, F. F., McCutcheon, I. E., Hassenbusch, S. J., Holland, E., Hess, K., Michael, C., Miller, D. and Sawaya, R. (2001) 'A multivariate analysis of 416 patients with glioblastoma multiforme: prognosis, extent of resection, and survival', *J Neurosurg,* 95(2), pp. 190-8.

Laperriere, N., Zuraw, L. and Cairncross, G. (2002) 'Radiotherapy for newly diagnosed malignant glioma in adults: a systematic review', *Radiother Oncol,* 64(3), pp. 259-73.

Lee, S. Y. (2016) 'Temozolomide resistance in glioblastoma multiforme', *Genes Dis,* 3(3), pp. 198-210.

Lee, T., Di Paola, D., Malina, A., Mills, J. R., Kreps, A., Grosse, F., Tang, H., Zannis-Hadjopoulos, M., Larsson, O. and Pelletier, J. (2014) 'Suppression of the DHX9 helicase induces premature senescence in human diploid fibroblasts in a p53-dependent manner', *J Biol Chem,* 289(33), pp. 22798-22814.

Lee, T. and Pelletier, J. (2016) 'The biology of DHX9 and its potential as a therapeutic target', *Oncotarget,* 7(27), pp. 42716-42739.

Lei, L., Wu, J., Gu, D., Liu, H. and Wang, S. (2016) 'CIZ1 interacts with YAP and activates its transcriptional activity in hepatocellular carcinoma cells', *Tumour Biol,* 37(8), pp. 11073-9.

Li, W., Zhao, X. L., Shang, S. Q., Shen, H. Q. and Chen, X. (2015) 'Dual Inhibition of Cdc7 and Cdk9 by PHA-767491 Suppresses Hepatocarcinoma Synergistically with 5-Fluorouracil', *Curr Cancer Drug Targets,* 15(3), pp. 196-204.

Li, Y., Zhou, X., Liu, J., Gao, N., Yang, R., Wang, Q., Ji, J., Ma, L. and He, Q. (2020) 'Dihydroartemisinin inhibits the tumorigenesis and metastasis of breast cancer via downregulating CIZ1 expression associated with TGF-β1 signaling', *Life Sci,* 248, pp. 117454.

Li, Z., Zhang, J., Zheng, H., Li, C., Xiong, J., Wang, W., Bao, H., Jin, H. and Liang, P. (2019) 'Modulating lncRNA SNHG15/CDK6/miR-627 circuit by palbociclib, overcomes temozolomide resistance and reduces M2-polarization of glioma associated microglia in glioblastoma multiforme', *J Exp Clin Cancer Res,* 38(1), pp. 380.

Liu, B., Guo, Z., Dong, H., Daofeng, T., Cai, Q., Ji, B., Zhang, S., Wu, L., Wang, J., Wang, L., Zhu, X., Liu, Y. and Chen, Q. (2015a) 'LRIG1, human EGFR inhibitor, reverses multidrug resistance through modulation of ABCB1 and ABCG2', *Brain Res,* 1611, pp. 93-100.

Liu, H. Y., Tuckett, A. Z., Fennell, M., Garippa, R. and Zakrzewski, J. L. (2018a) 'Repurposing of the CDK inhibitor PHA-767491 as a NRF2 inhibitor drug candidate for cancer therapy via redox modulation', *Invest New Drugs,* 36(4), pp. 590-600.

Liu, J., Zhang, X., Chen, G., Shao, Q., Zou, Y., Li, Z., Su, H., Li, M. and Xu, Y. (2023) 'Drug repurposing and structure-based discovery of new PDE4 and PDE5 inhibitors', *Eur J Med Chem,* 262, pp. 115893.

Liu, S., Tang, Y., Yuan, X., Yuan, D., Liu, J., Li, B. and Li, Y. (2018b) 'Inhibition of Rb and mTOR signaling associates with synergistic anticancer effect of palbociclib and erlotinib in glioblastoma cells', *Invest New Drugs,* 36(6), pp. 961-969.

Liu, T., Ren, X., Li, L., Yin, L., Liang, K., Yu, H., Ren, H., Zhou, W., Jing, H. and Kong, C. (2015b) 'Ciz1 promotes tumorigenicity of prostate carcinoma cells', *Front Biosci (Landmark Ed),* 20(4), pp. 705-15.

Louis, D. N., Perry, A., Wesseling, P., Brat, D. J., Cree, I. A., Figarella-Branger, D., Hawkins, C., Ng, H. K., Pfister, S. M., Reifenberger, G., Soffietti, R., von Deimling, A. and Ellison, D. W. (2021) 'The 2021 WHO Classification of Tumors of the Central Nervous System: a summary', *Neuro Oncol,* 23(8), pp. 1231-1251.

Lukasik, A., Uniewicz, K. A., Kulis, M. and Kozlowski, P. (2008) 'Ciz1, a p21 cip1/Waf1-interacting zinc finger protein and DNA replication factor, is a novel molecular partner for human enhancer of rudimentary homolog', *Febs j,* 275(2), pp. 332-40.

Lyon, M. F. (1961) 'Gene action in the X-chromosome of the mouse (Mus musculus L.)', *Nature,* 190, pp. 372-3.

Manikandan, C. and Jaiswal, A. K. (2023) 'Scaffold-based spheroid models of glioblastoma multiforme and its use in drug screening', *Biotechnol Bioeng,* 120(8), pp. 2117-2132.

McKinley, B. P., Michalek, A. M., Fenstermaker, R. A. and Plunkett, R. J. (2000) 'The impact of age and sex on the incidence of glial tumors in New York state from 1976 to 1995', *J Neurosurg,* 93(6), pp. 932-9.

McLaughlin, R. P., He, J., van der Noord, V. E., Redel, J., Foekens, J. A., Martens, J. W. M., Smid, M., Zhang, Y. and van de Water, B. (2019) 'A kinase inhibitor screen identifies a dual cdc7/CDK9 inhibitor to sensitise triple-negative breast cancer to EGFR-targeted therapy', *Breast Cancer Res,* 21(1), pp. 77.

Mitsui, K., Matsumoto, A., Ohtsuka, S., Ohtsubo, M. and Yoshimura, A. (1999) 'Cloning and characterization of a novel p21(Cip1/Waf1)-interacting zinc finger protein, ciz1', *Biochem Biophys Res Commun,* 264(2), pp. 457-64.

Mojas, N., Lopes, M. and Jiricny, J. (2007) 'Mismatch repair-dependent processing of methylation damage gives rise to persistent single-stranded gaps in newly replicated DNA', *Genes Dev,* 21(24), pp. 3342-55.

Montagnoli, A., Valsasina, B., Croci, V., Menichincheri, M., Rainoldi, S., Marchesi, V., Tibolla, M., Tenca, P., Brotherton, D., Albanese, C., Patton, V., Alzani, R., Ciavolella, A., Sola, F., Molinari, A., Volpi, D., Avanzi, N., Fiorentini, F., Cattoni, M., Healy, S., Ballinari, D., Pesenti, E., Isacchi, A., Moll, J., Bensimon, A., Vanotti, E. and Santocanale, C. (2008) 'A Cdc7 kinase inhibitor restricts initiation of DNA replication and has antitumor activity', *Nat Chem Biol,* 4(6), pp. 357-65.

Moya, I. M. and Halder, G. (2019) 'Hippo-YAP/TAZ signalling in organ regeneration and regenerative medicine', *Nat Rev Mol Cell Biol,* 20(4), pp. 211-226.

Narod, S. A., Stiller, C. and Lenoir, G. M. (1991) 'An estimate of the heritable fraction of childhood cancer', *Br J Cancer,* 63(6), pp. 993-9.

Natoni, A., Coyne, M. R., Jacobsen, A., Rainey, M. D., O'Brien, G., Healy, S., Montagnoli, A., Moll, J., O'Dwyer, M. and Santocanale, C. (2013) 'Characterization of a Dual CDC7/CDK9 Inhibitor in Multiple Myeloma Cellular Models', *Cancers (Basel),* 5(3), pp. 901-18.

Natoni, A., Murillo, L. S., Kliszczak, A. E., Catherwood, M. A., Montagnoli, A., Samali, A., O'Dwyer, M. and Santocanale, C. (2011) 'Mechanisms of action of a dual Cdc7/Cdk9 kinase inhibitor against quiescent and proliferating CLL cells', *Mol Cancer Ther,* 10(9), pp. 1624-34.

NCBI (2024) *PubChem Compound Summary for CID 46926350, Dinaciclib*. Available at: https://pubchem.ncbi.nlm.nih.gov/compound/Dinaciclib (Accessed: 1st September 2024).

Nishibe, R., Watanabe, W., Ueda, T., Yamasaki, N., Koller, R., Wolff, L., Honda, Z., Ohtsubo, M. and Honda, H. (2013) 'CIZ1, a p21Cip1/Waf1-interacting protein, functions as a tumor suppressor in vivo', *FEBS Lett,* 587(10), pp. 1529-35.

Nishikawa, R., Yamasaki, F., Arakawa, Y., Muragaki, Y., Narita, Y., Tanaka, S., Yamaguchi, S., Mukasa, A. and Kanamori, M. (2023) 'Safety and efficacy of tumour-treating fields (TTFields) therapy for newly diagnosed glioblastoma in Japanese patients using the Novo-TTF System: a prospective post-approval study', *Jpn J Clin Oncol,* 53(5), pp. 371-377.

Okur, E. and Yerlikaya, A. (2019) 'A novel and effective inhibitor combination involving bortezomib and OTSSP167 for breast cancer cells in light of label-free proteomic analysis', *Cell Biol Toxicol,* 35(1), pp. 33-47.

Ostrom, Q. T., Gittleman, H., Farah, P., Ondracek, A., Chen, Y., Wolinsky, Y., Stroup, N. E., Kruchko, C. and Barnholtz-Sloan, J. S. (2013) 'CBTRUS statistical report: Primary brain and central nervous system tumors diagnosed in the United States in 2006-2010', *Neuro Oncol,* 15 Suppl 2(Suppl 2), pp. ii1-56.

Pan, B., Wan, T., Zhou, Y., Huang, S., Yuan, L., Jiang, Y., Zheng, X., Liu, P., Xiang, H., Ju, M., Luo, R., Jia, W., Lan, C., Li, J. and Zheng, M. (2023) 'The MYBL2-CCL2 axis promotes tumor progression and resistance to anti-PD-1 therapy in ovarian cancer by inducing immunosuppressive macrophages', *Cancer Cell Int,* 23(1), pp. 248.

Parry, D., Guzi, T., Shanahan, F., Davis, N., Prabhavalkar, D., Wiswell, D., Seghezzi, W., Paruch, K., Dwyer, M. P., Doll, R., Nomeir, A., Windsor, W., Fischmann, T., Wang, Y., Oft, M., Chen, T., Kirschmeier, P. and Lees, E. M. (2010) 'Dinaciclib (SCH 727965), a novel and potent cyclin-dependent kinase inhibitor', *Mol Cancer Ther,* 9(8), pp. 2344-53.

Parsons, D. W., Jones, S., Zhang, X., Lin, J. C., Leary, R. J., Angenendt, P., Mankoo, P., Carter, H., Siu, I. M., Gallia, G. L., Olivi, A., McLendon, R., Rasheed, B. A., Keir, S., Nikolskaya, T., Nikolsky, Y., Busam, D. A., Tekleab, H., Diaz, L. A., Jr., Hartigan, J., Smith, D. R., Strausberg, R. L., Marie, S. K., Shinjo, S. M., Yan, H., Riggins, G. J., Bigner, D. D., Karchin, R., Papadopoulos, N., Parmigiani, G., Vogelstein, B., Velculescu, V. E. and Kinzler, K. W. (2008) 'An integrated genomic analysis of human glioblastoma multiforme', *Science,* 321(5897), pp. 1807-12.

Patnaik, A., Rosen, L. S., Tolaney, S. M., Tolcher, A. W., Goldman, J. W., Gandhi, L., Papadopoulos, K. P., Beeram, M., Rasco, D. W., Hilton, J. F., Nasir, A., Beckmann, R. P., Schade, A. E., Fulford, A. D., Nguyen, T. S., Martinez, R., Kulanthaivel, P., Li, L. Q., Frenzel, M., Cronier, D. M., Chan, E. M., Flaherty, K. T., Wen, P. Y. and Shapiro, G. I. (2016) 'Efficacy and Safety of Abemaciclib, an Inhibitor of CDK4 and CDK6, for Patients with Breast Cancer, Non-Small Cell Lung Cancer, and Other Solid Tumors', *Cancer Discov,* 6(7), pp. 740-53.

Pauzaite, T. (2019) *Identification and analysis of the signalling networks that regulate Ciz1 levels in normal and cancer cell lines.* PhD, Lancaster University.

Pauzaite, T., Thacker, U., Tollitt, J. and Copeland, N. A. (2016) 'Emerging Roles for Ciz1 in Cell Cycle Regulation and as a Driver of Tumorigenesis', *Biomolecules,* 7(1).

Pauzaite, T., Tollitt, J., Sopaci, B., Caprani, L., Iwanowytsch, O., Thacker, U., Hardy, J. G., Allinson, S. L. and Copeland, N. A. (2022) 'Dbf4-Cdc7 (DDK) Inhibitor PHA-767491 Displays Potent Anti-Proliferative Effects via Crosstalk with the CDK2-RB-E2F Pathway', *Biomedicines,* 10(8).

Preston-Martin, S. and Mack, W. (1996) 'Neoplasms of the nervous system', *Cancer Epidemiology and Prevention.* 2nd ed: New York: Oxford University Press, pp. 1231-1281.

Rahman, F., Ainscough, J. F., Copeland, N. and Coverley, D. (2007) 'Cancer-associated missplicing of exon 4 influences the subnuclear distribution of the DNA replication factor CIZ1', *Hum Mutat,* 28(10), pp. 993-1004.

Rahman, F. A., Aziz, N. and Coverley, D. (2010) 'Differential detection of alternatively spliced variants of Ciz1 in normal and cancer cells using a custom exon-junction microarray', *BMC Cancer,* 10, pp. 482.

Raub, T. J., Wishart, G. N., Kulanthaivel, P., Staton, B. A., Ajamie, R. T., Sawada, G. A., Gelbert, L. M., Shannon, H. E., Sanchez-Martinez, C. and De Dios, A. (2015) 'Brain Exposure of Two Selective Dual CDK4 and CDK6 Inhibitors and the Antitumor Activity of CDK4 and CDK6 Inhibition in Combination with Temozolomide in an Intracranial Glioblastoma Xenograft', *Drug Metab Dispos,* 43(9), pp. 1360-71.

Rayala, S. K., den Hollander, P., Balasenthil, S., Yang, Z., Broaddus, R. R. and Kumar, R. (2005) 'Functional regulation of oestrogen receptor pathway by the dynein light chain 1', *EMBO Rep,* 6(6), pp. 538-44.

Ridings-Figueroa, R., Stewart, E. R., Nesterova, T. B., Coker, H., Pintacuda, G., Godwin, J., Wilson, R., Haslam, A., Lilley, F., Ruigrok, R., Bageghni, S. A., Albadrani, G., Mansfield, W., Roulson, J. A., Brockdorff, N., Ainscough, J. F. X. and Coverley, D. (2017) 'The nuclear matrix protein CIZ1 facilitates localization of Xist RNA to the inactive X-chromosome territory', *Genes Dev,* 31(9), pp. 876-888.

Riess, C., Del Moral, K., Fiebig, A., Kaps, P., Linke, C., Hinz, B., Rupprecht, A., Frank, M., Fiedler, T., Koczan, D., Troschke-Meurer, S., Lode, H. N., Engel, N., Freitag, T., Classen, C. F. and Maletzki, C. (2022) 'Implementation of a combined CDK inhibition and arginine-

deprivation approach to target arginine-auxotrophic glioblastoma multiforme cells', *Cell Death Dis,* 13(6), pp. 555.

Riess, C., Koczan, D., Schneider, B., Linke, C., Del Moral, K., Classen, C. F. and Maletzki, C. (2021) 'Cyclin-dependent kinase inhibitors exert distinct effects on patient-derived 2D and 3D glioblastoma cell culture models', *Cell Death Discov,* 7(1), pp. 54.

Riess, C., Schneider, B., Kehnscherper, H., Gesche, J., Irmscher, N., Shokraie, F., Classen, C. F., Wirthgen, E., Domanska, G., Zimpfer, A., Strüder, D., Junghanss, C. and Maletzki, C. (2020) 'Activation of the Kynurenine Pathway in Human Malignancies Can Be Suppressed by the Cyclin-Dependent Kinase Inhibitor Dinaciclib', *Front Immunol,* 11, pp. 55.

Rojas-Prats, E., Tosat-Bitrián, C., Martínez-González, L., Nozal, V., Pérez, D. I. and Martínez, A. (2021) 'Increasing Brain Permeability of PHA-767491, a Cell Division Cycle 7 Kinase Inhibitor, with Biodegradable Polymeric Nanoparticles', *Pharmaceutics,* 13(2).

Sagberg, L. M., Solheim, O. and Jakola, A. S. (2016) 'Quality of survival the 1st year with glioblastoma: a longitudinal study of patient-reported quality of life', *J Neurosurg,* 124(4), pp. 989-97.

Sakaue-Sawano, A., Yo, M., Komatsu, N., Hiratsuka, T., Kogure, T., Hoshida, T., Goshima, N., Matsuda, M., Miyoshi, H. and Miyawaki, A. (2017) 'Genetically Encoded Tools for Optical Dissection of the Mammalian Cell Cycle', *Mol Cell,* 68(3), pp. 626-640.e5.

Serrano-Heras, G., Castro-Robles, B., Romero-Sánchez, C. M., Carrión, B., Barbella-Aponte, R., Sandoval, H. and Segura, T. (2020) 'Involvement of N-methylpurine DNA glycosylase in resistance to temozolomide in patient-derived glioma cells', *Sci Rep,* 10(1), pp. 22185.

Shi, J., Lv, S., Wu, M., Wang, X., Deng, Y., Li, Y., Li, K., Zhao, H., Zhu, X. and Ye, M. (2020) 'HOTAIR-EZH2 inhibitor AC1Q3QWB upregulates CWF19L1 and enhances cell cycle inhibition of CDK4/6 inhibitor palbociclib in glioma', *Clin Transl Med,* 10(1), pp. 182-198.

Shiau, A. K., Barstad, D., Loria, P. M., Cheng, L., Kushner, P. J., Agard, D. A. and Greene, G. L. (1998) 'The structural basis of estrogen receptor/coactivator recognition and the antagonism of this interaction by tamoxifen', *Cell,* 95(7), pp. 927-37.

Slamon, D. J., Neven, P., Chia, S., Fasching, P. A., De Laurentiis, M., Im, S. A., Petrakova, K., Bianchi, G. V., Esteva, F. J., Martín, M., Nusch, A., Sonke, G. S., De la Cruz-Merino, L., Beck, J. T., Pivot, X., Sondhi, M., Wang, Y., Chakravartty, A., Rodriguez-Lorenc, K., Taran, T. and Jerusalem, G. (2020) 'Overall Survival with Ribociclib plus Fulvestrant in Advanced Breast Cancer', *N Engl J Med,* 382(6), pp. 514-524.

Socié, G., Curtis, R. E., Deeg, H. J., Sobocinski, K. A., Filipovich, A. H., Travis, L. B., Sullivan, K. M., Rowlings, P. A., Kingma, D. W., Banks, P. M., Travis, W. D., Witherspoon, R. P., Sanders, J., Jaffe, E. S. and Horowitz, M. M. (2000) 'New malignant diseases after allogeneic marrow transplantation for childhood acute leukemia', *J Clin Oncol,* 18(2), pp. 348-57.

Sofi, S., Williamson, L., Turvey, G. L., Scoynes, C., Hirst, C., Godwin, J., Brockdorff, N., Ainscough, J. and Coverley, D. (2022) 'Prion-like domains drive CIZ1 assembly formation at the inactive X chromosome', *J Cell Biol,* 221(4).

Somarelli, J. A., Roghani, R. S., Moghaddam, A. S., Thomas, B. C., Rupprecht, G., Ware, K. E., Altunel, E., Mantyh, J. B., Kim, S. Y., McCall, S. J., Shen, X., Mantyh, C. R. and Hsu, D. S. (2020) 'A Precision Medicine Drug Discovery Pipeline Identifies Combined CDK2 and 9 Inhibition as a Novel Therapeutic Strategy in Colorectal Cancer', *Mol Cancer Ther,* 19(12), pp. 2516-2527.

Stewart, E. R., Turner, R. M. L., Newling, K., Ridings-Figueroa, R., Scott, V., Ashton, P. D., Ainscough, J. F. X. and Coverley, D. (2019) 'Maintenance of epigenetic landscape requires CIZ1 and is corrupted in differentiated fibroblasts in long-term culture', *Nat Commun,* 10(1), pp. 460.

Strobel, H., Baisch, T., Fitzel, R., Schilberg, K., Siegelin, M. D., Karpel-Massler, G., Debatin, K. M. and Westhoff, M. A. (2019) 'Temozolomide and Other Alkylating Agents in Glioblastoma Therapy', *Biomedicines,* 7(3).

Stupp, R., Mason, W. P., van den Bent, M. J., Weller, M., Fisher, B., Taphoorn, M. J., Belanger, K., Brandes, A. A., Marosi, C., Bogdahn, U., Curschmann, J., Janzer, R. C., Ludwin, S. K., Gorlia, T., Allgeier, A., Lacombe, D., Cairncross, J. G., Eisenhauer, E. and Mirimanoff, R. O. (2005) 'Radiotherapy plus concomitant and adjuvant temozolomide for glioblastoma', *N Engl J Med,* 352(10), pp. 987-96.

Sunwoo, H., Colognori, D., Froberg, J. E., Jeon, Y. and Lee, J. T. (2017) 'Repeat E anchors Xist RNA to the inactive X chromosomal compartment through CDKN1A-interacting protein (CIZ1)', *Proc Natl Acad Sci U S A,* 114(40), pp. 10654-10659.

Swarts, D. R. A., Stewart, E. R., Higgins, G. S. and Coverley, D. (2018) 'CIZ1-F, an alternatively spliced variant of the DNA replication protein CIZ1 with distinct expression and localisation, is overrepresented in early stage common solid tumours', *Cell Cycle,* 17(18), pp. 2268-2283.

Talapati, S. R., Nataraj, V., Pothuganti, M., Gore, S., Ramachandra, M., Antony, T., More, S. S. and Krishnamurthy, N. R. (2020) 'Structure of cyclin-dependent kinase 2 (CDK2) in complex with the specific and potent inhibitor CVT-313', *Acta Crystallogr F Struct Biol Commun,* 76(Pt 8), pp. 350-356.

Tang, J. B., Svilar, D., Trivedi, R. N., Wang, X. H., Goellner, E. M., Moore, B., Hamilton, R. L., Banze, L. A., Brown, A. R. and Sobol, R. W. (2011) 'N-methylpurine DNA glycosylase and DNA polymerase beta modulate BER inhibitor potentiation of glioma cells to temozolomide', *Neuro Oncol,* 13(5), pp. 471-86.

Taylor, J. W., Parikh, M., Phillips, J. J., James, C. D., Molinaro, A. M., Butowski, N. A., Clarke, J. L., Oberheim-Bush, N. A., Chang, S. M., Berger, M. S. and Prados, M. (2018) 'Phase-2 trial of palbociclib in adult patients with recurrent RB1-positive glioblastoma', *J Neurooncol,* 140(2), pp. 477-483.

Thacker, U., Pauzaite, T., Tollitt, J., Twardowska, M., Harrison, C., Dowle, A., Coverley, D. and Copeland, N. A. (2020) 'Identification of DHX9 as a cell cycle regulated nucleolar recruitment factor for CIZ1', *Sci Rep,* 10(1), pp. 18103.

Thakkar, J. P., Peruzzi, P. P. and Prabhu, V. C. (2024) *Glioblastoma Multiforme*. Patients. American Association of Neurological Surgeons (Accessed: 13th August 2024).

Thalappilly, S., Suliman, M., Gayet, O., Soubeyran, P., Hermant, A., Lecine, P., Iovanna, J. L. and Dusetti, N. J. (2008) 'Identification of multi-SH3 domain-containing protein interactome in pancreatic cancer: a yeast two-hybrid approach', *Proteomics,* 8(15), pp. 3071-81.

Thanasupawat, T., Natarajan, S., Rommel, A., Glogowska, A., Bergen, H., Krcek, J., Pitz, M., Beiko, J., Krawitz, S., Verma, I. M., Ghavami, S., Klonisch, T. and Hombach-Klonisch, S. (2017) 'Dovitinib enhances temozolomide efficacy in glioblastoma cells', *Mol Oncol,* 11(8), pp. 1078-1098.

Tollitt, J., Briggs, T., Allinson, S. L., Staples, C. J., Parsons, J. L., Mort, R. L. and Copeland, N. A. (2024) 'CIZ1 regulates G1 length and the CDK threshold for initiation of DNA replication to prevent DNA replication stress', *bioRxiv*, pp. 2024.09.02.610838.

Turner, N. C., Ro, J., André, F., Loi, S., Verma, S., Iwata, H., Harbeck, N., Loibl, S., Huang Bartlett, C., Zhang, K., Giorgetti, C., Randolph, S., Koehler, M. and Cristofanilli, M. (2015) 'Palbociclib in Hormone-Receptor-Positive Advanced Breast Cancer', *N Engl J Med,* 373(3), pp. 209-19.

Verhaak, R. G., Hoadley, K. A., Purdom, E., Wang, V., Qi, Y., Wilkerson, M. D., Miller, C. R., Ding, L., Golub, T., Mesirov, J. P., Alexe, G., Lawrence, M., O'Kelly, M., Tamayo, P., Weir, B. A., Gabriel, S., Winckler, W., Gupta, S., Jakkula, L., Feiler, H. S., Hodgson, J. G., James, C. D., Sarkaria, J. N., Brennan, C., Kahn, A., Spellman, P. T., Wilson, R. K., Speed, T. P., Gray, J. W., Meyerson, M., Getz, G., Perou, C. M. and Hayes, D. N. (2010) 'Integrated genomic analysis identifies clinically relevant subtypes of glioblastoma characterized by abnormalities in PDGFRA, IDH1, EGFR, and NF1', *Cancer Cell,* 17(1), pp. 98-110.

Walker, A. E., Robins, M. and Weinfeld, F. D. (1985) 'Epidemiology of brain tumors: the national survey of intracranial neoplasms', *Neurology,* 35(2), pp. 219-26.

Wan, H., Wang, L., Huo, B., Qiao, Z. and Zhang, Y. (2023) 'CIZ1 aggravates gastric cancer progression via mediating FBXL19-AS1 and miR-339-3p', *Heliyon,* 9(11), pp. e21061.

Wander, S. A., O'Brien, N., Litchfield, L. M., O'Dea, D., Morato Guimaraes, C., Slamon, D. J. and Goel, S. (2022) 'Targeting CDK4 and 6 in Cancer Therapy: Emerging Preclinical Insights Related to Abemaciclib', *Oncologist,* 27(10), pp. 811-821.

Wang, D. Q., Wang, K., Yan, D. W., Liu, J., Wang, B., Li, M. X., Wang, X. W., Peng, Z. H., Li, G. X. and Yu, Z. H. (2014) 'Ciz1 is a novel predictor of survival in human colon cancer', *Exp Biol Med (Maywood),* 239(7), pp. 862-870.

Wang, X., Xie, H., Zhu, Z., Zhang, J. and Xu, C. (2023) 'Molecular basis for the recognition of CIZ1 by ERH', *Febs j,* 290(3), pp. 712-723.

Warder, D. E. and Keherly, M. J. (2003) 'Ciz1, Cip1 interacting zinc finger protein 1 binds the consensus DNA sequence ARYSR(0-2)YYAC', *J Biomed Sci,* 10(4), pp. 406-17.

Weathers, S.-P. (2019) *7 glioblastoma myths*. Cancerwise. MD Anderson Cancer Center. Available at: https://www.mdanderson.org/cancerwise/7-glioblastoma-brain-tumor-myths.h00-159299889.html (Accessed: 25th August 2024).

Weller, M., van den Bent, M., Preusser, M., Le Rhun, E., Tonn, J. C., Minniti, G., Bendszus, M., Balana, C., Chinot, O., Dirven, L., French, P., Hegi, M. E., Jakola, A. S., Platten, M., Roth, P., Rudà, R., Short, S., Smits, M., Taphoorn, M. J. B., von Deimling, A., Westphal, M., Soffietti, R., Reifenberger, G. and Wick, W. (2021) 'EANO guidelines on the diagnosis and treatment of diffuse gliomas of adulthood', *Nat Rev Clin Oncol,* 18(3), pp. 170-186.

Whittaker, S., Madani, D., Joshi, S., Chung, S. A., Johns, T., Day, B., Khasraw, M. and McDonald, K. L. (2017) 'Combination of palbociclib and radiotherapy for glioblastoma', *Cell Death Discov,* 3, pp. 17033.

Wojcik, E., Murphy, A. M., Fares, H., Dang-Vu, K. and Tsubota, S. I. (1994) 'Enhancer of rudimentaryp1, e(r)p1, a highly conserved enhancer of the rudimentary gene', *Genetics,* 138(4), pp. 1163-70.

Wong, S. T., Zhang, X. Q., Zhuang, J. T., Chan, H. L., Li, C. H. and Leung, G. K. (2012) 'MicroRNA-21 inhibition enhances in vitro chemosensitivity of temozolomide-resistant glioblastoma cells', *Anticancer Res,* 32(7), pp. 2835-41.

Wu, J., Lei, L., Gu, D., Liu, H. and Wang, S. (2016) 'CIZ1 is upregulated in hepatocellular carcinoma and promotes the growth and migration of the cancer cells', *Tumour Biol,* 37(4), pp. 4735-42.

Xu, P., Westhoff, M. A., Hadzalic, A., Debatin, K. M., Winiarski, L., Oleksyszyn, J., Wirtz, C. R., Knippschild, U. and Burster, T. (2022) 'Diisothiocyanate-Derived Mercapturic Acids Are a Promising Partner for Combination Therapies in Glioblastoma', *ACS Omega,* 7(7), pp. 5929-5936.

Yang, A. L., Wu, Q., Hu, Z. D., Wang, S. P., Tao, Y. F., Wang, A. M., Sun, Y. X., Li, X. L., Dai, L. and Zhang, J. (2021) 'A network pharmacology approach to investigate the anticancer mechanism of cinobufagin against hepatocellular carcinoma via downregulation of EGFR-CDK2 signaling', *Toxicol Appl Pharmacol,* 431, pp. 115739.

Yang, B. Z., Liu, M. Y., Chiu, K. L., Chien, Y. L., Cheng, C. A., Chen, Y. L., Tsui, L. Y., Lin, K. R., Chu, H. C. and Wu, C. P. (2024) 'DHX9 SUMOylation is required for the suppression of R-loop-associated genome instability', *Nat Commun,* 15(1), pp. 6009.

Yin, J., Wang, C., Tang, X., Sun, H., Shao, Q., Yang, X. and Qu, X. (2013) 'CIZ1 regulates the proliferation, cycle distribution and colony formation of RKO human colorectal cancer cells', *Mol Med Rep,* 8(6), pp. 1630-4.

Yin, L., Li, H., Liu, W., Yao, Z., Cheng, Z., Zhang, H. and Zou, H. (2018) 'A highly potent CDK4/6 inhibitor was rationally designed to overcome blood brain barrier in gliobastoma therapy', *Eur J Med Chem,* 144, pp. 1-28.

Yusa, K., Zhou, L., Li, M. A., Bradley, A. and Craig, N. L. (2011) 'A hyperactive piggyBac transposase for mammalian applications', *Proc Natl Acad Sci U S A,* 108(4), pp. 1531-6.

Zafrakas, M., Losen, I., Knüchel, R. and Dahl, E. (2008) 'Enhancer of the rudimentary gene homologue (ERH) expression pattern in sporadic human breast cancer and normal breast tissue', *BMC Cancer,* 8, pp. 145.

Zeverijn, L. J., Looze, E. J., Thavaneswaran, S., van Berge Henegouwen, J. M., Simes, R. J., Hoes, L. R., Sjoquist, K. M., van der Wijngaart, H., Sebastian, L., Geurts, B. S., Lee, C. K., de Wit, G. F., Espinoza, D., Roepman, P., Lin, F. P., Jansen, A. M. L., de Leng, W. W. J., van der Noort, V., Leek, L. V. M., de Vos, F., van Herpen, C. M. L., Gelderblom, H., Verheul, H. M. W., Thomas, D. M. and Voest, E. E. (2023) 'Limited clinical activity of palbociclib and ribociclib monotherapy in advanced cancers with cyclin D-CDK4/6 pathway alterations in the Dutch DRUP and Australian MoST trials', *Int J Cancer,* 153(7), pp. 1413-1422.

Zhang, D., Wang, Y., Dai, Y., Wang, J., Suo, T., Pan, H., Liu, H. and Shen, S. (2015) 'CIZ1 promoted the growth and migration of gallbladder cancer cells', *Tumour Biol,* 36(4), pp. 2583-91.

Zhang, J., Stevens, M. F. and Bradshaw, T. D. (2012) 'Temozolomide: mechanisms of action, repair and resistance', *Curr Mol Pharmacol,* 5(1), pp. 102-14.

Zhang, P., Chen, X. B., Ding, B. Q., Liu, H. L. and He, T. (2018) 'Down-regulation of ABCE1 inhibits temozolomide resistance in glioma through the PI3K/Akt/NF-κB signaling pathway', *Biosci Rep,* 38(6).

Zhang, P., Miska, J., Lee-Chang, C., Rashidi, A., Panek, W. K., An, S., Zannikou, M., Lopez-Rosas, A., Han, Y., Xiao, T., Pituch, K. C., Kanojia, D., Balyasnikova, I. V. and Lesniak, M. S. (2019) 'Therapeutic targeting of tumor-associated myeloid cells synergizes with radiation therapy for glioblastoma', *Proc Natl Acad Sci U S A,* 116(47), pp. 23714-23723.

Zhou, X., Liu, Q., Wada, Y., Liao, L. and Liu, J. (2018) 'CDKN1A-interacting zinc finger protein 1 is a novel biomarker for lung squamous cell carcinoma', *Oncol Lett,* 15(1), pp. 183-188.

Zou, Y., Wang, Q., Li, B., Xie, B. and Wang, W. (2014) 'Temozolomide induces autophagy via ATM-AMPK-ULK1 pathways in glioma', *Mol Med Rep,* 10(1), pp. 411-6.

7. Appendices

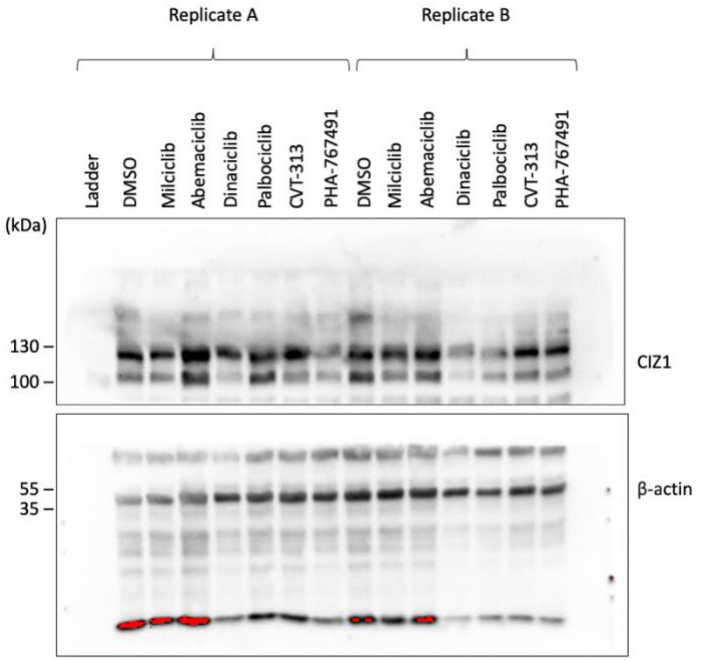

Appendix 1. Full gels from Figure 3.14 A.

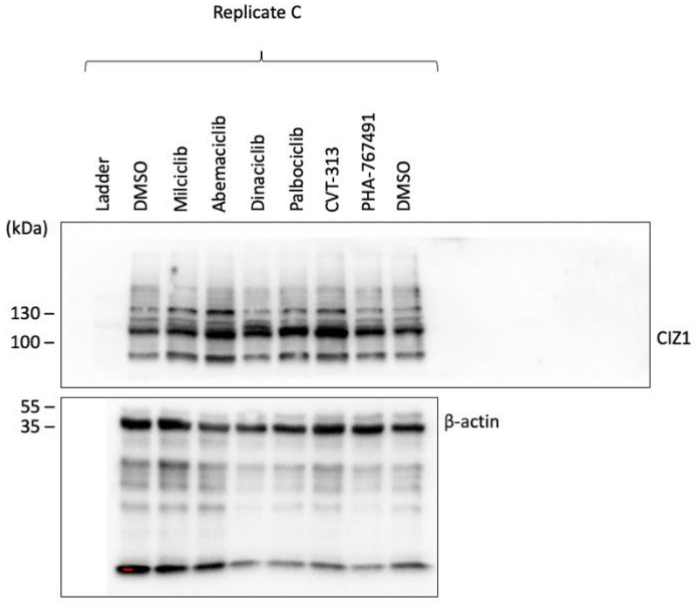

Appendix 2. Full gels from Figure 3.14 B.

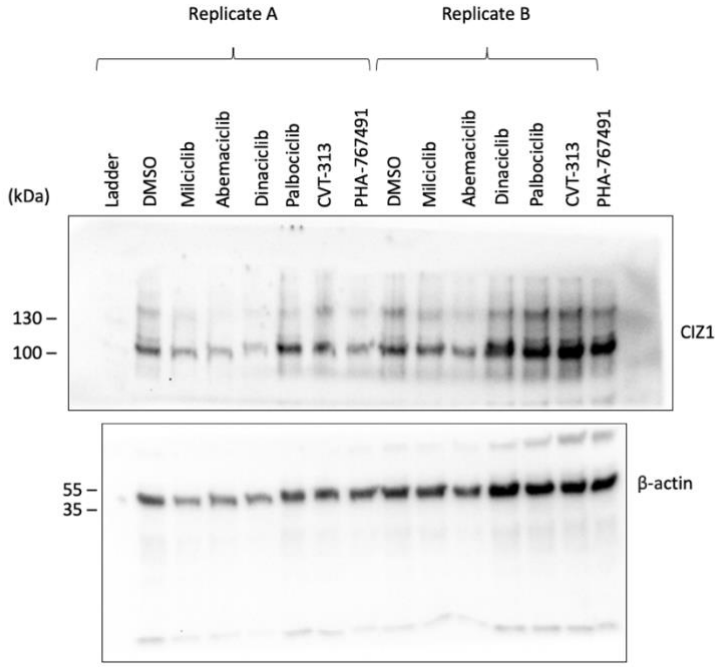

Appendix 3. Full gels from Figure 3.15 A.

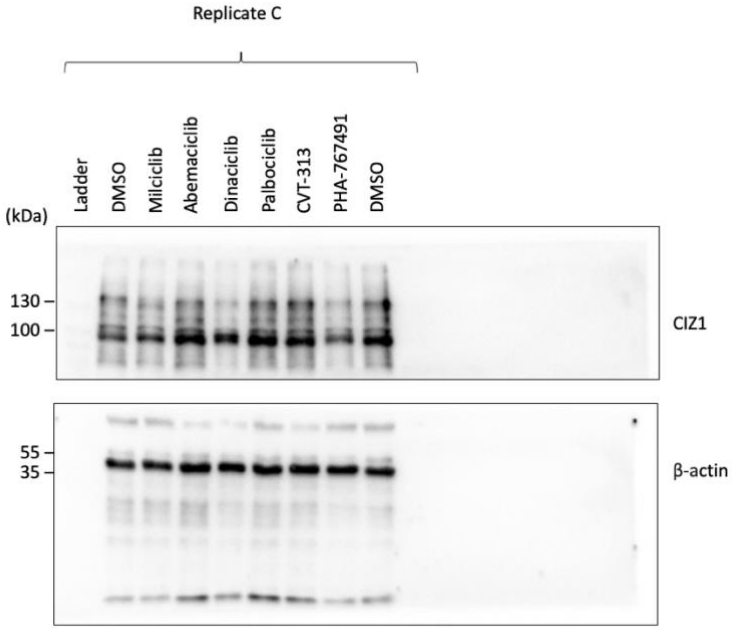

Appendix 4. Full gels from Figure 3.15 B.